SISSA - SCUOLA
INTERNAZIONALE
SUPERIORE
DI STUDI AVANZATI
TRIESTE
Strada Costiera 11

ISAS - INTERNATIONAL SCHOOL FOR ADVANCED STUDIES

Thesis submitted for the degree of

Doctor Philosophiae:

ON THE STRUCTURE AND BONDING OF NEUTRAL AND IONIZED MOLECULES

Candidate:

Giulia Galli

Supervisor:

Prof. Mario P. Tosi

Trieste, December 1986

TRIESTE

C. R.

Thesis submitted for the degree of

Doctor Philosophiae:

ON THE STRUCTURE AND BONDING OF NEUTRAL AND IONIZED MOLECULES

Candidate:

Giulia Galli

Supervisor:

Prof. Mario P. Tosi

Trieste, December 1986

ACKOWLEDGEMENTS

I would like to express my gratitude to Dr. Wanda Andreoni and Prof. Mario P. Tosi for their supervision and their constant help and support throughout this work.

I thank Dr. Pietro Ballone for his constant encouragement during the preparation of this thesis and for his critical reading of several parts of the manuscript.

The kind hospitality of Prof. Carlo Calandra at the Computer Center of the University of Modena and of the Institut of Experimental Physics of Lausanne is gratefully acknowledged.

Finally, I thank Dr. Francesco Buda and Dr. Guido L. Chiarotti for their kind and patient help in the final version of this thesis.

CONTENTS

INTRODUCTION

The problem of predicting the structure that an atomic aggregate will adopt at equilibrium, starting from knowledge of its atomic constituents, is still a challenging one for both physicists and chemists. The prediction from first-principles quantum mechanical calculations of the electronic structure in either molecules or solids now counts a number of successes[1]. The usually small energy differences between different molecular or crystal conformations can be computed with a high degree of accuracy, at least for sufficiently simple systems. On the other hand, several semiempirical approaches have been developed, especially in the case of solids, which allow the structural trends in large families of compounds to be systematized and understood.

Both first-principles and semiempirical approaches to molecular shapes and crystal structures have so far been developed on different footings. While successful quantum mechanical calculations for solids have been performed within the Local density approximation of the Density Functional theory[2], molecules have mainly been investigated by the so called quantum chemistry methods, i.e., Hartree-Fock, Generalized Valence Bond and Configuration Interaction methods[3].

The most successful and promising of the semiempirical approaches adopted for solids have been based on bidimensional structural plots, where each compound is characterized by two parameters and compounds with the same

structure appear to cluster in separate domains[4]. In the case of molecules, instead, phenomenological criteria based on molecular orbital theory have been mainly used to rationalize and account for the geometries of the main group species.[5]

The growing interest in the new field of cluster physics, to which a widespread attention has recently been devoted by both physicists and chemists[6], has pointed out the need for unified methods and schemes to investigate molecules together with solids. This is seen as an essential prerequisite to the study of the structural ,and in general of the physical properties of clusters, which represent an intermediate state of aggregation between the molecular and the solid phases. At the same time, theoretical investigations on simple molecules and/or bulk properties of crystals from which a comprehension of some physical properties of clusters can be extrapolated are much in demand.

In relation to the questions that we have underlined just above, we have investigated tri- and tetra-atomic aggregates both by exploring the construction of unified structural plots for their molecular and crystalline phases at the semiempirical level, and by carrying out first-principles calculations for specific molecular systems in neutral and ionized states. These latter calculations have been aimed both at assessing the physical content of empirical structural coordinates and at making contact with experimental evidence on ionic clusters.

The unified scheme for molecular shapes and crystal structures which we

have developed appeals to recent progress made in structural classification of solids through simple a priori parameters of the atomic constituents[7-12]. Such "quantum structural diagrams" are usually defined by two Cartesian coordinates, derived as linear combinations of valence electron orbital radii, the latter being obtained from first-principles calculations on the free atoms.

Our contribution to the construction of a parallel scheme for clusters and polyatomic molecules is twofold :

(i) We have shown that the same quantum structural parameters which classify $s-p$ bonded crystals can predict successfully the shapes of AB_2, AB_3 and A_2B_2 small aggregates[13,14].

In the case of a triatomic molecule, the pertinent question about structure is simple and well defined : is the molecule linear or bent? On the other hand, in the case of tetra-atomic species the number of possible equilibrium configurations increases and with it the number of questions that one should answer.

The quantum diagrams that we have constructed perfectly discriminate between linear and bent structures for AB_2 molecules. In the case of AB_3 species, they allow the distinction between planar and threedimensional geometries and also between several different distortions of ideal symmetric shapes. The different planar conformations adopted within the family of A_2B_2 compounds are also resolved in our plots.

(ii) The approach not only discriminates between different molecular geometries, but also accounts for the trend in the apex angle displayed

by bent AB_2 and rhombohedral A_2B_2 molecules. This has allowed us to establish simple semiempirical relationships between our quantum coordinates and the bond angles of these species[13,14]. The existence of these correlations has in turn indicated a direction where a physical interpretation of the structural coordinates may be sought. Such an interpretation is mainly aimed at understanding the reasons why structural parameters defined for the atomic constituents contain sufficient information to account for structural regularities in the molecular and in the solid phase. Significant insight into this problem has indeed been gained by an ab initio study of the linear-to-bent transition in the family of double-octet (DO) AB_2 molecules. We have performed first-principles calculations to characterize this structural transition and analyzed in a fully theoretical framework the role played by our structural parameters in driving it.

Our calculations have also permitted a critical discussion of some of the phenomenological criteria widely used in the literature, by both experimentalists and theoreticians, to predict and rationalize the shapes of main group molecules.

The remaining part of our work devoted to first-principles investigations of specific systems has been concentrated on sodium chloride microclusters. The alkali halides , and in particular sodium chloride, have long served as model materials in solid state physics[16] because of the simplicity of the bonding and of sample preparation. The same properties make them ideally suited to represent a class of clusters. Alkali halides aggregates

of different sizes and compositions have been recently produced by several experimental techiques and carefully characterized through mass spectra or time of flight measurements[17]. A main feature of these spectra is the observation of a larger abundance of halogen-deficient clusters relative to the stoichiometric ones.

In relation to these experimental findings, we have performed ab initio calculations for the equilibrium properties of Na_2Cl_2 and Na_2Cl in both the neutral and singly ionized states, with specific attention to their ionization processes[18]. Our calculations have been carried out within the Hartree-Fock approximation, in a pseudopotential framework.

We have found that in both Na_2Cl_2 and Na_2Cl ionization is a drastic process, followed by symmetry breaking. Specifically, a linear Na_2Cl^+ is the final product of the ionization of the bent triatomic species, while the rhombohedral dimer adopts a triangular conformation upon removal of one electron. The latter turns out to be very weakly bound against dissociation into Na_2Cl^+ and a chlorine atom. These results provide a natural explanation for mass spectra, accounting for the much higher stability of the chlorine-deficient ionized aggregates relative to the stoichiometric one.

Our results are also in broad agreement with experimental data on dissociation energies, ionization potentials and equilibrium structural parameters and allow a discussion of chemi-ionization experiments on compound formation.

The layout of this thesis is as follows. In chapter 1 we briefly review

the main semiempirical approaches adopted so far for solids and molecules, in order to establish the framework in which our structural classifications of AB_2, AB_3 and A_2B_2 compounds have been developed. These are described in chapters 2 and 4 for tri- and tetra-atomic species, respectively. In chapter 3 we report the results of our ab initio calculations to investigate the linear-to-bent transition in DO AB_2 molecules and discuss their connection with the results of the quantum structural diagrams developed in chapter 2 and also with phenomenological criteria proposed in the literature to account for the shapes of main group molecules. The results of first-principles calculations on sodium chloride microclusters, as well as those of test calculations on NaCl and $NaCl^+$ monomers[19], are described in chapter 5. Chapter 6 concludes the thesis with a summary of our main results and with a brief discussion of work in progress.

Chapter 1

SEMIEMPIRICAL APPROACHES TO CRYSTAL STRUCTURES AND MOLECULAR SHAPES.

Quantum mechanical calculations have become increasingly refined recently and have revealed a great deal of *detailed* information about the electronic structures of specific systems, either molecules or solids[1]. It seems nevertheless difficult to extract from these calculations and understanding of the *general* physical factors determining the origin of structural regularities. Semiempirical approaches to crystal structures and molecular shapes, on the other hand, concentrate on the construction of physically simple and transferable criteria (i.e. from system to system and among different classes of compounds), according to which the structural trends in large families of compounds can be rationalized. The quantum mechanical and semiempirical treatements of structural problems are clearly complemental.

As we have mentioned in the Introduction, the most successful of the semiempirical approaches adopted so far for solids have been based on bidimensional plots ("structural maps")[4]. During the last ten years, this method has moved from a mere phenomenological level, owing to the introduction of structural parameters which are linear combinations

of orbital radii of the valence electrons, derived from quantal treatements of the component atoms.[7-12]. Structural diagrams defined by Cartesian coordinates which are obtained from these parameters turn out to provide a simple and general scheme which:

1) allows the ordering of a large amount of experimental data for several classes of compounds;

2) allows one to distinguish between different crystal structures;

3) accounts for several trends in the structural and physical properties of families of compounds with different chemical bonding, e.g., metallic, covalent and ionic;

4) may lead to predictions on compounds stability and formation;

5) may lead to a global understanding of the physical factors which determine one specific configuration as the equilibrium structure, via the interpretation of the coordinates used.

In the case of molecules, several models[5] based on molecular orbital theory have been formulated to account for the shapes of the main group species .The application of most of them is often not straightforward but requires some chemical intuition on the bonding that a compound is going to form. As we shall see, these models are usually appropriate to classify molecular shapes within restricted classes of compounds, but fail in accounting for geometries of large families such as all the known AB_2 or AB_3 systems. Even with this limitation, the phenomenological criteria proposed for molecules are very useful in pointing out some key physical factors to

look at in structural classifications.

In this chapter we briefly review the semiempirical approaches adopted so far for structural classifications of solids (section 1.1) and molecules (section 1.2), in order to establish the framework in which the unified approach to crystal structure and molecular shapes described in chapters 2 and 4 has been developed.

1.1 Quantum structural diagrams for solids

The origin of crystal structure classifications through bidimensional maps is the Mooser-Pearson plot of octet A_nB_m crystals [4,20]. The Mooser-Pearson argument in tackling the problem of a possible correlation between the chemical composition of a crystal phase and the coordination configuration met in its structure runs as follows. With increasing principal quantum number n of the valence shell of an atom, the directional character of the bonds formed by that atom decreases. Moreover, covalent bonds have strongly pronounced directional properties, while ionic bonds are nondirectional. Taking the difference $\delta\chi$ between the Pauling electronegativities of anions and cations as a measure of the bond ionicity, Mooser and Pearson plotted the A_nB_m type of octet phases in $\bar{n}$ versus $\delta\chi$ diagrams, $\bar{n}$ being the average principal quantum number. These plots are indeed successful in separating solids with different coordination configurations. At low values of $\bar{n}$ and/or $\delta\chi$, low coordinated (tetrahedral) structures are met, the high coordinated ones (octahedral)

being instead found at high $\bar{n}$ and/or $\delta\chi$ values. Though successful for octet solids, a ($\bar{n}$,$\delta\chi$) diagram cannot properly separate differently coordinated structures for non-octet compounds, as shown by Zunger[9] for AB crystals.

Fully quantum mechanical structural coordinates were first introduced by Phillips and Van Vecten [21] in order to classify AB type, $s-p$ bonded octet compounds. These coordinates are the average covalent energy gap E_h and the ionic energy gap C. In an E_h versus C diagram, shown in fig. 1.1, the $A^N B^{8-N}$ solids fall into two completely separated regions : one corresponding to fourfold coordination (covalent compounds), the other to sixfold coordination (ionic compounds). The boundary dividing the seventy compounds in fig. 1.1 into ionic and covalent structures corresponds to $f_i = \frac{C}{(E_h^2+C^2)} = 0.79 \pm 0.01$. Since $C = 0$ for diamond-type crystals, this line can be defined as the critical ionicity line. The success of the Phillips-Van Vechten coordinates can be achieved for crystals which have isotropic dielectric properties and are non-metallic, so that the covalent and ionic interactions can each be described by only one parameter.

The need of a classification scheme which could be generalized to materials other than $s-p$ bonded $A^N B^{8-N}$ solids has led to the introduction of new structural parameters: these are linear combinations of valence electron orbital radii (VEOR) derived from first-principles calculations on the free atoms. The definition of the pseudopotential VEOR is based on ideas first developed by St. John and Bloch [7]. In an isolated atom one defines, for each orbital angular momentum l, a hard-core pseudopotential $V_l(r)$ such

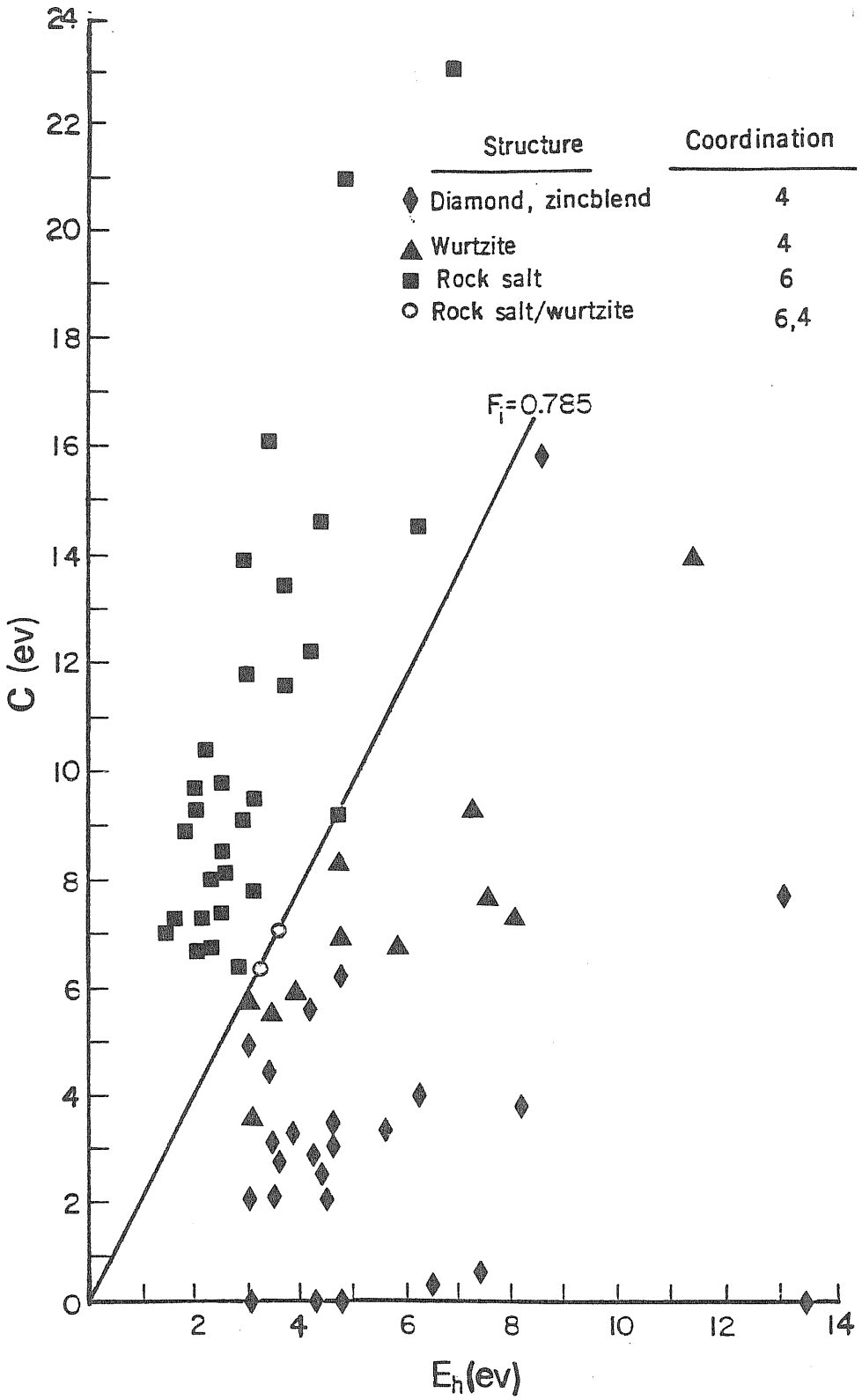

Fig. 1.1 Covalent (E_h) and ionic (C) contributions to the average energy gap E_g ($E_g^2 = E_h^2 + C^2$)are used as Cartesian coordinates to separate the crystal structures of $s-p$ bonded $A^N B^{8-N}$ solids with coordination number four and six. (From ref.21).

that,for large r the potential is the same as the one-electron potential $V(r)$, whereas for small r a large positive term simulates the effects of valence electron repulsion from the core region, due to orthogonalization effects. The way in which the repulsive term is chosen has been greatly refined in the last decade and the success of ab initio pseudopotential calculations for specific solids [1] suggests that this term can now be known quite accurately. Given a set of pseudopotentials $V_l(r)$ for neutral atoms, one defines the quantum core radii r_l by the condition $V_l(r_l) = 0$. The radii r_l define the size of the core, the region from which valence electrons with l angular character are excluded. The effect of the core on the valence electrons can be regarded as unchanged as the chemical environment of the atom is modified, as long as the frozen core approximation is valid.

The first demonstration that quantum core radii were valid structural coordinates was given by Bloch and St.John[7], by showing that a successful quantum structural diagrams for eigthy $A^N B^{8-N}$ compounds resulted from using suitable combinations of $r_s(A), r_p(A), r_s(B)$ and $r_p(B)$ as Cartesian coordinates. This is shown in fig. 1.2. Apart from the broad covalent-ionic structural dichotomy already displayed in Fig. 1.1,there are more subtle structural distinctions which are faithfully resolved, leading thus to a substantial improvement on the Phillips- Van Vechten plot.

Altogether five different crystal structures are separated in Fig. 1.2. The new quantum structural parameters introduced by Bloch and St.John - generally improved in the choice of the atomic pseudopotentials $V_l(r)$ -

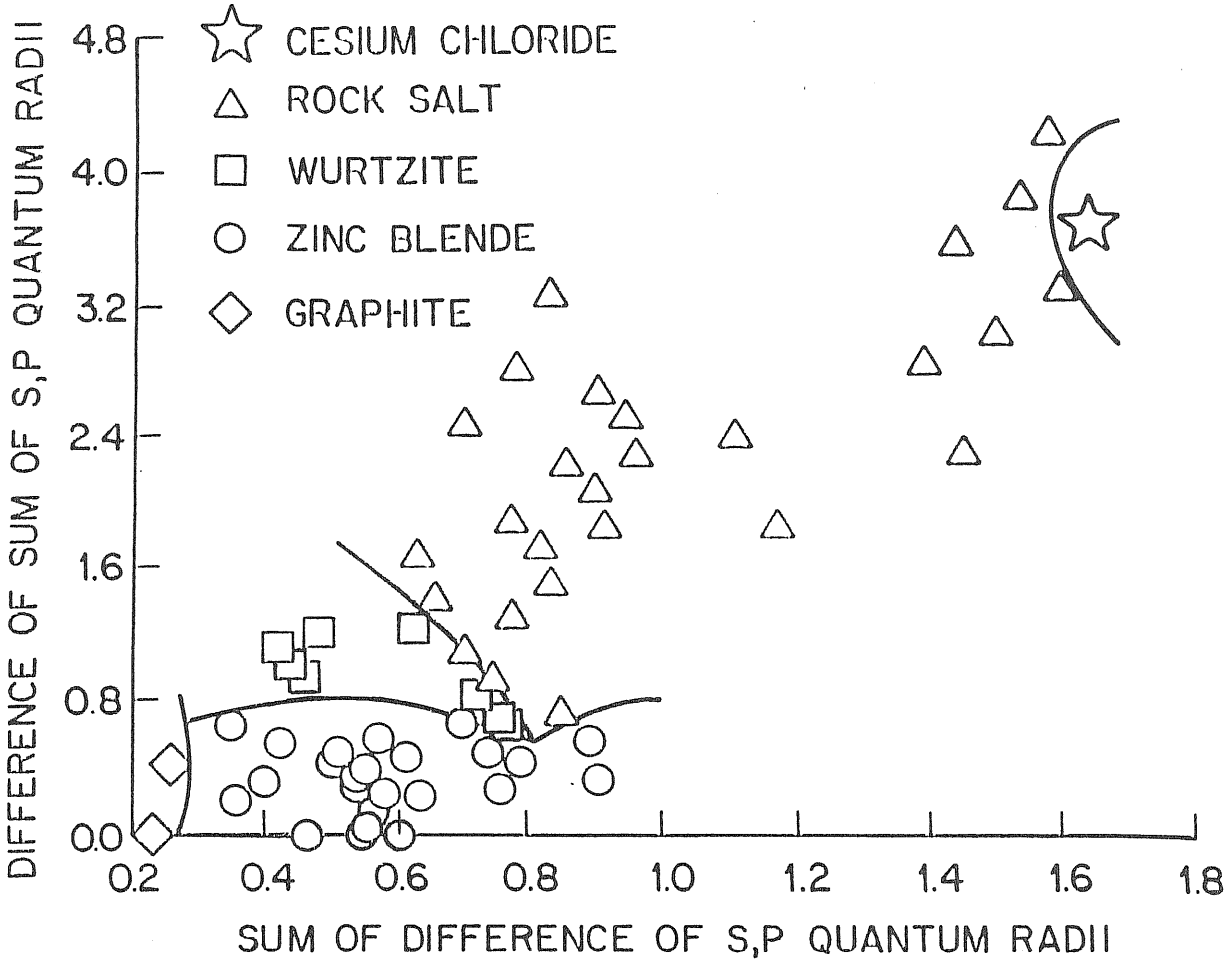

Fig.1.2 Linear combinations of the s and p orbital radii as defined by Bloch and St. John are used to separate the crystal structures of $s-p$ bonded $A^N B^{8-N}$ solids. (From ref. 7)

has been applied by different authors[8,9,12] also to metallic and non octet compounds. Quantum Structural Diagrams (QSDs) have been reported for AB crystals, exhibiting successful structural separations involving up to 500 compounds. (In many cases, different combinations of the parameters r_l have been used by different authors to set up the two Cartesian coordinates of the QSD. These correspond to affine transformations of the metric, which generally do not affect the separability of different structrures in significant

ways). Zunger[9] has provided a rather satisfying classification of both $s-p$ and $p-d$ bonded AB crystals using the same quantum coordinates, obtained as linear combinations of s and p radii. The structural map derived for the 356 binary non-octet compounds is shown in Fig. 1.3.

Although remarkable, the success in the structural separation of AB solids comprehensive of transition metal (TM) compounds without including r_d radii is not easily interpretable and should not be taken as a manifestation of the irrelevance of the d valence electrons in the bonding of these materials. In fact, Machlin and Loh[22], and subsequently Chelickowsky[23], have proposed two alternative coordinates to classify the restricted class of TM-TM compounds, based upon δN and $\bar{N}$, N being the periodic table group number. Their parameters effect a better crystal structure separation than the Zunger coordinates do for about 100 TM-TM compounds. This supports the view that d orbital contributions are indeed important for crystal structural properties.

VEOR radii derived from first-principles all-electron calculations on the free atoms have been introduced by Andreoni *et al.*[24] They are defined as nodal radii (N_l), i.e. as the outermost nodes of valence wavefunctions with l angular character. They measure the size of the core othogonalization hole in a straightforward way. A brief discussion of the nodal radii properties, together with those of the pseudopotentials radii introduced by Zunger will be given in chapter 2, where both sets of structural parameters will be used to construct QSD for a parallel classification of AB_2 molecules and crystals.

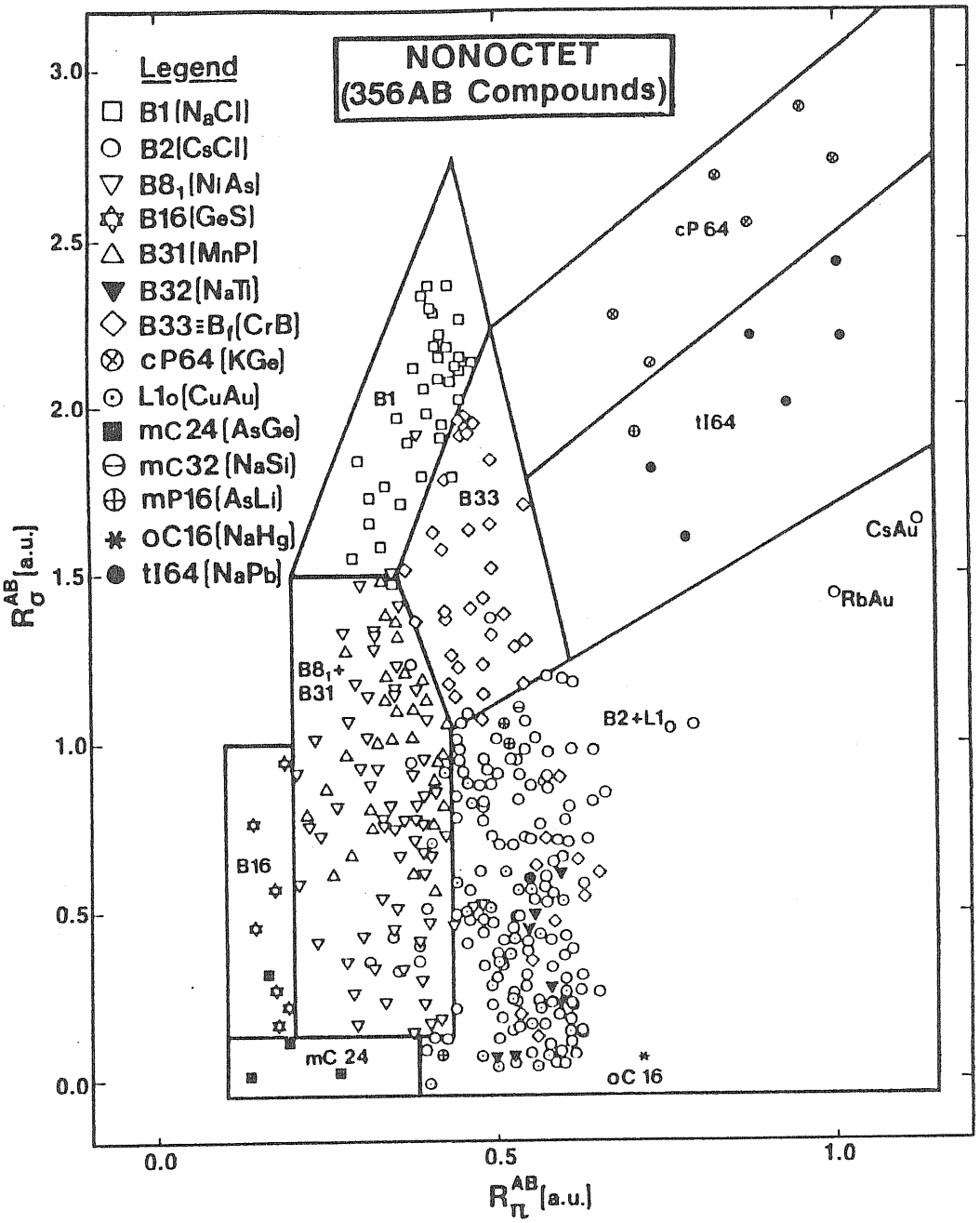

Fig. 1.3 Structural separation plot for 356 nonoctet AB compounds obtained with the s and p orbital radii as defined by Zunger, with $R_\sigma^{AB} = |(r_s^A + r_p^A) - (r_s^B + r_p^B)|$ and $R_\pi^{AB} = |r_s^A - r_p^A| + |r_s^B - r_p^B|$. (From ref. 9).

We notice that the structural indices r_l associated with electron repulsion from atomic cores are more significant than the atomic radius R associated with attractive interatomic interactions. The origin of the inadequacy of R for structural classification lies in the following relation discussed by Pauling[25]:

$$R(f) = R(1) - 0.6log(f). \tag{1.1}$$

$f < 1$ measures the fractional bond character; for an atom with v resonating valence bond electrons and with η nearest neighbors, $f = \frac{v}{\eta}$. R as defined above is not a property of each element, since it depends on η through f. In different structures with different η, each element will have a different atomic radius.

Quite sussessful structural classifications for different A_nB_m crystal phases, namely AB, AB_2 and (AB_3 + A_3B_5) compounds, have been reported by Villars[10]. At variance from previous works, he has introduced three coordinates, which are the same for $s-p$ bonded materials as for transition and rare earth metal compounds involving d and f electrons. The three orthogonal axes used in the classification of the different families of compounds are defined by : (i) the sum N of the valence electrons of the constituent atoms; (ii) the difference of the Zunger's s and p pseudopotential radii sum $\Delta = [r_s(A) + r_p(A) - r_s(B) - r_p(B)]$; and (iii) the difference of the atomic electronegativities $\chi(A) - \chi(B)$. The ionization potentials

(IPs)used in the definition of χ are obtained by taking a weighted average of the ionization potentials of all the valence electrons. One can picture the IPs as measuring the total valence (including s, p and d) electron charge transfer, and $(r_s + r_p)$ as a measure of the s and p directed valence exclusion from the core region. It is a remarkable success that the application of the Villars' scheme to more than 3000 compounds, inclusive of transition and rare earth solids, turns out to have an overall accuracy of about 97%.

A chemical scale χ has recently been proposed by Pettifor[26], which characterizes each atom in the periodic table and allows two dimensional structural separation for the individual stoichiometries AB_n ($n = 1-6, 11-13$), A_2B_n (n=3,5,17), A_3B_n (n=4,5,7), A_4B_5 and A_6B_{23} in the plane (χ_A, χ_B). These families of compounds are comprehensive of $s-p$ and $p-d$ bonded materials. The Pettifor's chemical scale is set up by ordering the elements along a single axis χ, so that the Mendeleev-type features of the periodic table are preserved. Therefore the variation of the χ coordinate within a group is requested not to overlap and mix with neighboring groups; χ is also constrained to vary linearly across the transition metal series and again across the $s-p$ elements to the right of the noble metals. The magnitude of the chemical scale is fixed by requiring it to take the Pauling electronegativity values for Beryllium to Fluorine . The separations achieved in the plane (χ_A, χ_B) for the mentioned families of compounds can be regarded as successful as the corresponding ones reported by Villars.

The eventual choice between structural classifications based upon VEOR

or the χ chemical scale is to be determined not only by statistical criteria, but also by its susceptibility to direct physical interpretation[27]. To this respect, VEOR-based QSDs seem more appealing, since the χ scale is entirely phenomenological and has no a priori significance other that it orders the elements relative to one another along a one-dimensional axis. A simple test for the different structural classification parameters can be provided by a parallel analysis of A_nB_m systems in the molecular and in the crystalline phase. Such an analysis will be presented in chapters 2 and 4 for AB_2 and AB_3 compounds, respectively.

We now turn to describe the semiempirical approaches developed in the literature to systematize and understand molecular geometries. In our brief review we will mainly concerned with AB_2 and AB_3 compounds, that we are going to treat in detail in chapters 2 and 4.

1.2 Phenomenological criteria for molecular shapes

One of the best known models proposed to account for molecular shapes dates back to Walsh[28]. The key idea of the Walsh approach is that the energy changes associated with the deformation of a molecular structure into another are determined by the energetic behavior of the highest occupied molecular orbital (HOMO) on distortion. A model for molecular structure is then constructed as follows : for a given class of AB_n compounds, two high symmetrical reference geometries are chosen and the single particle orbital

energy variations corresponding to the nuclear distortion from one shape to the other estimated in a qualitative fashion. These reference geometries are the linear ($D_{\infty h}$) and the bent (C_{2v}) configurations for AB_2 species; the planar equilateral triangle conformation (that with the highest symmetry among the possible planar shapes : D_{3h}) and the pyramidal one (C_{3v}) for AB_3 systems. For each of the two chosen geometries, an orbital correlation diagram can be traced, which relates the single particle energies of the united atoms to those of the separated atoms configurations. By combining the results of the two mappings, one can plot a diagram which shows the variation in orbital energies as functions of the molecular apex angle(θ). Such a diagram is commonly known as a Walsh diagram. General qualitative considerations on orbital hybridization and on hybrid repulsion and attraction from molecular orbital (MO) theory are needed, in order to establish the relative energy ordering of the diagram. We notice that both the energy ordering and the orbital behavior as functions of θ are assumed to be the same for any molecule of a given chemical formula. Figure 1.4 shows the Walsh diagram for AB_2 molecules, constructed from s and p atomic levels.

In the original formulation, only $s - p$ bonded materials have been considered and therefore only s-like and p-like orbitals used in building up the structural correlation diagrams. In later generalizations of the model to include transition metal compounds, d orbitals have been explicitly taken into account[5].

Let us consider the class of AB_2 compounds (fig.1.4). For molecules

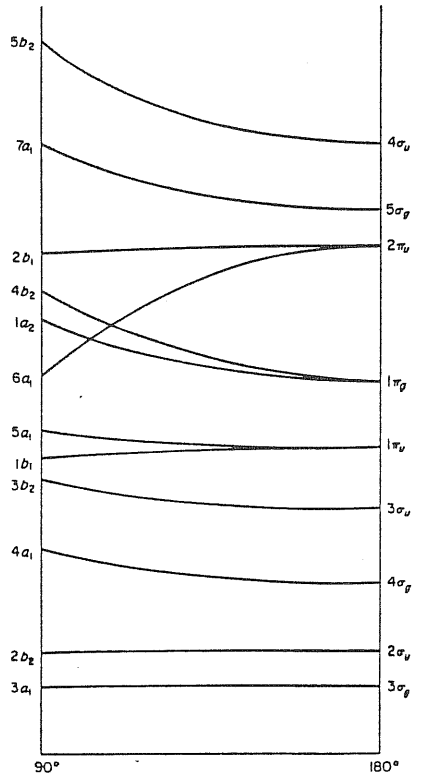

Fig. 1.4 Walsh diagrams for $s - p$ bonded AB_2 molecules. (From ref. 28)

with a number N of valence electrons less than 16 and with $N = 16$ or 22, the sum of the single particle energies is lower in the linear configuration than in the bent one, while the opposite is true for molecules with N greater than 16 and different from 22. This is valid under the condition of regular filling of orbitals. Assuming then that the total energy variation as a function of the apex angle parallels that of the eigenvalue sum, the so called Walsh rule for AB_2 molecules can be established . They are linear if $N \leq 16$ and $N = 22$; they are bent if $N > 16$ but different from 22. The result of the same assumptions and reasoning applied to AB_3 molecules leads to the following structural rules : they are planar if $N \leq 24$, while pyramidal if they contain 25 or 26 valence electrons; for $N = 28$ they are planar or nearly so.

The Walsh approach clearly indicates, in agreement with even earlier suggestions by Mulliken[29], that a crucial parameter to look at in predicting molecular shapes is the number of valence electrons (VE)in the molecule. However, as we shall discuss in detail in chapters 2 and 4, many exceptions to the Walsh rules are now known. Actually most of the AB_2 molecules with less than 16 VE are bent and several AB_3 species with less than 24 VE are pyramidal. Furthermore, planar AB_3 compounds present a large spectrum of structures other than the high symmetrical D_{3h} conformation.

Several critical analyses of the Walsh rules based on ab initio treatements of the electronic structures of molecules have been proposed in the literature[30–32]. In particular, the relationship between the total energy E of a molecular system and the sum of its single particle energy levels, $\sum \epsilon_i$, established by March[32] within the DF theory in the LD approximation, indicates both the limiting cases in which the Walsh criterion is justified and the corrections to be added to $\sum \epsilon_i$ to make it proportional to E. This relationship will be discussed in detailed in chapter 3 (section 3.3).

After the introduction of Walsh diagrams, several models for molecular structure based on a single particle picture of the molecular bond have been developed. In the model first formulated by Bartell[33] and Pearson[34] and usually known as the second order Jahn-Teller (JT) approach[5], symmetry arguments are introduced for looking at features of molecular geometry. More precisely, this model exploits symmetry rules to inquire whether the energy of a molecular system is lowered when a fixed reference shape is distorted

along a normal coordinate of a given symmetry species. If first order JT instabilities are neglected, the energy E of a molecule distorted within the coordinate S_i can be expressed in the following way, using first and second order perturbation theory:

$$\Delta E = E(S_i) - E_0 = \frac{S_i^2}{2}(f_{00} + 2\sum_{m\neq 0} f_{0m}), \tag{1.2}$$

where E_0 is the energy of the undistorted geometry, corresponding to the non degenerate ground state ψ_0, and

$$f_{00} = \int \psi_0 (\frac{\partial^2 \mathbf{H}}{\partial S_i^2}) \psi_0 d\bar{r} \tag{1.3}$$

$$f_{0m} = \int \frac{|\psi_0 (\frac{\partial \mathbf{H}}{\partial S_i}) \psi_m d\bar{r}|^2}{\Delta E_{om}} \tag{1.4}$$

$\mathbf{H}(S_i)$ is the system hamiltonian and $\Delta E_{om}(< 0)$ is the zeroth order energy separation between the states ψ_0 and ψ_m of the undistorted molecule. f_{00} can be regarded as a classical force constant representing the nuclear motion in a static electronic distribution. $\sum_{m\neq 0} f_{om}$ is instead a relaxation term, which describes the energy change associated with the electronic charge distribution as it adjusts to "follow" the nuclei. Since f_{00} is always a positive term, ΔE is positive if the integrals defining $\Sigma_{m\neq 0} f_{om}$ vanish, i.e. the energy of the system is not lowered by the distortion along S_i. If, on the other hand, these integrals do not vanish, the sign of ΔE depends upon the magnitudes of the energy gaps ΔE_{0m}. In the second order JT approach, it is assumed

that the smallest energy gap is associated with the separation between the electronic ground state ψ_0 and the first excited state ψ_1. The sum defining the relaxation force constant is then approximated by the term f_{01}. By writing ψ_o and ψ_1 as Slater determinants of single particle orbitals, the integral $\int d\bar{r}\psi_0 \frac{\partial \mathrm{H}}{\partial S_i}\psi_1$ can be reduced to the scalar product $< \phi_o|\mathrm{H}|\phi_1 >$, ϕ_o and ϕ_1 being respectively the highest occupied orbital (HOMO) and the lowest unoccupied orbital (LUMO) in a MO picture. Therefore, only the symmetry species of the transition density $\phi_0\phi_1$ need to be known and considered to establish whether f_{01} vanishes or not. An example can be useful to illustrate the application of the method.

The HOMO and LUMO symmetries for a given system are usually fixed according to the Walsh diagrams. For the molecules CY_2 and OY_2, Y indicating an atom of the group VII, the transition density is of species $\pi_u * \sigma_g = \pi_u$, as can be argued from fig.1.4. π_u is the symmetry type of the bending normal coordinate for an AB_2 linear species and hence the scalar product entering the f_{01} definition in not zero. Since the energy gap ΔE_0 here may well be small, the force constant for bending the linear geometry is expected to be negative and these molecules to be bent,in agreement with the experimental result. The influence of ligand electronegativity on the geometry is easily introduced in this approach. With reference to the previous example, increasing the electronegativity of Y relative to the central atom A lowers the Yσ atomic orbitals relative to those of A. This has the effect of lowering the entire set of σ orbitals relative to $1\pi_u$. The result is a decrease

in the energy separation ΔE_{01} between $1\pi_u$ and $2\sigma_g$, which makes bending of the molecule even more advantageous.

The behavior of the single particle energy levels ϵ_i of a molecular system can be quantified by using the angular overlap model (AOM)[5,35]. In this approach, the orbital energies are expressed according to the Hückel MO theory[36], in which all overlap integrals between different orbitals are allowed to be non zero. These integrals are represented as single products of a radial and an angular term. For AB_2 and AB_3 species, this leads to a generalization of Walsh diagrams, in which an analytic functional dependance of the ϵ_i from the apex angle θ is explicitly derived. Burdett[5] has applied this model to the main group molecules. The predictions on the molecular structures of AB_2 and AB_3 systems are substantially the same as those extracted from the second order JT model. The AOM approach allows in addition to estimate the trends in the equilibrium bond angles for several species. Moreover it can be applied to rationalize the different structural types for planar AB_3 molecules, all of them assumed to exhibit D_{3h} symmetry in the original Walsh model.

The second order JT model and the AOM approach introduce significant refinements to the Walsh model for molecular shapes. They can be easily applied to specific systems or to groups of compounds with the same chemical formula. They do not leave, however, to general structural rules for wide classes of compounds, such as all the AB_2 or AB_3 species.

Two models for molecular shapes not directly deduced from Walsh-type

ideas, but again refering to a single particle approach to the energetics of molecular systems, are the valence shell electron pair method (VSEPR)[37] and the directed valence (DV)[38] method. The basic idea of these approaches is that the most favorable packing of pairs of electrons in the valence shell of the central atom dictates the shape and also the bond angles in molecules. In the VSEPR scheme the valence electrons around the central atom are supposed to be arranged in localized pairs containing two electrons of opposite spin ; these pairs are assumed to be arranged in space such that the distances between them are maximized. The mechanism invoked to keep these pairs apart is the "Pauli repulsion force" which operates to prevent electrons of the same spin from occupying the same region of space. This force should be the expectation value of an operator, in a quantum mechanical language.

It is however difficult to formulate this operator mathematically, which makes the estimation of the relevance of the "Pauli force" not well defined. Actually, most of the objections leveled to the VSEPR model have been concerned with its lack of physical reality. In spite of this, it has been widely used in molecular geometry prediction. The geometries which give rise to the lowest energy structures according to the VSEPR rule can be determined by calculating the minimum energy arrangement of n-like charges (modeling the n electron pairs)subject to a given mutual interaction potential, constrained to move on the surface of a sphere, with the central atom and its core electrons sitting in the middle. This gives rise to the geometric arrangements of electron pairs shown in Fig. 1.5a for systems with electron pairs up to 6,

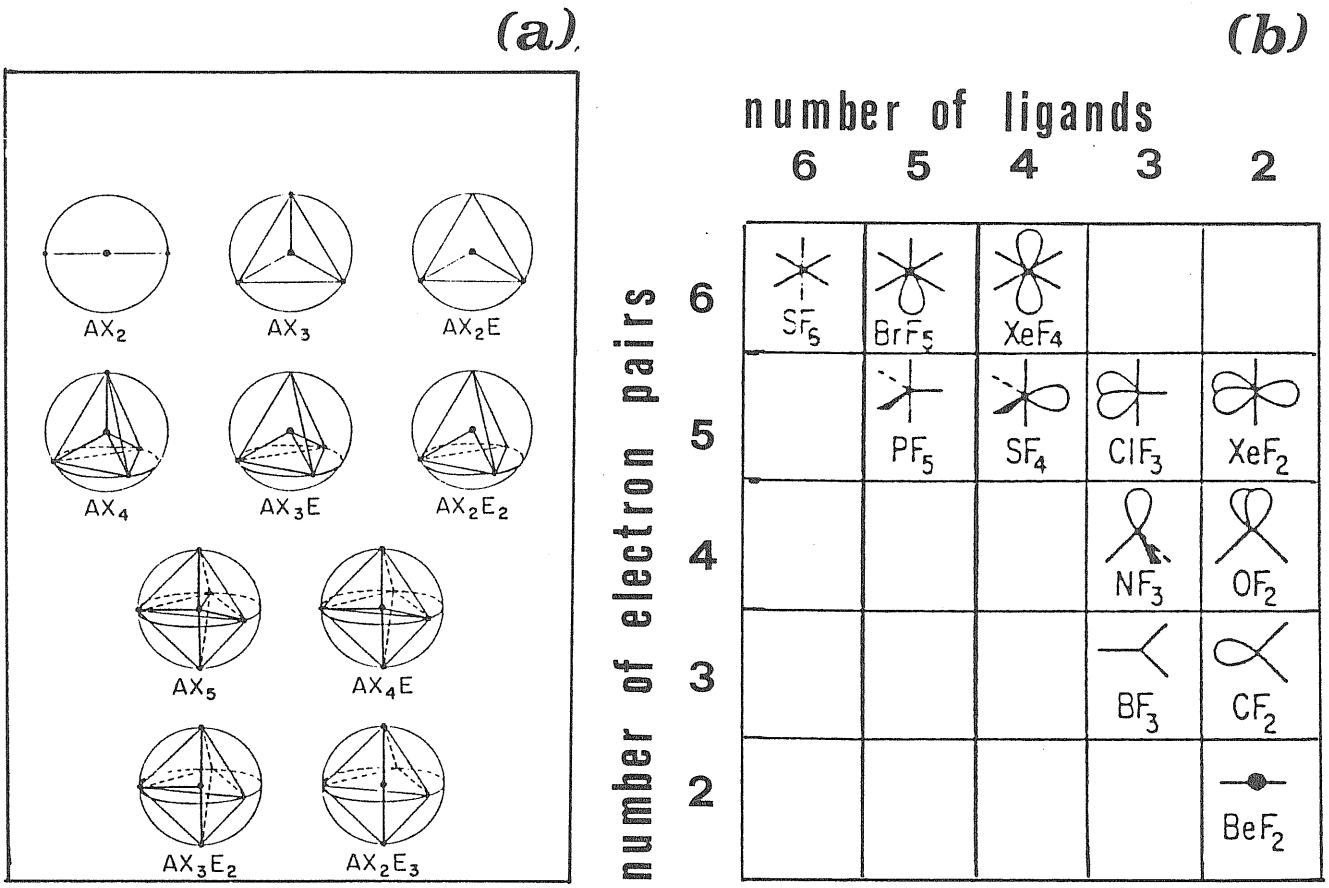

Fig. 1.5 (a) Minimum energy arrangements of n points on sphere to simulate arrangement of bonded (X) and unshared (E) electron pairs around a central atom A, according to the VSEPR model; (b) range of structures adopted by molecules governed by the VSEPR rule. (From ref. 5).

as functions of bonded (X) and unshared pairs of electrons (E).

Fig.1.5b shows the range of structures adopted by molecules governed by the VSEPR rule. In several cases, hypothesis on the chemical behavior of the system must be made in applying this rule. The central atom in the compound must be known or at least established in advance. The electrons to be included when counting the number of electron pairs around the central

Table 1.1 Spatial arrangement adopted by directional hybrid molecular orbitals, syntetized by relevant combinations of s, p and d atomic orbitals, according to the DV model. N indicates the number of hybrids. (From ref.5.)

N	Type	Spatial arrangement
2	sp	Linear
	dp	Linear
	p^2	Angular
	ds	Angular
	d^2	Angular
3	sp^2	Trigonal plane
	dp^2	Trigonal plane
	ds^2	Trigonal plane
	d^3	Trigonal plane
	dsp	Unsymmetrical plane
	p^3	Trigonal pyramid
	d^2p	Trigonal pyramid
4	sp^3	Tetrahedron
	d^3s	Tetrahedron
	dsp	Trigonal plane
	d^2p^2	Trigonal plane
	d^2sp	Distorted tetrahedron
	dp^3	Distorted tetrahedron
	d^3p	Distorted tetrahedron
	d^4	Trigonal pyramid

atom are its valence electrons plus the ligand ones involved in σ interactions with the central atom. The latter number cannot be defined a priori, but only guessed. In most cases one electron is the regarded contribution per ligand, if the ligands are counted as uncharged entities. Molecules with an odd electron (a half pair) often provide difficulties in the VSEPR classification scheme. Few examples can clarify these difficulties : NF_2 (3 and a half pair) is bent commensurate with the bent species CF_2 (3 pairs) and OF_2 (4 pairs). BH_2 is however bent (2 and a half pairs) and lies between $BeCl_2$ (2 pairs, linear) and CF_2 (3 pairs, bent). On the contrary, CH_3 is planar (3 and a halfpairs), whereas BF_3 (3 pairs) is planar and NF_3 (4 pairs) is pyramidal.

The DV[38] model differs from the VSEPR model for the physical factors invoked to control the spatial arrangements of electron pairs. In the former , the angular direction of the lowest energy hybrid orbitals of the central atom is assumed to be responsible for the spatial distribution of the electron pairs. Table 1.1 gives the angular disposition of various hybrids synthesized by relevant combinations of s, p and d orbitals. The energies of the atomic orbitals increase in this order and therefore the lowest energy hybrids will contain the largest possible amount of s and p character and the smallest amount of d. The geometries adopted by AX_2, AX_3, AX_2E, AX_4, AX_3E and AX_2E_2 species are unambigously established by the DV rule, since the bond angles are set by the hybrid orbital directions which are identical to those of the VSEPR scheme. When the number of electron pairs n is equal to or greater than 5, different kinds of hybrid orbitals are likely to be set

up in the molecule and assumptions are required to choose between them.(Usually these assumption are based on experimental data for hybrid orbital energies). As in the case of the Walsh model, the VSEPR and DV approaches fail to account for the shapes of most of AB_2 molecules with 16 or less valence electrons as well as of AB_3 moleules with $N < 24$.

Chapter 2

UNIFIED STRUCTURAL CLASSIFICATION OF AB_2 MOLECULES AND SOLIDS

As is clear from the brief review given in the previous chapter, semiempirical approaches to molecules and solids have so far been developed on different footings. Burdett[39] has extended ideas from molecular orbital theory to structural problems of solids. The models developed are simple and useful in understanding the basic features of several structural problems such as, e.g., pressure and temperature induced structural transformations. However, a general classification scheme for crystal structures paralleling that for molecular shapes has not been extracted so far from these models.

We have instead found that successful classifications of the structural properties of given classes of compounds in both the molecular and the solid phase can be achieved through the use of Quantum Structural Diagrams (QSD). Plots based on valence electron orbital radii (VEOR) have been applied to $s-p$ bonded AB_2 and AB_3 solids and to small aggregates of the same composition[13,14]. In principle, in fact, provided the frozen core approximation is valid in both phases, VEOR should be good parameters in both cases. We have also tested whether the same linear combinations of s

and p radii are adequate to describe the bond in both phases, i.e.,whether VEOR based structural parameters are transferable.

In section 2.1 of this chapter we discuss some properties of the VEOR and define the coordinates used in our diagrams. These will be reported in section 2.3 (molecules and solids with 16 valence electrons) and 2.4 (molecules and solids with less than 16 valence electrons). In section 2.2 we briefly illustrate the experimental situation for triatomic molecules and clusters.

2.1 VEOR based structural coordinates

Quantum structural parameters for the classification of AB_2 and AB_3 systems have been derived from either the pseudopotential radii r_l of Zunger and Cohen[9] (ZC) or from the nodal radii[24,40] N_l (l=0,1).

r_l is defined to be the turning point of the screened l-dependent pseudopotential V_l, derived from atomic calculations performed in the local density (LD) approximation of Density functional theory[2]. The all electron (AE) and pseudopotential single-particle equations for atoms are:

$$\{-\frac{\nabla^2}{2}-\frac{(Z_c+Z_v)}{r}+\frac{l(l+1)}{2r^2}+v_{xc}[\rho_c+\rho_v]+v_{ee}[\rho_c+\rho_v]\}\psi_{nl}(r)=\epsilon_{nl}\psi_{nl}(r) \tag{2.1}$$

and

$$\{-\frac{\nabla^2}{2}-\frac{Z_v}{r}+v_{ps}^{(l)}(r)+\frac{l(l+1)}{2r^2}+v_{ee}[n]+v_{xc}[n]\}\chi_{nl}(r)=\lambda_{nl}\chi_{nl}(r) \tag{2.2}$$

respectively. v_{ee} and v_{xc} denote the density functional Couloumb and exchange potentials. ρ_c and ρ_v are the core and valence charge densities, while $n = \sum_j \chi_j^*(r)\chi_j(r)$ is the valence pseudo charge density. Z_c and Z_v are the core and valence charges. The atomic pseudopotentials $v_{ps}^{(l)}(r)$ are derived in the following way. First physically desirable pseudowavefunctions χ_{nl} are constructed and then equation (2.2) is solved for that pseudopotential $v_{ps}^{(l)}$ which will reproduce these wavefunctions, together with the theoretically correct orbital energies $\lambda_{nl} = \epsilon_{nl}$. χ_{nl} is written as linear combination of the true AE core and valence orbitals of equation (2.1):

$$\chi_{nl} = \sum_m C_{n,m}^{(l)} \psi_{m,l}^{c,v}(r) \tag{2.3}$$

The coefficients $C_{n,m}^{(l)}$ are chosen to satisfy the following conditions for the pseudowavefunction : i) χ_{nl} must be nodeless for each of the lowest angular symmetries and normalized; and ii) such that the spatial range out of the atomic core where it coincides with the true wavefunction ψ_{nl}^v is maximized, and its amplitude and lowest derivatives in the core region are minimized. Conditions ii) are imposed to minimize the energy and quantum state dependance of $v_{ps}^{(l)}$, i.e., to construct a pseudopotential whose dependance on the chemical environment be minimal and thus have desirable transferability properties. As a consequence of the chemically motivated constraints on the pseudowavefunction, $v_{ps}^{(l)}$ turns out to be a hard-core-type

pseudopotential with a characteristic crossing point at $r = r_l^0 (v_{ps}^{(l)}(r_l^0) = 0)$, for each angular momentum.

The pseudopotential radii r_l are defined as the crossing points of the ground state screened effective pseudopotential $v_{eff}^{(l)}(r)$:

$$v_{eff}^{(l)}(r_l) = 0 \tag{2.4}$$

where

$$v_{eff}^{(l)}(r) = v_{ps}^{(l)}(r) + \frac{l(l+1)}{r^2} + v_{ee}[n] + v_{xc}[n] \tag{2.5}$$

Two main reasons dictate the definition of the structural indices through $v_{eff}^{(l)}$ and not through $v_{ps}^{(l)}$. The screened and bare pseudopotentials can both be expressed as the sum of two terms:

$$v_{eff}^{(l)}(r) = U_l(r) + g(Z, \rho_c + \rho_v) \tag{2.6a}$$

$$v_{ps}^{(l)}(r) = U_l(r) + f(Z_c, Z_v, \rho_c, \rho_v, n) \tag{2.6b}$$

$U_l(r)$ is the only non-local (i.e., angular dependent) part of the pseudopotential; in a sense it replaces the core-valence orthogonality constraint of the AE approach. While f depends on $n(r)$, which in turn depends on all orbitals that are assigned as valence states, g does not. Therefore the screened pseudopotential, contrary to the bare one, is invariant under a change in the

assignement of the valence electrons. Furthermore, the definition of the orbital radii from $v_{eff}^{(l)}(r)$ permits a direct inclusion of electronic exchange and correlation effects in the structural indices r_l. Table 2.1 lists the ZC radii r_s and r_p for the non transition elements of the periodic table.

The nodal radii N_l are defined to be the outermost nodes of the AE atomic valence orbitals of angular momentum l. They express the same "physical effect" as the pseudopotential radii r_l do : they measure the core orthogonalization hole in a straightforward way. It has been shown[24] that the N_l do not change as the atomic ionization and excitation state varies and that they are independent, to a large extent, from the way of solving the atomic single particle Schroedinger equation (three different approximation have been tested[24]: local density, Hartree-Fock, Hartree-Fock-Slater). The $N_l(l = 0, 1)$ radii for non transition elements are reported in Table 2.2.

Both sets r_l and N_l can be used to construct system invariant energy scales[9,24]. Figure 2.1 displays the multiplet- average experimental ionization energies E_l for some atoms, plotted against the reciprocal orbital radius r_l^{-1}. For each group of elements two lines are shown: E_s versus r_s^{-1} and E_p versus r_p^{-1}. The theoretical r_l^{-1} are seen to give an accurate measure of the experimental orbital energies and hence can be employed as an elementary orbital-dependent energy scale. The same results are recovered when the nodal radii are used.

We are now going to define the Cartesian coordinates which will be used in QSDs for molecules and solids. In the ZC pseudopotential approach, each

Table 2.1 s and p Zunger-Cohen pseudopotential radii for 36 non transition elements of the periodic table. (From ref. 9).

Atom	r_s	r_p
Li	0.985	0.625
Be	0.640	0.440
B	0.480	0.315
C	0.390	0.250
N	0.330	0.210
O	0.285	0.180
F	0.250	0.155
Ne	0.220	0.140
Na	1.100	1.550
Mg	0.900	1.130
Al	0.770	0.905
Si	0.680	0.740
P	0.600	0.640
S	0.540	0.560
Cl	0.500	0.510
Ar	0.460	0.460
K	1.540	2.150
Ca	1.320	1.680
Cu	0.880	1.160
Zn	0.820	1.060
Ga	0.760	0.935
Ge	0.720	0.840
As	0.670	0.745
Se	0.615	0.670
Br	0.580	0.620
Kr	0.560	0.600
Rb	1.670	2.430
Sr	1.420	1.790
Ag	1.045	1.330
Cd	0.985	1.230
In	0.940	1.110
Sn	0.880	1.000
Sb	0.830	0.935
Te	0.790	0.880
I	0.755	0.830
Xe	0.750	0.810
Cs	1.710	2.600
Ba	1.515	1.887

Table 2.2 s and p Nodal radii for 36 non transition elements of the periodic table. (From ref. 24)

Atom	r_s	r_p
Li	0.832	0.000
Be	0.590	0.000
B	0.458	0.000
C	0.375	0.000
N	0.318	0.000
O	0.276	0.000
F	0.244	0.000
Ne	0.218	0.000
Na	1.035	1.113
Mg	0.899	0.941
Al	0.797	0.822
Si	0.717	0.720
P	0.653	0.643
S	0.600	0.582
Cl	0.555	0.531
Ar	0.516	0.488
K	1.614	1.898
Ca	1.441	1.617
Cu	0.899	1.000
Zn	0.854	0.931
Ga	0.821	0.883
Ge	0.782	0.832
As	0.746	0.787
Se	0.714	0.746
Br	0.683	0.710
Kr	0.656	0.677
Rb	1.861	2.239
Sr	1.700	1.959
Ag	1.163	1.296
Cd	1.113	1.229
In	1.067	1.169
Sn	1.026	1.113
Sb	0.988	1.064
Te	0.953	1.019
I	0.920	0.979
Xe	0.890	0.941
Cs	2.252	1.057
Ba	2.076	2.373

element E of the periodic table is characterized by two structural parameters:

$$R_\sigma^E = r_s + r_p \tag{2.7}$$
$$R_\pi^E = |r_s - r_p|$$

From them, two sets of coordinates can be constructed : (i) the "compounds coordinates" , which for a binary compound AB are defined by[9]

$$Y_{ZC} = |R_\sigma^A - R_\sigma^B| \tag{2.8}$$
$$X_{ZC} = R_\pi^A + R_\pi^B$$

and (ii) the "elemental coordinates" :

$$R_\sigma^A \tag{2.9}$$
$$R_\pi^B$$

In the nodal radii scheme, the two structural parameters defined for each element are[11]

$$y_E = \frac{(N_s^E + wN_p^E)}{(w+1)} \qquad (2.10)$$
$$x_E = \frac{(wN_s^E - N_p^E)}{(w+1)}$$

of which y_E can be used as "elemental coordinate". y_E is defined by requiring the weighting factor w to be proportional to the atomic state degeneracy[8]. This fixes $w = 3$. The orthogonality constraint then imposed on the couple of parameters (y_E, x_E) specifies the linear combination expressing x_E. The compound coordinates which will be used for AB_2 and AB_3 compounds are

$$Y = y_B - y_A \qquad (2.11)$$
$$X = \alpha x_A + x_B$$

The choice of the constant $\alpha(1 or 2)$ will be commented further on, while discussing the sorting of QSD for these systems.

In Figure 2.2 we compare the elemental coordinates of the nodal and pseudopotential radii scheme for 36 non transition elements. A good correlation exists between the two sets of values, but the first row atoms have a type of functional relation different from that of the others. This naturally comes from the fact that for first row atoms $N_p = 0$, in contrast to r_p. Some discrepancies betwee the ZC and nodal radii approaches can be expected, in the classification of compounds of these elements.

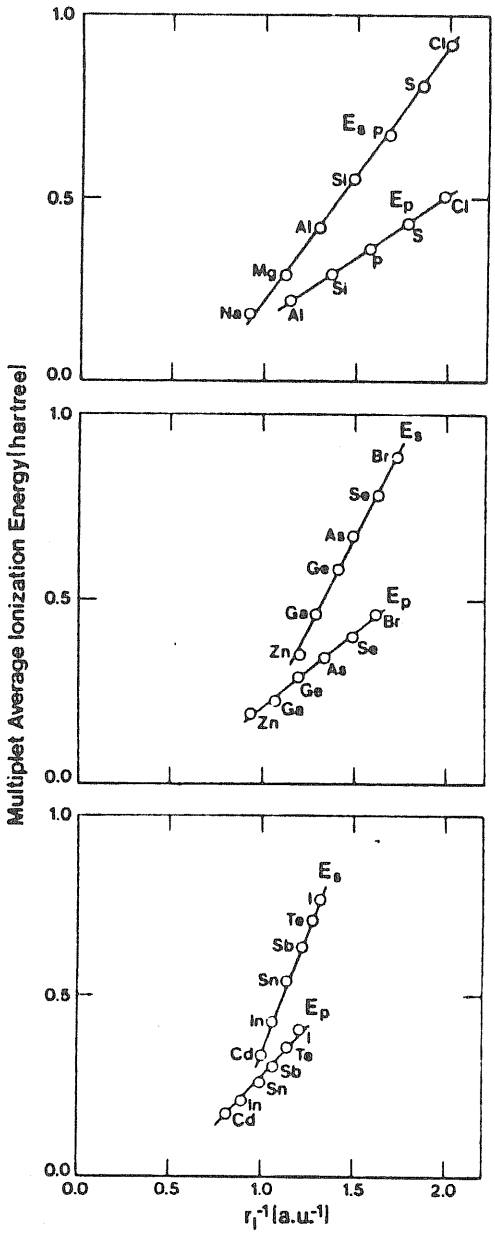

Fig. 2.1 Correlation between the observed $l-th$ orbital multiplet-averaged ionization energies E_l and the reciprocl pseudopotential radius r_l^{-1} (see Table 2.1) for some elements of the periodic table. (From ref. 9)

Phillips[41] has proposed an interpretation of the structural parameters derived from VEOR, in which R_σ^E (or y^E) corresponds to $s-p\sigma$ hybrids on atom E, while R_π^E (or x^E) corresponds to p^2-sp hybrids, i.e., measures the residual strenght of π bonding after subtraction of the more stable σ interactions. A physical interpretation of the coordinates Y_{ZC} and X_{ZC} (and correspondingly of Y and X) can be given in term of bond charges[42].

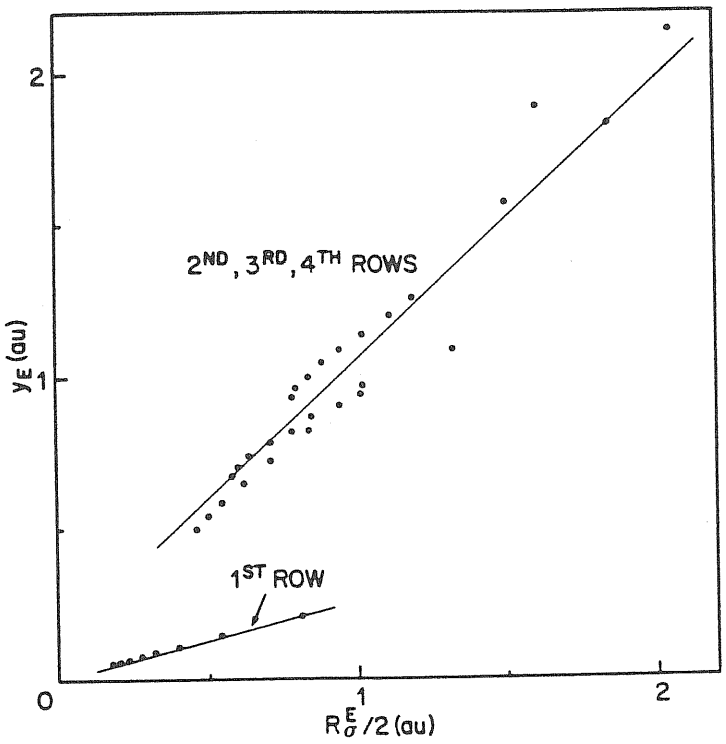

Fig.2.2 Comparison of elemental coordinates in the pseudopotential ($R^E_\sigma/2$) and nodal (y_E) radii schemes.

The fact that the sets (Y_{ZC}, X_{ZC}) and (Y, X) were found to be powerful structural coordinates for AB compounds has suggested that the bond charge may be decomposed into σ and π components. Then the sign in equations (2.8) and (2.11) suggests that the π charge is shared (+ sign), while the σ bond charges are transferred. This leads to think of Y_{ZC} and Y as a measure, in a loose sense, of the bond ionicity and to X_{ZC}^{-1} and X^{-1} as the expression of covalent effects in the bond.

2.2 AB_2 compounds

While crystal structures are known for many solids and very accurately for most of them[43,44], the experimental situation for molecules and clusters is not so well established. AB_2 molecules have been investigated with several techniques and in many cases it is clear whether a given species is linear or bent. The electric deflection of mass-spectrometrically detected molecular beams can be used to study the molecular geometry of high temperature species, by determining whether they possess a permanent dipole moment or not[45]. This technique can therefore clearly distinguish between bent species, carrying a permanent dipole moment, and linear ones, which are non polar. Infrared (IR) and Raman (R) spectroscopy are widely used methods to investigate molecular structures[46]. The pattern resulting from either infrared absorption or non-polarized Raman scattering distinguishes between linear symmetric AB_2 molecules (two IR and one R lines) and linear asymmetric or bent ones (three IR and three R lines). Further analysis of these data (e.g. through the comparison of different spectra obtained from the same compound with different isotopes as central atoms) and consistency with other experiments help to identify the bent geometry. Polarized Raman scattering, if available, would actually define a clear cut between linear (one line, independent of symmetry) and bent (two lines) species. Most of the IR and R experiments refer to molecules embebbed in matrices. This is always the case for electron spin resonance (ESR) experiments which also constitute

a rather accurate structural probe[47]. In general, electron diffraction on vapors gives only rough estimates for both bond lengths and bond angles in molecules. The values of the apex angle of bent molecules have been estimated rather rarely, mostly through the analysis of infrared spectra. This analysis is usually based on a normal coordinate treatement of the measured vibrational frequencies and can yield the bond angle within an accuracy not higher than ± 5 degrees.

As we have already mentioned, we have classified AB_2 molecular shapes and crystal structures according to the same VEOR based structural coordinates. Both the compound and the elemental coordinate schemes presented in the previous section have been used. The first result of our QSDs is that the number N of total valence electrons in the compound is a relevant parameter, in the sense that compounds with $N < 16$ cannot be placed on the same map as those with $N = 16$, although one can use the same structural parameters. This is true in both the nodal and pseudopotential radii approaches and for different choices of the structural Cartesian coordinates.Therefore, in the following, we shall treat these two classes of compounds separately. The importance of N in molecular structure classification is in agreement with the Walsh criterion[28]. Its relevance also for solids is not surprising, especially in view of the remarkable success of the structural classifications by Villars[10], based on three dimensional plots in which N represents one (and a crucial) coordinate. We have found that at least in the case of molecules, it is sufficient to divide $N = 16$ from $N < 16$

(and indeed necessary, since further subdivision of the systems with $N < 16$ in different structural plots for different values of N would drastically reduce the statistical meaning of each plot). We have not considered trimers with $N > 16$, since, in full agreement with the Walsh criterion, all of them are bent apart from the dihalides of rare gases[48]. In classifying AB_2 molecules, we have labeled as 'supposed' all the geometries which were only guessed from incomplete experimental data. Amongst theoretical approaches, we have considered as reliable only advanced configuration-interaction (CI) calculations. Only rare calculations exist in the LDA which, however, confirm pre-existing CI determinations. The results of Hartree-Fock calculations are not regarded as definitive but rather as proposals for a given structure (and therefore marked with empty symbols in our QSDs).

2.3 Molecules and Solids with 16 valence electrons

AB_2 molecules with 16 valence electrons have been classified within the same schemes proposed by Andreoni[11] and Burdett *et.al.*[12] for double octet (DO) solids. Before examining the sorting out of our plots for the molecular phase, we describe in some detail the results which have been obtained for crystal structures.

2.3.1 AB_2 solids with $N = 16$

DO AB_2 solids of non-transition elements[43,44,49] contain oxides and other chalcogenides of tetravalent ions (e.g. Si) and halides of divalent ions

(e.g. Ca). Moreover, for A=Pb or Sn, there exist materials with A acting either as divalent (B = F,Cl,Br,I) or as tetravalent (B = O,S,Se). Ditellurides, as well as CS_2, CSe_2 and $PbSe_2$ are not stable. DOs adopt a variety of structures which can be systematized according to different criteria, i.e. the coordination number (CN, fron 2 to 9), the type of atomic grouping which can be either packed (3 d) or layered (2 d) or formed by weakly bound molecular units (CO_2). Moreover, a number of them, e.g. SiO_2, form good glasses. A good structural map must show all these distinctive features.

In Figure 2.3 we reproduce the structural plot obtained by Andreoni[11] for solids with 16 valence electrons, with compound coordinates based on nodal radii. The coordinate X is defined by taking $\alpha = 1$ in equation (2.11). We notice that the quality of the structural separation we are going to discuss would be unchanged if $X(\alpha = 1)$ be replaced by $X(\alpha = 2)$.

Fist of all, a net distinction between "3d" and "2d" structures can be recognized in Fig. 2.3. The border is marked by Zn (Cl_2,Br_2) which in fact are found in both layer and non-layer configurations. Amongst the four different phases of $ZnCl_2$, three adopt three dimensional structures with CN=4 and one has the "2d" tetragonal (red) HgI_2-structure, with CN=6. $ZnBr_2$ crystallizes in three forms, i.e. one with a "3d" tetragonal structure with CN=4 (tetrag. $ZnBr_2$) and two with true layer structures, both with CN=6. ZnI_2, which is also close to the border "2d"/"3d", adopts essentially layer structures but is also found in the tetragonal $ZnBr_2$ configuration. It is significant that Zn-dihalides (B = Cl,Br,I) are located at the border

between CN=4 and CN=6. Within the "2d" domain, the $CdCl_2$ and CdI_2 configurations differ in the close- packing of the anions, which is cubic in the former and hexagonal in the latter. The difference is subtle and a few compounds crystallize in both structures depending on the growth mechanism. A net separation is not found in Figure 2.3.

Especially interesting information comes from the location of glass-forming materials, e.g. GeS_2, $GeSe_2$, SiO_2, SiS_2, BeF_2 and $ZnCl_2$, which lie between the molecular regime (represented only by CO_2 in the plot) and the layered materials. This is consistent with Phillips' view of glasses[50], as formed by covalent clusters which interact via strong van-der-Waals forces.

The coordination number increases with increasing $|Y|$ and/or increasing X. This is consistent with the interpretation of Y as bond ionicity and of $\frac{1}{X}$ as directionality of the bond. Separation between structures with different CN's is very well represented in Fig.2.3 ; the unique arrangements adopted by $SrBr_2$ and SrI_2, and the $PbCl_2$-configuration, for which only average CN's can be defined, also emerge quite clearly in the plot. The more complex CN=6 domain is well separated into structures with sheets (2d) and close-packing (3d) of the anions.

The only compounds which are somewhat misplaced in Fig .2.3 are mercury dihalides, with the exception of the difluoride found at the correct position. In fact, $HgCl_2$ has a unique structure which is layered (as the map indicates) but it is classified with CN=2, while found in the CN=6 domain. $HgBr_2$ possesses an unusual structure which is orthorombic and

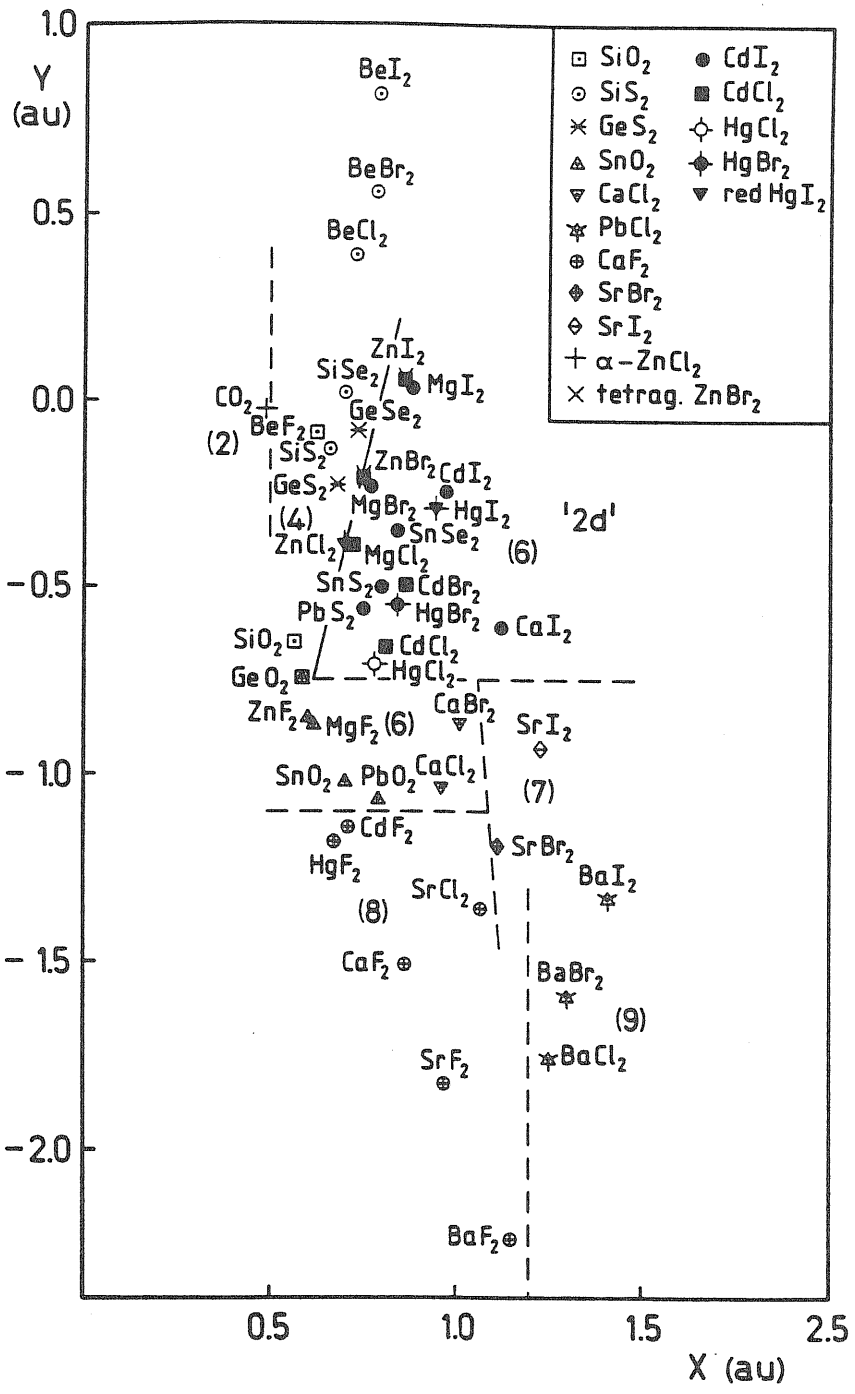

Fig. 2.3 Structural plot for AB_2 double-octet solids. (From ref. 11)

layer-like, but the first coordination can be considered as a strongly distorted octahedron. Thus its occurence in the 6-fold and layer domain of the plot is still meaningful. HgI_2 adopts the $HgBr_2$ structure at high temperatures, but is otherwise found in a special layered configuration (red-HgI_2) with CN=4. The reason for the misplacement of mercury compounds is not obvious. However, one can reasonably expect that the basic approximation involved in the use of nodal (as well as pseudopotential) radii (i.e. the frozen core approximation) loses validity for heavy and highly polarizable ions like Hg. Also the assumption that only s and p states partecipate in the bond is probably not well founded. It is not possible to classify in the same plot (Fig. 2.3) both the (oxides, chalcogenides) and the dihalides of multivalent cations like Pb and Sn. The reason for this is in the type of bonding of these materials. In the halides, Pb and Sn ($Sn(F_2,Cl_2)$) behave as divalent ions and the s-states are not involved directly in the bond, while in oxides and chalcogenides they behave as tetravalent ions. In a steric picture with ionic radii, one would consider different cation radii for the two states of ionization and for different CN[25,38,51].

It has been shown in ref.(11) that also structural transformations of DO AB_2 compounds driven under pressure or by heating can be analyzed according to Fig. 2.3, in remarkable consistency with experiment. This is a stringent criterion for the validity of the (Y, X) structural plot.

The ZC compound coordinates Y_{ZC} and X_{ZC}, which have been used with great success for AB compounds, do not seem to work for AB_2 crystals.

Burdett *et. al.*[12] have shown that an elemental coordinate scheme in which $X = R_\sigma(A)$ and $Y = R_\sigma(B)$ can instead be used to achieve a good structural separation of DO AB_2 structures. The difficulties found in the nodal radii scheme previously discussed are also present in Burdett et.al.'s scheme, i.e. Hg-dihalides are misplaced and Pb/Sn dihalides cannot be included in their plot. We notice that nodal radii based elemental coordinates produce a sorting very much similar to that obtained using the corresponding ZC structural parameters.

2.3.2 AB_2 molecules with $N = 16$

In searching for parallelism between solids and molecules, we have applied the compound and elemental coordinate schemes to $s-p$ bonded AB_2 molecules with 16 valence electrons[13]. These are the dihalides of elements belonging to the groups IIA and IIB, the oxides of group IV, the diselenide and sulfide of carbon, the diselenide of tin and the dinitrogen-oxide and sulfide.

In a QSD with compound coordinates, the linear and bent geometries[52] can be distinguished perfectly and in a very simple way, in either the pseudopotential or the nodal radii based schemes. The simple coordinate Y_{ZC} sufficies to discriminate between bent and linear molecules, since all molecules with $Y_{ZC} < 2.1$ are linear, with the only exception of BaI_2 which is bent but has $Y_{ZC} = 1.82$. The (Y, X) plot leads again to a simple result : all DO AB_2 molecules with $Y < Y_c = -1.25$ are found to be bent, the

value of X being immaterial. The individual y_E, in analogy with R_σ^E, gives a measure of the average core size and increasingly negative values of Y and Y_{ZC} correspond to increasing ionicity. This can e.g. be seen from the ordering of the various halides of each metal in Fig. 2.3. Bent species correspond to an ionic type of bond (all the fluorides of alkaline earth elements) and to highly polarizable cations (all the halogenides of Ba). These properties seem to be somewhat "condensed" in either Y_{ZC} or Y and in the solid phase, as previously mentioned, give rise to the compounds with the highest CN (8 or 9). In particular, these are the fluorites which attain a fast-ion conducting state at high temperature, or crystal with the $PbCl_2$ structure, which transform to the fluorite modification at high temperature. Although the Y coordinate alone can distinguish between bent and linear molecules, it is significant that the most covalent species such as CO_2 have large values of $\frac{1}{X}$, while the most ionic ones have small values of $\frac{1}{X}$.

The structural parameter Y has been found to be related to the measured bond angles θ_{eq} of bent species in a simple way : the square of the angular deviation from planarity, $(\theta - \pi)^2$ varies linearly with Y. A plot of $(\Delta\theta_{eq})^2 = (\theta - \pi)^2$ versus Y is shown in Fig.2.4.

Although the values reported in the literature[52] for θ are derived from approximate tratements of the measured vibrational frequencies and are known at best within 10 degrees, this result has suggested a double-well form for the binding energy curve of these compounds of the type :

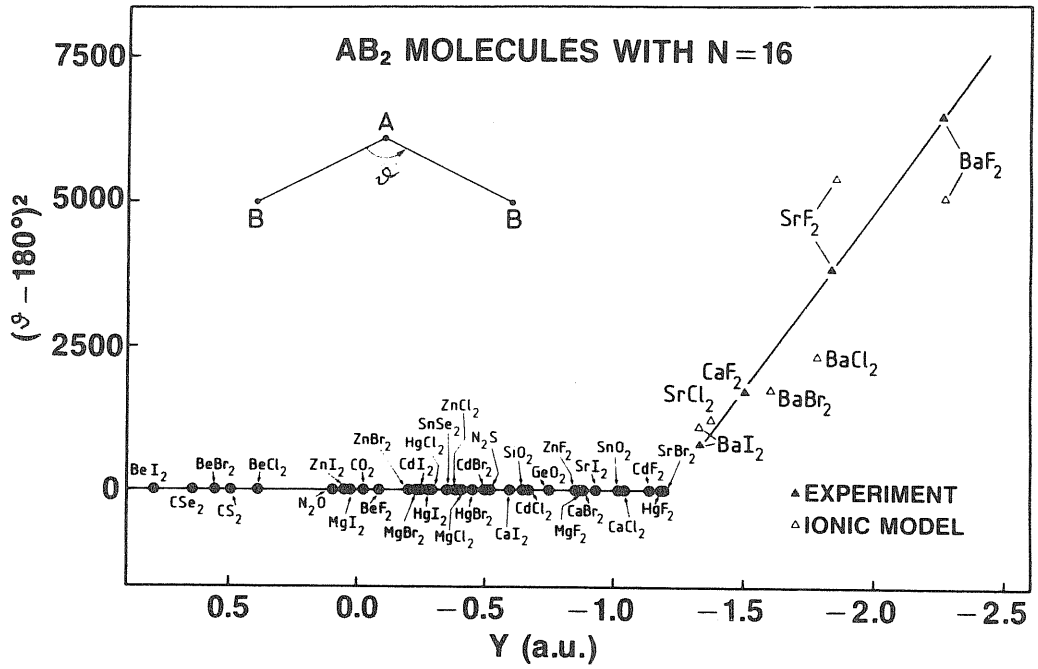

Fig. 2.4 Correlation between apex angle θ and the the nodal radii based coordinate Y for double-octet AB_2 molecules. The measured values for θ are from ref. 52; the results of an ionic model are from ref.56.

$$E = E_\pi + a(Y - Y_c)(\theta - \pi)^2 + b(\theta - \pi)^4, \qquad (2.12)$$

whose equilibrium solutions are :

$$\theta = \pi \qquad |Y| < |Y_c|$$

$$\theta = \pi - (\tfrac{a}{2b}^{(\frac{1}{2})}(Y - Y_c) \qquad |Y| < |Y_c|$$

The form for the binding energy proposed in equation (2.12) will be accurately investigated in the next chapter, where the structural transition from linear to bent in the class of DO AB_2 molecules will be studied in a

fully theoretical framework. We note here already that eq. (2.12) should not be taken to apply in the immediate neighborhood of Y_c.

A successful classification of DO AB_2 molecules can also be achieved using elemental coordinate schemes. If the coordinates initially proposed by Burdett[12] *et.al.* for solids, $(R_\sigma^A, R\sigma^B)$, are used, a dividing line $R\sigma^A = 0.41R\sigma^B + 2.74$ is found, which completely separates bent molecules (above) from linear molecules (below). Actually, it is interesting to note that a similar plot based on Pauling's ionic radii[38] for the two elements A and B works almost as well and fails only for mercury dihalides.

We notice that only seven DO molecules out of 42 are bent. All but one of the phenomenological criteria discussed in chapter 1 fail in predicting a right shape for the seven bent alkaline-earth dihalides species. The second order JT effect method is the only one which roughly accounts for their geometries if the electronegativity of the ligands A-B is explicitly taken into account in its application.

2.4 Molecules and Solids with less than 16 valence electrons

2.4.1 AB_2 molecules and A_3 clusters with $N < 16$

First of all, we notice that most known molecules with $N < 16$ are bent[53,54], in full disagreement with the Walsh rule which predicts them all to be linear. Sub-DO species present a broad spectrum of apex angles and their classification requires a full bidimensional plot. The available information

is not sufficient to construct statistically meaningful separate plots for the various values of N.

Fig. 2.5 and 2.6 show the structural maps for these compounds obtained with nodal radii-based coordinates. Both diasgrams nicely discriminate between linear and bent molecules, the only exceptions being empty symbols (labelling compounds whose structure is not known but only guessed by incomplete experimental data or Hartree-Fock calculations). The elemental and the compound coordinate scheme are essentially equivalent for the heteronuclear species, while clusters are better included when described with y_E. Here, X is defined to be $(2x_A + x_B)$. This coordinate is much superior to $X = x_A + x_B$, which would not discriminate between, say, LiO_2 and Li_2O which have different structures. This indicates the relative importance of the central atom, in agreement with several phenomenological approaches to molecular geometry presented in chapter 1 (see,e.g the VSEPR and the DV rules).

Although rather little is known about the values of the bond angle in these bent AB_2 molecules, a clear trend emerges in both plot for the apex angle of bent species to increase from the bottom right to the top left. This would correspond, in an ionic picture, to a shift from $A^+(B_2)^-$ (small angles) to $(B^+)_2A^{2-}$ (large angles). However, our structural parameters cannot be expected to account for Jahn-Teller effects in the A_3 clusters, since the three atoms are necessarily treated as equivalent. Therefore, the cluster-line in the bent region must be viewed as representing a bond angle of 60 degrees.

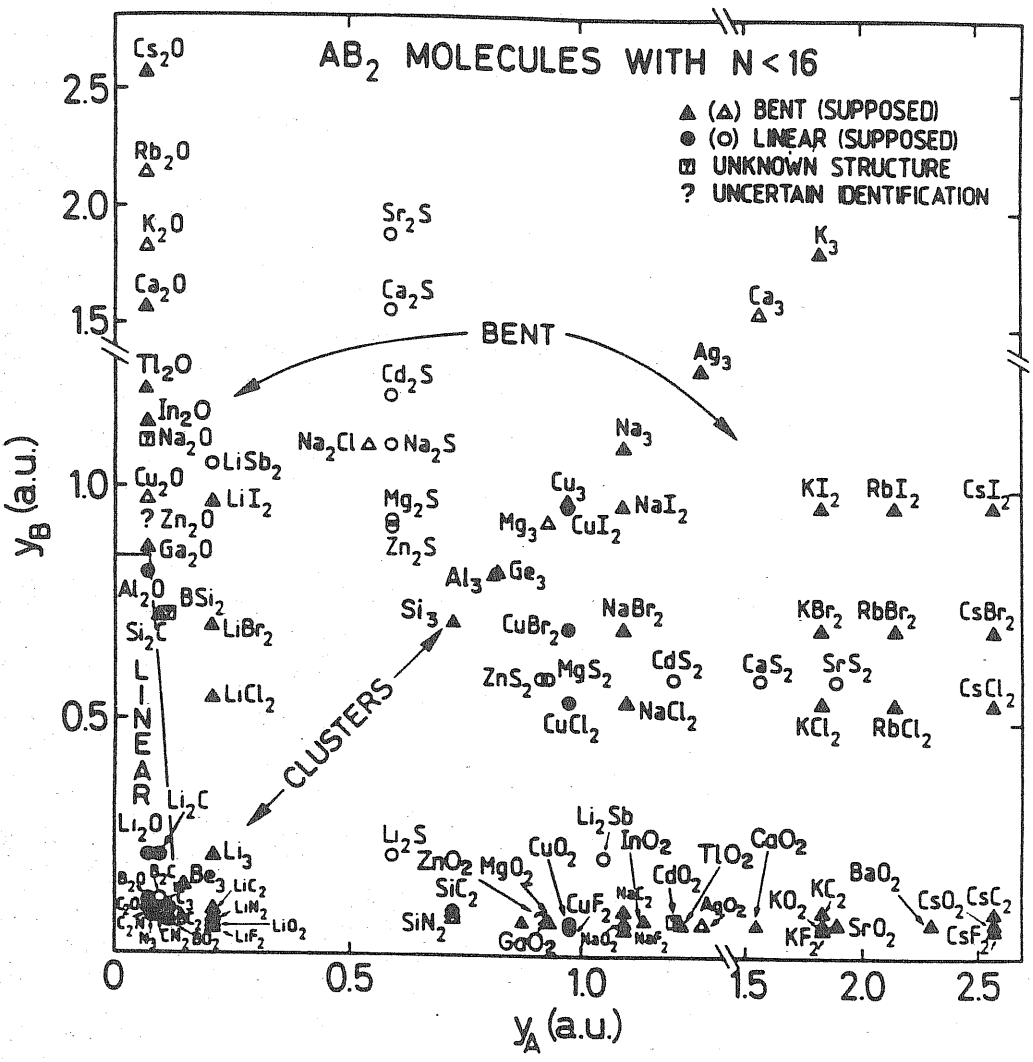

Fig. 2.5 Elemental coordinate plot for AB_2 molecules and A_3 clusters with $N < 16$. The structural information used for these compounds are from references 53 and 54.

According to estimates from experimental data[53], the dioxides of Li, Mg, Ca, Ba and Ga (below the cluster line) have bond angles between 30 and 50 degrees, while the suboxides of K, Rb, In, Tl (above the cluster line) all have apex angles larger than 140 degrees. As apparent from Figures 2.5 and

2.6, Y no longer correlates with an ionicity scale and X is crucial. Again, as found for DO AB_2 molecules, the most covalent species lie at small values of X.

The ZC elemental coordinates are essentially equivalent to the nodal-radii ones, insofar as the final molecular classification is concerned. Also, copper dihalides are misplaced in both cases, which could be a manifestation of d character in the bonding.

We have also examined the usefulness of the chemical scale χ proposed by Pettifor[26] (see chapter 1). For the DO molecules, we again find a critical line $\chi_A = 0.52\chi_B - 0.83$ which nicely discriminates between bent (below) and linear (above) species. When applied to the molecules with $N < 16$, however, Pettifor's scheme fails for Li_2O, Li_2C and Al_2O and again for Cu-dihalides. The difficulty we find with Pettifor's coordinates for the first row elements is also apparent in his structural plot for the DO AB_2 solids where Cd_2, HgF_2 and Be-dihalides are misplaced. We notice that if we modify the ordering of the first-row elements in Pettifor's chemical scale in such a way to have a good agreement for the AB_2 compounds, the octet AB compounds are no longer correctly classified in the structural map of AB solids.

2.4.2 AB_2 solids with $N < 16$.

In the case of solid AB_2 compound with $N < 16$, we have considered both di-and mono-oxides as well as chalcogenides of di- and mono-valent cations, which also are known in the molecular phase, plus other compounds

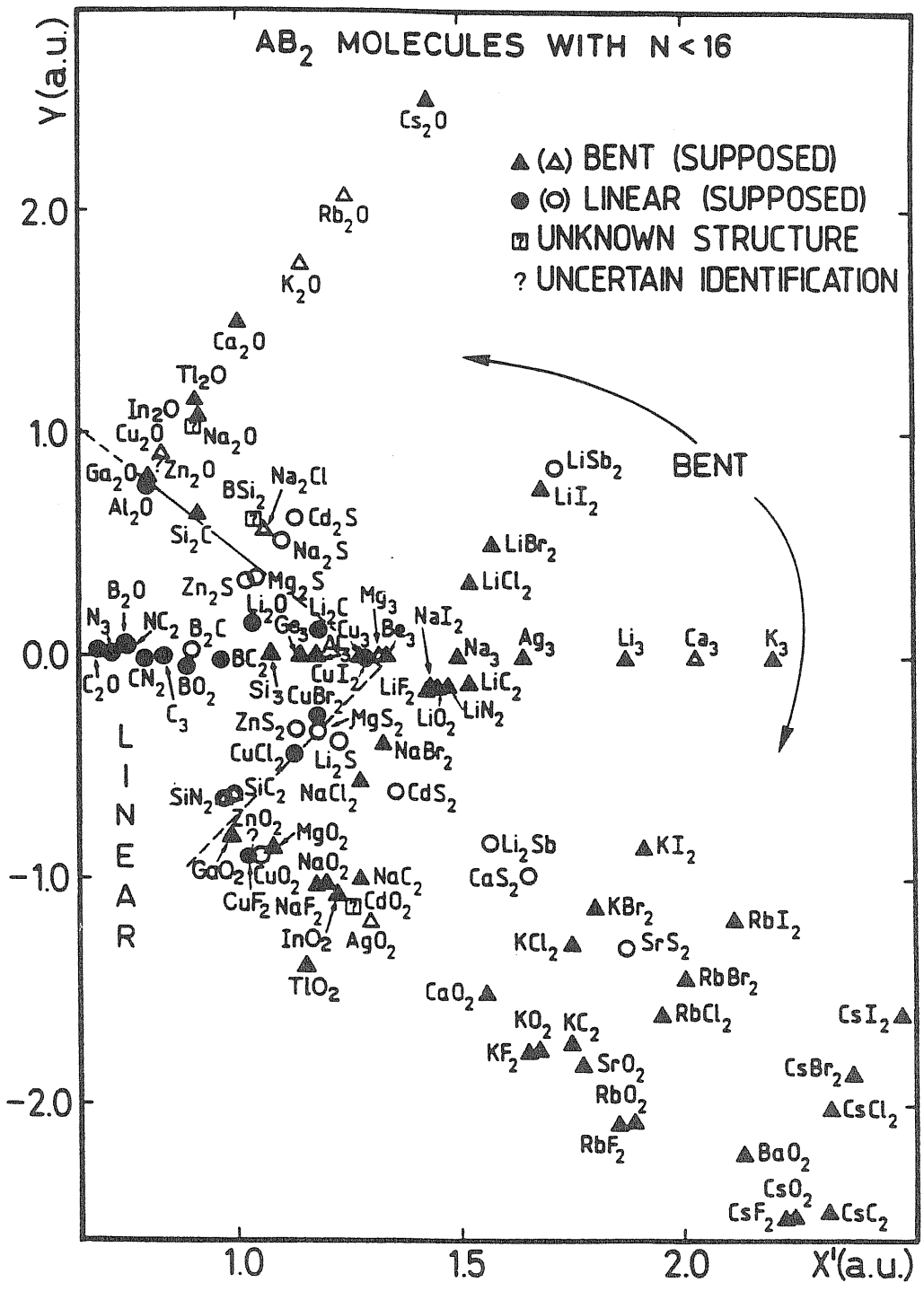

Fig. 2.6 Compound coordinates plot for AB_2 molecules and A_3 clusters with $N < 16$.The structural information used for these compounds are from references 53 and 54.

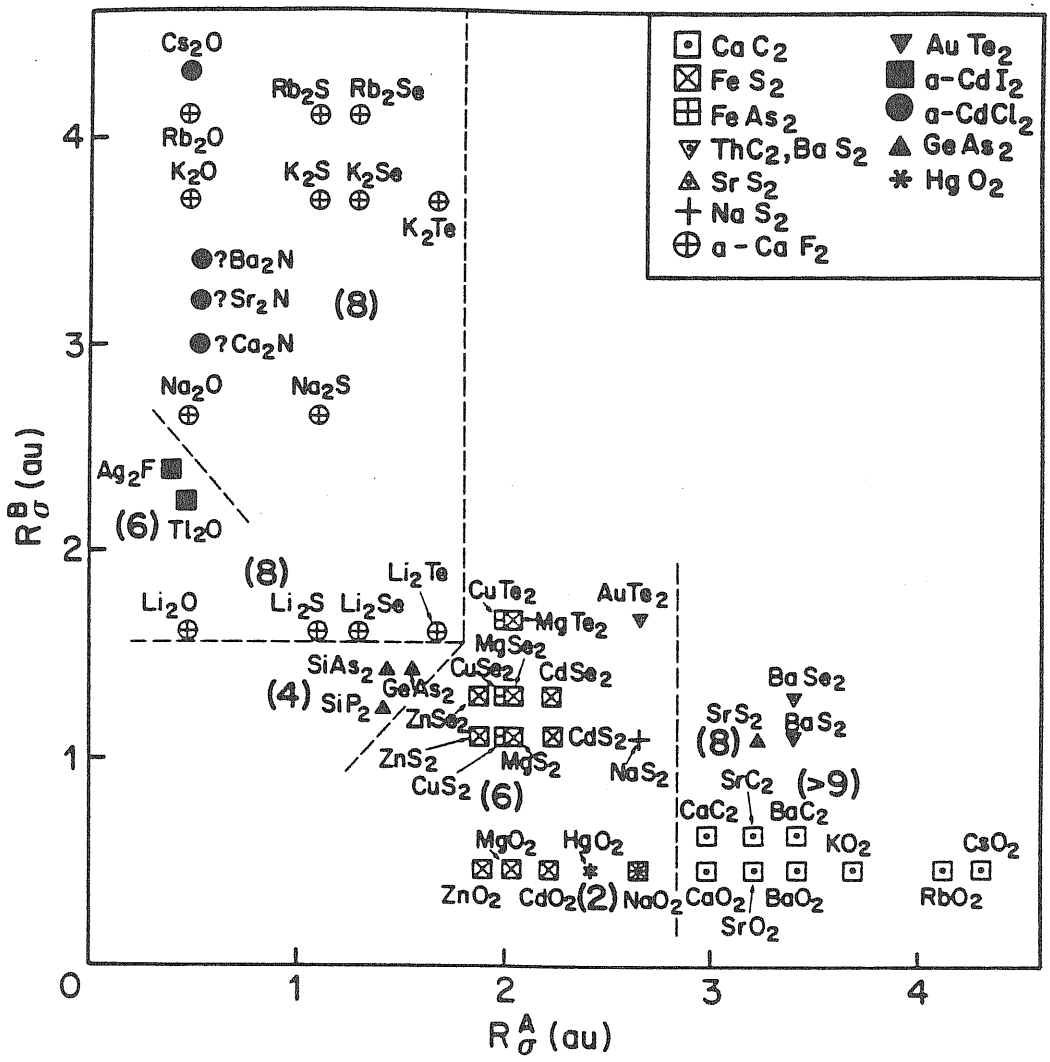

Fig. 2.7 Elemental coordinates plot for some AB_2 solids with $N < 16$.

with the same number of valence electrons. We have not included intermetallic compounds like AlB_2 or alloys, and have excluded non-stoichiometric materials. We are left with a few compounds which, however, can be nicely compared to the molecules in Fig. 2.5 and 2.6.

Fig. 2.7 and 2.8 are constructed with the ZC elemental coordinates and with the compound coordinates of Fig. 2.3, respectively.

The ZC compound coordinates are found to be not adequate, as in the case of DO solids. The elemental coordinates y_A and y_B ,instead, give a plot similar to Fig. 2.7, where the only relavent difference is in Li di-chalcogenides which are not as well separated as in the ZC scheme. The same comments can be made about both figures 2.7 and 2.8, again with the exception of Li-dichalcogenides, whose misplaced positions are much more evident in the latter figure than in the former one.

Both structural maps separate rather successfully compounds with different coordination numbers (CN) and according to their atomic arrangement, either packed (3d) or layered (2d). We notice that we have indicated explicitly the coordination number of the A atom, irrespective of its cation- or anion-nature. Compounds, such as, e.g., Rb_2O and RbO_2 however, lies in two different domains of the maps, just as in the molecular plots.

Only a few species crystallize in layer structures. Of these, the position of the tetrahedrally coordinated $GeAs_2$ structure is significant in view of the fact that $GeAs_2$ is known to transform to the pyrite structure under pressure[55]. The nitrides appear in the 3d domain incorrectly: however, the chemical composition of these materials reported in the literature as subnitrides is questionable (see ref. 55 pag. 277). We have not included the two compounds with the cuprite structure[44], i.e. Cu_2O and Ag_2O, since the former is indeed classified as a high-pressure structure and the latter is stable above room temperature. It is however interesting to notice that they would be correctly classified according the A atom coordination

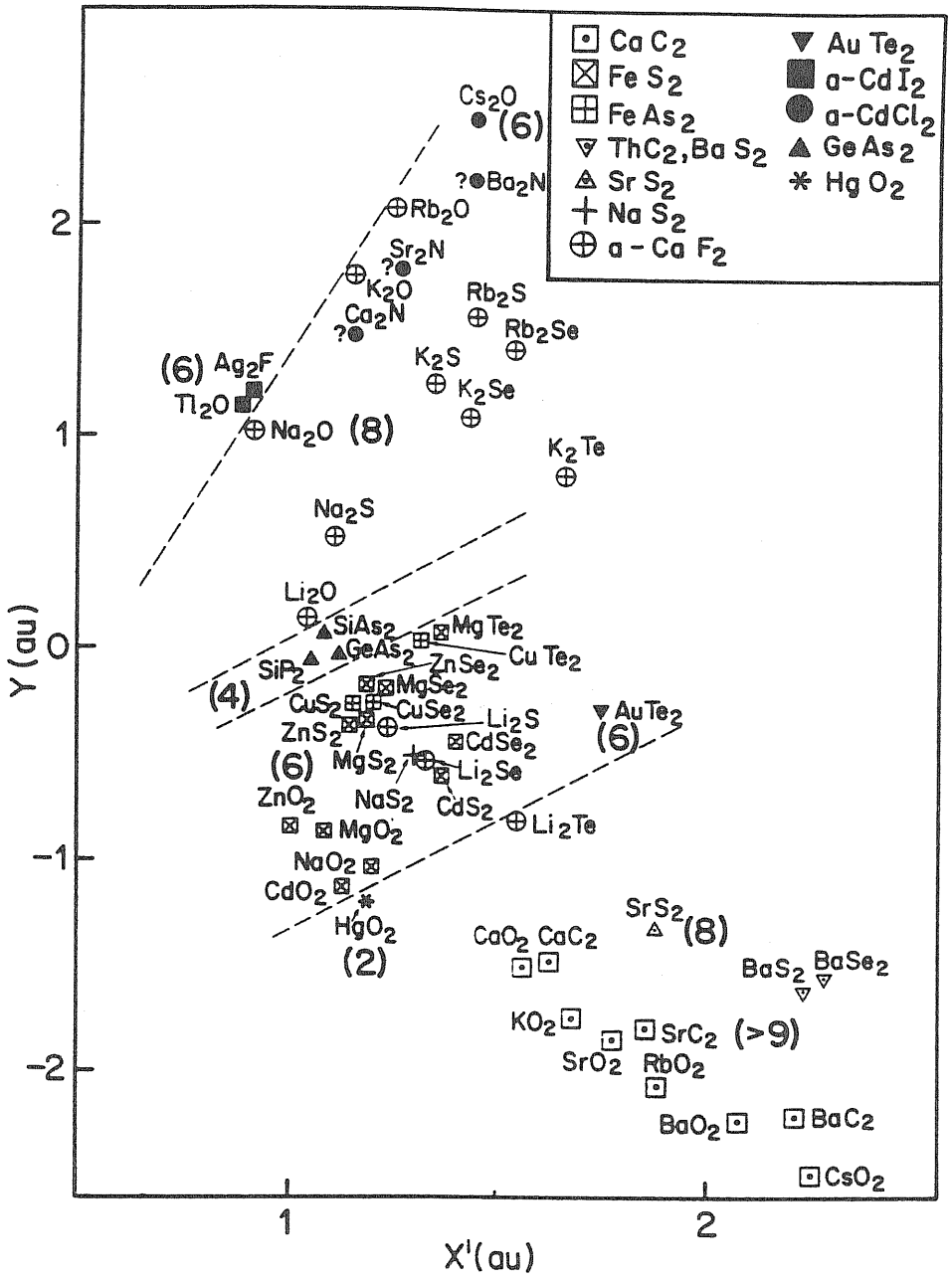

Fig. 2.8 Compound coordinates plot for some AB_2 solids with $N < 16$.

number. Moreover Ag_2O, that in either case is very close to Ag_2F (α-CdI_2 structure), has also an α-CdI_2 modification at high temperature and high pressure[44]. We also notice that the di-chalcogenides of both Zn and Cd are

obtained under special conditions, i.e., high pressure (60-65 Kbar) and also high temperature. This is also the case for $CuTe_2$.[We remark that MgS_2 and $MgSe_2$ are not classified by Villars and Calvert[44]; we have classified them according to Hulliger[55].]

Finally, we see that HgO_2 which assumes a very special structure with very low coordination, is misplaced in Fig. 2.7, although correctly located in the 3d domain. This fact is analogous to the misplacement of the Hg-dihalides in Fig. 2.3. $CuCl_2$ and $CuBr_2$ also crystallize in unique structures which are four-fold oordinated and layered. These are misplaced in all our plots, in analogy with their incorrect position in the molecular maps. No compound which is linear in the molecular phase is known in the solid phase, apart from Li_2O. At variance with what could be expected from the molecular bonds, Li_2O assumes the same crystal structure (antifluorite) as Na_2O, K_2O and Rb_2O.

Chapter 3

STRUCTURAL TRANSITION OF AB_2 MOLECULES FROM AB-INITIO AND IONIC MODEL CALCULATIONS

The results of our structural classification of double octet (DO) AB_2 molecules according to the single Y coordinate have shown that there exist a "critical" value Y_c, such that AB_2 compounds with an associated Y smaller than Y_c are linear, while those with Y greater than Y_c have a ground state bent geometry. Moreover, our results have suggested the following relationship between the equilibrium bond angle θ_{eq} of bent species and their so called bond ionicity:

$$\theta_{eq} = \pi \qquad |Y| < |Y_c| \qquad (3.1a)$$

$$\theta_{eq} = \pi - const.(Y - Y_c) \qquad |Y| < |Y_c| \qquad (3.1b)$$

Equations (3.1a) and (3.1b) suggest, in turn, a double well form for the binding energy curve of DO AB_2 compounds of the type:

$$E(\theta, Y) = E(\pi, Y) + A(Y)(\theta - \pi)^2 + B(Y)(\theta - \pi)^4 \qquad (3.2)$$

Indeed, if A is assumed an analytic function of Y and then expressed by the linear form $A(Y) = a(Y - Y_c)$, a being a positive constant, and B is supposed independent of Y, the two equilibrium solutions of equation (3.2) are given by (3.1a) and (3.1b), with $const. = (\frac{a}{B})^{\frac{1}{2}}$. The above considerations are not expected to apply for Y in the immediate neighborhood of Y_c.

In order to investigate the transition from linear to bent in a theoretical framework and to what extent equation (3.2) is a good approximation for the binding energy $E(\theta, Y)$, we have performed all-electron (AE) frozen core Hartree-Fock (HF) calculations on model DO AB_2 molecules and have determined their equilibrium structure for several core sizes[15]. Theoretically, model atoms A and B with any desired value for their valence electron orbital radii (VEOR) can be constructed. This is accomplished by expressing their single particle atomic orbitals as linear combinations of suitably chosen expansion functions, e.g., gaussian primitive functions. In principle, it is therefore possible to vary the y_E parameter associated with A and B and hence the Y coordinate of the model AB_2 in a continuum way. This in turn allows an accurate analysis of the behaviour of the bond ionicity Y as a function of the optimized equilibrium apex angle θ_{eq} and of the binding energy E as both Y and θ_{eq} vary. Furthermore it is possible to characterize the transition region where the structural transition occurs.

Our calculations allow us also to investigate the role of the single particle orbitals of the central atom A in determining the molecular geometry and

how the nodal radii of the atomic constituents are related to their single particle energy levels.

Moreover, the comparison between the prediction about molecular geometry that one would obtain by looking at the sum of eigenvalues with the "correct" ones derived from total energy calculations for all of the AB_2 examined, permit a critical discussion of Walsh's rules for molecular shapes[28].

In section 3.1 of this chapter we briefly describe the method used to construct model AB_2 molecules and discuss the correlation found between single particle atomic orbitals and molecular geometry. Our results for $Y(\theta)$ and $E(\theta, Y)$ are presented in section 3.2,while section (3.3) is devoted to the discussion of the Walsh rules.

We finally report in section 3.4 the predictions about the molecular geometries of DO alkaline-earth molecules, obtained by an entirely different approach, based on a phenomenological description of these compounds within an ionic model adjusted to cohesive properties of their crystalline state[56].

3.1 An ab-initio analysis of relevant parameters for molecular shapes

Model $s-p$ bonded DO AB_2 molecules are constructed from atomic constituent with fixed nuclear charge, number of electrons and electronic configuration but having different core sizes. A and B are chosen to be

respectively a model magnesium atom and a model fluorine atom. Their single particle atomic wavefunctions ψ_j are expressed as linear combinations with coefficient c_i^j of gaussian primitives of exponents α_i :

$$\psi_j(\bar{r}) = \sum_{i=1}^{M_j} c_i^j \frac{exp(-\alpha_i r^2)}{N_i(\alpha_i)} f_j(\bar{r}) \tag{3.1}$$

M_j is the number of gaussians chosen to describe the atomic orbital ψ_j, whose angular character is specified by the function f_j. N_i is the normalization factor for the ith gaussian. The outermost nodes of the valence wavefunctions are determined and hence the atomic core size fixed, once the basis set exponents α_i are specified. The latter can be suitably chosen in order to reproduce desired values of the structural atomic indices N_l and therefore to define desired atomic dimensions. The same basis sets chosen to describe the atomic orbitals of A and B are used in the frozen core calculations performed to optimize the AB_2 molecular geometry. These are all-electron (AE) frozen core total energy calculations carried out in the HF approximation for the total wavefunction. The latter is expressed as linear combination of molecular orbitals, which in turn are symmetry adapted combinations of atomic wavefunctions. In all our calculations, the core size of B is kept fixed, while varying that of A.

A basis set for the real fluorine has been initially chosen for the B constituent[57]. Starting from a basis set appropriate to describe the magnesium atom[58], we have changed the α_i exponents to have desired values

of the y_A coordinate which are increasingly larger than y_{Mg}. The core of the central atom has been enlarged with certain physical constraints on its single particle orbitals. The most important from the present viewpoint is that their variation in energy resembles the corresponding variation which accompanies the increase in size when going from Mg to Ba, through the group II elements. The increase in the y coordinate from Mg to Ba is accompanied by an increase in energy of the outermost p core level, due to the increased number of electrons. We have found that this is a necessary and sufficient condition to be imposed on the A energy spectrum, in order to obtain a linear-to-bent transition for an AB_2 species, as y_A is increased from y_{Mg}. The position of the $2s$ core level of A is seen to be irrelevant for the bending of the molecule. We have therefore established that, provided the atomic constituent A gives rise together with B to an ionic compound AB_2, i.e., provided the $3s$ valence level ϵ_{3s} of A is high enough to permit a charge transfer A $\rightarrow$ B, it is the position of the ϵ_{2p} core level which determines the molecular equilibrium structure as linear or bent.

Our molecular calculations to investigate the functional relationships $Y(\theta)$ and $E(\theta, Y)$ have been carried out with minimal basis sets for both the A and B atoms. The set chosen for B contains four s and two p primitive gaussians to model its four electrons in s states and five electrons in the $2p$ state respectively. A further extended p function is included to allow the description of the B^- anion. The basis set of A, for each choice of the Gaussian width parameters, is built up with four s and two p primitive

gaussians chosen in such a way that the requirement upon the outermost p core level discussed above is satisfied. After recognizing the ϵ_{2p} position as the crucial one in determining the molecular shape, the s gaussian exponents were kept fixed, while those of the p gaussians were varied in going from one basis set to another. The ensemble of basis sets constructed defines the ensemble of AB_2 molecules which have been examined to investigate the correlation between Y and θ and the form of the binding energy.

We notice that the nodal radii $N_p(A)$ turns out to be related to the core eigenvalue $\epsilon_p(A)$ by a simple relation. As shown in Fig. 3.1a, N_p varies linearly with $|\epsilon_{2p}|^{\frac{-1}{2}}$. The same behaviour of N_l with the highest core level ϵ_{np} is recovered in going from Mg to Ba, through the group II elements ($n = 2, 3, 4, 5$ for Mg, Ca, Sr and Ba respectively). This is displayed in Fig. 3.1b, which reports results of a numerical local density treatement.

3.2 Linear-to-bent transition in model DO AB_2 molecules

Table 3.1 reports the computed equilibrium bond angles of the model AB_2 molecules and the corresponding Y coordinates associated to them.

The behaviour of $(\Delta\theta)^2 = (\theta_{eq} - \pi)^2$ as a function of Y is displayed in Fig. 3.2. First of all we notice that, in substantial agreement with the results of our quantum structural diagrams for DO trimers, we have again found a critical value $Y_c = -1.40$ a.u. of the Y coordinate associated to a DO AB_2 molecule such that species with $|Y| < |Y_c|$ have a linear shape,

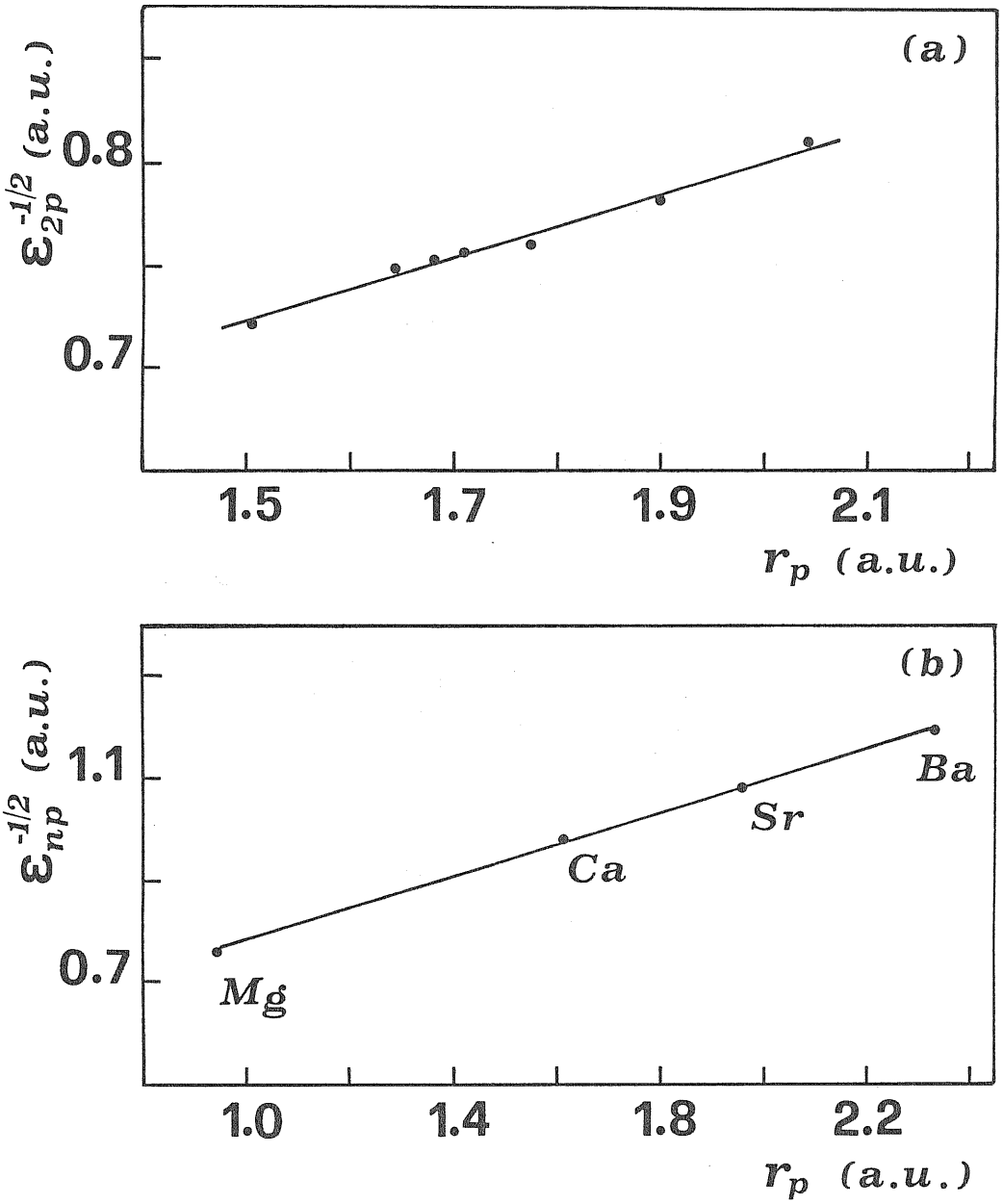

Fig. 3.1 Correlation between the p-nodal radii r_p and the highest single particle core level, respectively ϵ_{2p} for group II model atoms (a), and ϵ_{np} (n=2,3,4,5 for Mg, Ca, Sr and Ba) for group II actual atoms (b).

while those with $|Y| > |Y_c|$ have a bent geometry in their ground state. $(\Delta\theta)^2$ turns out to vary linearly with Y for $|Y| > 1.44$ a.u., while in the small region $1.40 < |Y| < 1.44$, which we will call the transition region, its

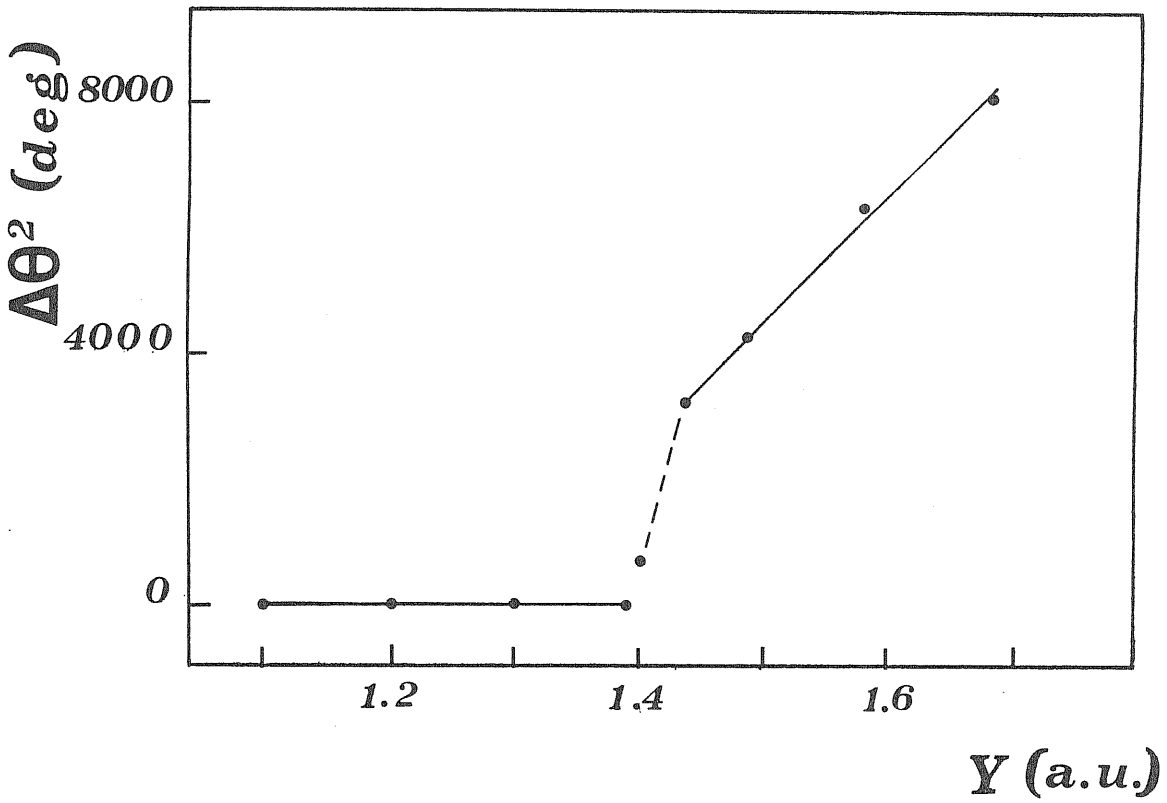

Fig. 3.2 Correlation between computed apex angles θ and the Y coordinate for model double-octet AB_2 molecules.

functional dependance on bond ionicity is more complicated. This behaviour suggests that the form (3.2) proposed for the binding energy of DO AB_2 molecules should have three possible minima : amongst them, two are indeed those given by equations (3.1a) and (3.1b), verified respectively in the regions $|Y| < 1.40$ a.u. and $|Y| > 1.44$ a.u..

In order to investigate whether equation (3.2) is a good approximation to the binding energy of an AB_2 species outside the transition region, we have

Table 3.1 Calculated equilibrium apex angles and corresponding Y coordinates for double-octet AB_2 molecules. For $Y < -1.39$, we always find $\theta = 180$ deg.

Y (a.u.)	θ_{eq} (deg.)
-1.390	180.00
-1.418	153.00
-1.441	127.25
-1.490	114.25
-1.582	100.00
-1.687	89.60

compared the results for $E(\theta)$ at fixed Y, obtained from equation (3.2) with those of optimized total energy calculations. To this end, we first determine the parameters A and B in eq. (3.2) from our present results, in the following manner.

The general equilibrium solutions of (3.2), as determined from the condition for $\frac{\partial E}{\partial \theta}$ to be zero at $\theta = \theta_{eq}$, are:

$$(\Delta\theta) = 0 \tag{3.4a}$$

$$(\Delta\theta)^2 = -\frac{A(Y)}{2B(Y)} \tag{3.4b}$$

If (3.4b) is solved for $A(Y)$ and the result substituted in (3.2), we get:

$$\frac{\Delta E_{B,L}}{(\Delta\theta)^4} = -B \tag{3.5}$$

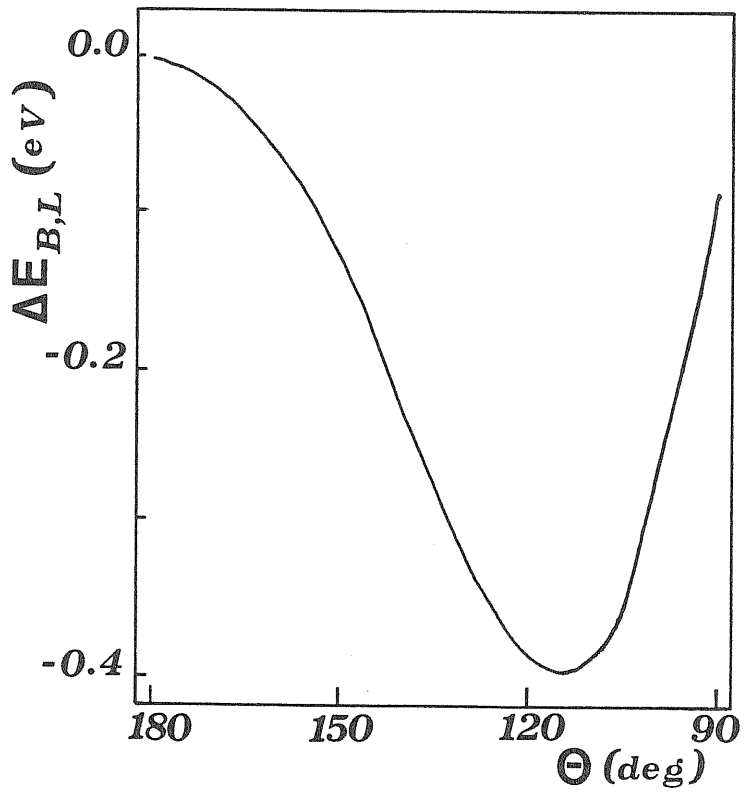

Fig. 3.3 Difference $\Delta E_{B,L}$ between the binding energies of a model double-octet AB_2 molecule ($Y = 1.49$ a.u.) in the bent and in the linear structures as a function of the bond angle θ. $\Delta E_{B,L}$ is an interpolation of results from optimized total energy calculations.

where we have defined $\Delta E_{B,L} = E(\theta_{eq}, Y) - E(\pi, Y)$ as the difference betwen the binding energies of the molecule in the bent (B) and in the linear (L) structure. On the other hand, if (3.4b) is solved for $B(Y)$ and the result inserted in (3.2), we have:

$$\frac{\Delta E_{B,L}}{(\Delta\theta)^2} = -\frac{A}{2} \tag{3.6}$$

Having fixed $Y = 1.49$, we have therefore computed $\Delta E_{B,L}$ and the

corresponding $\Delta\theta_{eq}$ by optimizing both the bent and the linear geometries (the latter geometry corresponding to a local minimum). The B and A coefficients are then obtained from equations (3.5) and (3.6) respectively. When inserted into (3.2), the latter gives the behaviour of $\Delta E_{B,L}$ as a function of θ. Fig. 3.3 displays the difference $\Delta E_{B,L}(\theta)$ as obtained from an interpolation of optimized total energy calculation results for several bond angles. On the scale reported in the picture, it coincides with $\Delta E_{B,L}(\theta)$ as derived above from equation (3.2). The latter turns out to be shifted downward relative to the "true" one by at most 0.003 eV. It is then a good approximation to the molecular binding energy, expecially near the equilibrium apex angle $\theta = 114.25$, where the shift between the two curves is almost constant and as small as 0.0002 eV over an interval of about 20 degrees.

Equations (3.5) and (3.6) can be used to compute the values of the B and A coefficients as a functions of Y, once the $\Delta E_{B,L}(Y)$ and the corresponding $\Delta\theta_{eq}$ are known. This has been done for the values of the Y parameter reported in Table 3.1. The results are shown in Fig. 3.4a and 3.4b. B turns out to increase rapidly for $1.39 < |Y| < 1.49$, from 0.06 to of 0.23eV(rad)^{-4} . Then its variation with Y becomes weak and approximately linear. The A coefficient is found to have a linear form in the bent region, when $|Y| > 1.49$. As already stated, it is however the behabiour of the ratio $A/2B$ which specifies the variation of $(\Delta\theta_{eq})^2$ as a function of Y. This is indeed linear in $(Y - Y_c)$ for $|Y| > 1.44$ a.u.(see Fig. 3.2)

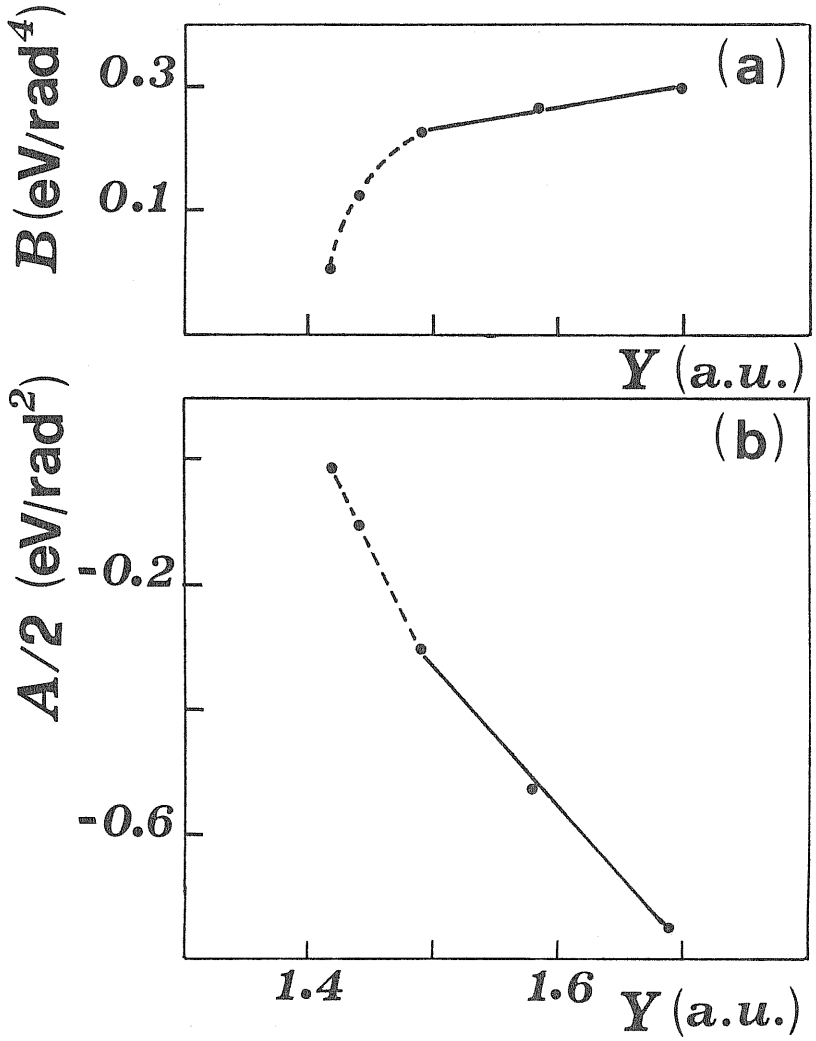

Fig. 3.4 Behaviour of the expansion coefficients B (a) and (b) of eq. (3.2) (see text) as functions of the Y coordinate.

3.3 Connection with the Walsh rules for molecular shapes

We are now going to discuss the Walsh rules for AB_2 molecular shapes[28] according to the results for the total energy E and the sum of eigenvalues $\sum_i \epsilon_i$ as functions of θ obtained for our model triatomic molecules. We first notice that the difference of eigenvalue sums $\Delta(\sum_i \epsilon_i)_{B,L} = \sum_i \epsilon_i(\theta_{eq}) -$

$\sum_i \epsilon_i(\pi)$ correctly predicts whether a compound is linear or bent in all of the cases that we have studied. Indeed, $\Delta E_{B,L}$ and $\Delta(\sum_i \epsilon_i)_{B,L}$ are found to have the same sign for each of the Y values reported in Table 3.1 and for several values of $|Y| < 1.39$. The functional relationship between $\Delta(\sum_i \epsilon_i)_{B,L}$ and θ is however different from that correlating $\Delta E_{B,L}$ with θ, and in the case of bent species the equilibrium bond angle which minimizes $E(\theta)$ is generally not an estremum point for $\sum_i \epsilon_i$. In the formulation of the Walsh rules for molecular shapes, both the relative position of s and p eigenvalues and each single particle orbital behaviour as functions of θ are assumed to be the same for any molecule of a given chemical formula and hence for each AB_2. This is not found to be the case in our results. The variation in size of the central atom leads to different energy level dispersions for the AB_2 molecules. As an example, Fig. 3.5 shows the single particle energies as functions of θ for a linear AB_2 (Fig 3.5a), whose associated Y coordinate is 0.93 and for a bent species, for which $Y = 1.49$ (Fig.3.5b). Therefore our calculations suggest that the weak point in Walsh's arguments lies in the form assumed for the dispersion of the single electron energy levels, at least in the case of AB_2 species.

As we have mentioned in chapter 1 (section 1.2), some critical analyses of the Walsh rules, based on ab initio treatements of the electronic structure in molecular systems have been proposed in the literature[30,33]. In particular, Ruedemberg[32] has derived a relationship between the total energy E in Hartree-Fock Self-Consistent-Field (HF SCF) theory and the orbital energies

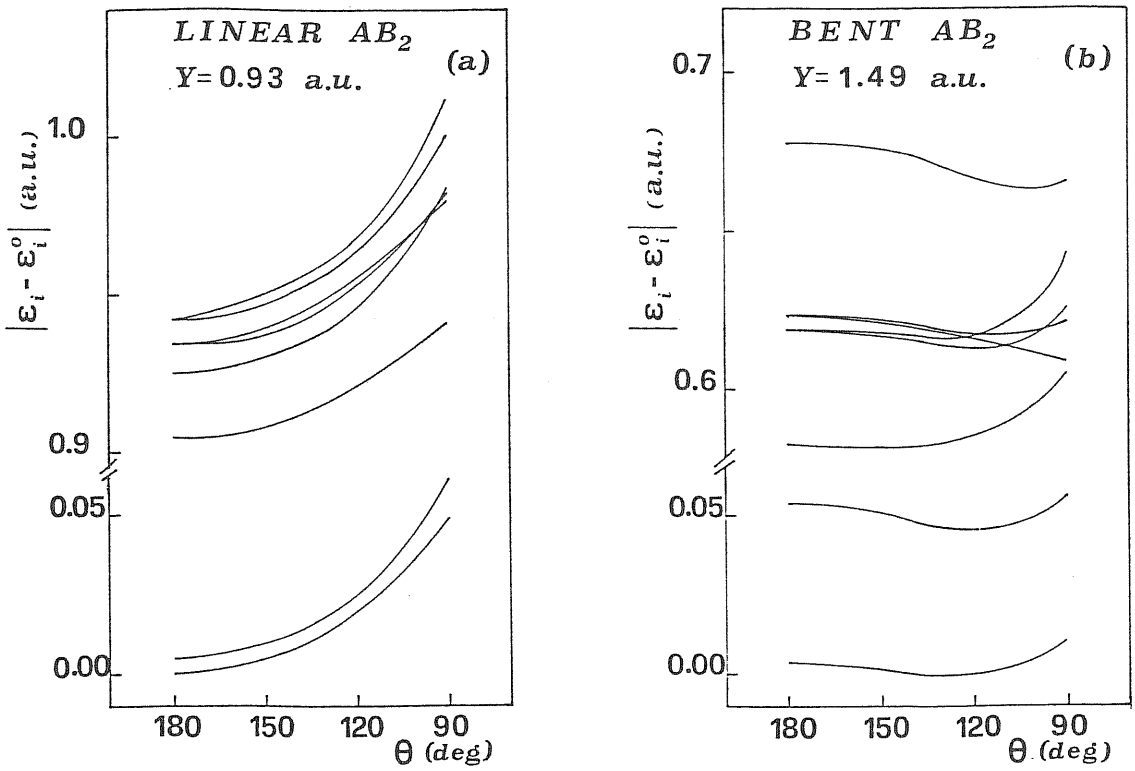

Fig. 3.5 Behaviour of the single particle energy levels as functions of the molecular bond angle θ for a linear ($Y = 0.93$ a.u.) and a bent ($Y = 1.49$ a.u.) double-octet model molecule.

ϵ_i of a molecular system, i.e. $E = k \sum_i n_i \epsilon_i$, where $k \simeq 1.55$ This equation holds only at the equilibrium geometry of a molecule and hence does not guarantee, evidently, that changes in orbital energies ϵ_i should dominate the variations in the total energy, as the shape of the system is distorted or modified.

March[32] has instead established a correlation between E and $\sum_i \epsilon_i$ of a molecule, within the local density approximation (LD) of the density functional (DF) theory. The relationship between these two quantities, which he

has derived, is the following:

$$E = \frac{3}{2}\sum_i \epsilon_i - \frac{3}{2}N\mu + \frac{3}{2}(\int d\bar{r}\rho\frac{\partial T_s}{\partial \rho} - \frac{5}{3}T_s) + \Delta T \qquad (3.7)$$

Here μ is the chemical potential of the molecule, T_s is the free-particle kinetic energy associated with the system of charge density ρ. ΔT is its correlation kinetic energy defined as $\Delta T = T - T_s$, T being the kinetic energy of the real system. ΔT can be expressed as follows:

$$\Delta T = -\int d\bar{r}\rho[4\epsilon_c - 3v_c] \qquad (3.8)$$

where $v_c = \frac{d}{d\rho}(\rho\epsilon_c)$ and $\int d\bar{r}\rho\epsilon_c$ is the correlation energy functional of the system. In the Thomas-Fermi approximation, eq. (3.7) reduces simply to $E = \frac{3}{2}\sum_i \epsilon_i$, in substantial agreement with the result obtained by Ruedemberg within the HF-SCF theory. In general, however, the chemical potential and kinetic energy contributions at the right hand side of eq. (3.7) are relevant and cannot be neglected. Thus a simple proportionality relationship between E and $\sum_i \epsilon_i$ does not hold, even at the equilibrium geometrical configuration of the molecule.

We finally mention that a relationship between total energy differences and eigenvalue sums has been investigated also in the case of solids. Within the DF-LD approach, Weinert *et.al.* have derived a variational expression for the total energy difference between two crystal structures in terms of

the difference in the sum of the one-electron energies and of additional exchange-correlation and Coulomb contributions. They have then discussed the conditions and approximations under which these additional terms can be made to vanish. In particular, they have shown that for compounds which exhibit a relevant charge transfer, the total energy cannot be approximated with the eigenvalue sum.

3.4 Ionic model results

Our ab initio calculations on model AB_2 molecules have elucidated the role of the central atom core size and of its single particle energy levels in determining the molecular structure. Further insight on the correlation between physical properties of the atomic constituents and molecular structure of AB_2 molecules, with A belonging to group II and B to group VII, can be gained by an investigation of these compounds within an ionic model.

Early experimental and theoretical works[60] have suggested that the classical ionic model should indeed provide a reasonable first order description of alkaline earth dihalide molecules, exeption made for Beryllium compounds, whose chemical bond is expected to show significant covalent features. We have calculated the equilibrium structures of the species MgX_2, CaX_2, SrX_2, BaX_2 (X = F, Cl, Br, I), within an ionic model which treats both the metal and the halogen as polarizable ions[56]. Our results show that the electronic

polarizability of the alkali ion plays a crucial role in determining the molecular conformation as linear or bent : it seems to provide a compensating mechanism to stabilize a bent molecular shape against the increase of the Coulombic repulsion of the halogen ions under bending, leading to an effective medium range attraction between the two halogens.

In our model calculation, the energy E of the molecule relative to the free ion state is expressed in a tight-dinding approach through a multipolar expansion, which includes short range couplings between the various poles in addition to the classical electrostatic couplings[61]. After truncation of the expansion at dipolar terms and linearization of the dipolar contribution, the expression for E as a function of the bond angle 2θ and the metal-halogen bond lenght R is :

$$\begin{aligned} E = & -\frac{4e^2}{R} + \frac{e^2}{Rl} + 2\varphi_{+-}(R) + \varphi_{--}(R) - \frac{2e}{R^2}|m_+|cos(\theta) - \\ & 2|m_x|\{[\frac{2e}{R} - B(R)]sin(\theta) - \frac{e}{Rl}\} - 2|m_y|[\frac{2e}{R} - B(R)]cos(\theta) \\ & - \frac{6}{R^3}|m_x||m_y|sin(\theta)cos(\theta) - \frac{2}{R^3}|m_x||m_y|(3cos^2(\theta) - 1) \\ & + 2\frac{|m_x|^2}{Rl^3} + \frac{|m_y|^2}{Rl^3} + \frac{|m_+|^2}{2\alpha_+} + (\frac{|m_x|^2 + |m_y|^2}{\alpha_-}) \end{aligned} \quad (3.9)$$

Here $Rl = 2Rsin(\theta)$. $|m_+|$ is the magnitude of the dipole moment on the metal ion, which vanishes in the limit of a linear molecule and $|m_x|$ and $|m_y|$ are the magnitudes of the components of the dipole moment on a halogen ion . The first four terms in Equation (3.9) are monopolar contributions, including short-range (overlap and van der Waals) interactions described by

the functions $\varphi_{+-}(R)$ and $\varphi_{--}(Rl)$ for metal-halogen and halogen- halogen pairs. The next three terms arise from dipole-monopole interactions and include, in addition to classical electrostatic contributions, an overlap dipole contribution to the screening of the metal ion by the deformation of the electronic shells of the anions. This effect is expressed through the function $B(R)$. Finally, the remaining terms are the electrostatic dipole- dipole interactions and the linearized polarization energy, which involves scalar polarizabilities α_+ and α_-. Our choice for the functions $B(R)$ and φ_{+-} and φ_{--} remains to be specified. In order to determine $B(R)$, we have developed a shell-model calculation of the vibrational motions in a triatomic molecule with C_{2v} symmetry, in which each ion is viewed as composed of an outer electronic shell elastically bound to a rigid inner core. When treated by the same approximations which are usually involved in simple lattice dynamics calculations[62], this model leads, for the alkaline-earth molecules, to the result:

$$\alpha_- B(R) = -[\frac{Y_+}{K_+} - \frac{Y_-}{K_-}]\frac{\partial\phi(R)}{\partial R}. \tag{3.11}$$

Here $\phi(R)$ is the overlap repulsive contribution to $\varphi_{+-}(R)$, Y_+ and K_+ are the shell charge and the shell-core force constant for the metal ion, and Y_- and K_- are the analogous parameters for the halogen ion. The main sources for the values of the model parameters used in our calculation are the tables of electronic polarizabilities of ions of Tessman *et.al.*[63] and the determination

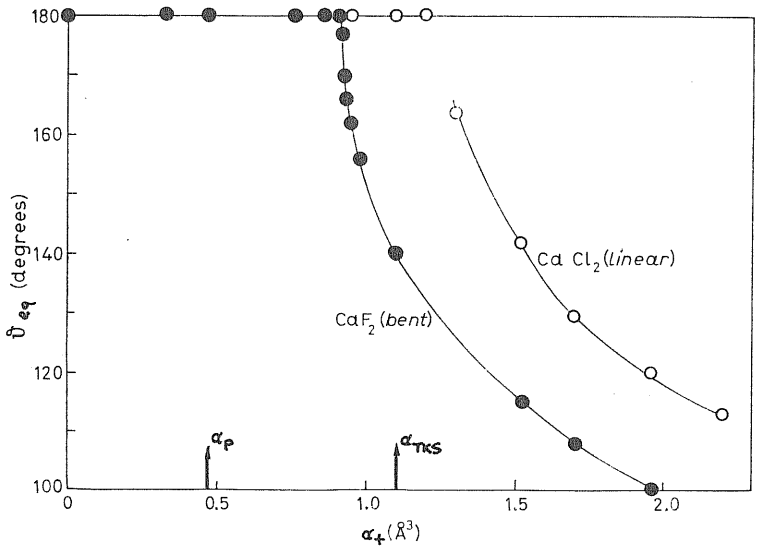

Fig. 3.6 The equilibrium bond angle θ_{eq} in CaF_2 (dots) and $CaCl_2$ (circles) as a function of the polarizability α_+ of the metal ion. The curves are only meant to guide the eye through calculated points. The arrows mark the values of the Pauling polarizability α_p and of the polarizability α_{TKS} of Tessman. et. al. for Ca^{2+}. Experimentally CaF_2 is bent, while $CaCl_2$ is linear.

of short- range interactions and shell-model parameters by Yuen *et.al.*[64] All these data are consistently based on analyses of crystalline properties for the family of alkaline earth dihalides. The use of information on the interionic forces from works on solid phase avoids a fit of model parameters to molecular properties.

Our model is in complete agreement with experiment on whether a particular molecule has a linear or a bent equilibrium configuration. Fig. 3.6 illustrates on CaF_2 and $CaCl_2$ the main physical factors which determine the molecular geometry, by plotting the calculated equilibrium bond angle as a function of the polarizability of the Ca^{2+} ion, all the other parameters being kept constant. The primary factor is precisely the value of α_+, with

a secondary effect from the halogen ionic radius, which determines the bond lenght and thus the internal electric field on the metal ion. Evidently, there is only a narrow range of values of α_+ which are consistent with the observation that CaF_2 is bent while $CaCl_2$ is linear. This range would tend to widen if α_+ were varied at constant molar refractivity rather than at constant α_-, as will became clear below.

In the case of CaF_2, we have examined in detail the region of values for α_+ near the "critical" value where the molecule starts bending. The minimum in the energy $E(2\theta, R)$ at $2\theta = 180$ flattens out as the critical value of α_+ is approached from below, and the bending sets in continuosly as a function of α_+. In support of the above interpretation of the main origin of the molecular geometry, we should mention the tests that we have made by changing either the value of the halogen polarizability or the magnitude of the overlap dipole in both CaF_2 and $CaCl_2$, again at fixed values of the other parameters and taking α_+ as given by Tessman *et.al.*[63]. The bond angle in CaF_2 tends to increase as α_- is lowered from the value of $0.76A^3$ given by Tessman et.al., but the molecules remains bent even if α_- vanishes. On the other hand, $CaCl_2$ would start taking a bent configuration only if α_- were pushed up to about $3.7\mathring{A}^3$ from the value of $2.96\mathring{A}^3$ given by Tessman et.al. for Cl^-. Similarly, rather wide variations of $(\frac{Y_+}{K_+} - \frac{Y_-}{K_-})$ from the values of ref. 64 affect only the quantitative value of the bond angle in CaF_2 and leave $CaCl_2$ in a linear configuration.

From a quantitative viewpoint, the results of the model are compared

Table 5.1 Equilibrium bond length $\mathbf{R_{eq}}$, bond angle $\theta_{\mathbf{eq}}$ and binding energy $\mathbf{E_0}$ of alkaline-earth dihalides molecules .

	R_{eq}(Å)		θ_{eq}(deg.)		E_0(kcal/mol)	
	theory	expt.[a]	theory	expt.	theory	expt.[d]
MgF_2	1.72	1.77	180	L[b]	606	615
$MgCl_2$	2.14	2.18	180	—	543	543
$MgBr_2$	2.26	2.34	180	—	524	524
MgI_2	2.42	2.52	180	—	504	500
CaF_2	2.07	2.10	140	140[c]	504	522
$CaCl_2$	2.52	2.51	180	L[b]	446	460
$CaBr_2$	2.66	2.76	180	L[b]	430	443
CaI_2	2.83	2.88	180	—	413	422
SrF_2	2.20	2.20	118	108[c]	474	490
$SrCl_2$	2.68	2.67	154	B[b]	416	437
$SrBr_2$	2.81	2.82	180	L[b]	402	417
SrI_2	2.99	3.03	180	L[b]	386	398
BaF_2	2.32	2.32	108	100[c]	449	469
$BaCl_2$	2.82	2.82	132	B[b]	392	414
$BaBr_2$	2.95	2.99	139	B[b]	380	394
BaI_2	3.15	3.20	153	148[c]	363	374

[a] From ref. 65. [b] From ref. 45. [c] From ref. 52. [d] Estimated values fom ref. 60.

in Table 3.2 with the available experimental evidence on the equilibrium bond lenght R_{eq}, the equilibrium apex angle θ_{eq} and the binding energy E_o. The calculated values of R_{eq} agree reasonably well with the measured values, which refer to the free molecules, with deviations lying within the estimated uncertainties of $0.02 \div 0.03\mathring{A}$ in these data, except for Mg halides and for the iodides. Measured values for θ_{eq} are available for the fluoride trapped in solid-kripton matrices from infrared spectra and for BaI_2 from electron difraction experiments. The agreement between our model and these data seems quite reasonable if also one bears in the mind that the effect of the matrix, though presumably not large, is not known quantitatively and that the experimental values are determined at most within $\pm$5degrees. Finally, we notice that the model tends to understimate the binding energy of the molecule, with a mean deviation of about 3% from the expeimental values estimated by Brackett and Brackett[60]. This discrepancy is probably significant and suggests that additional contributions to the binding, such as those coming from quadrupole deformations, may be quantitatively relevant.

Chapter 4

UNIFIED STRUCTURAL CLASSIFICATION OF TETRA-ATOMIC MOLECULES AND SOLIDS

In chapter 2 we have shown that the same quantum structural parameters which classify $s-p$ bonded crystals enable one to predict successfully the shapes of AB_2 molecules. Of course, in this case the question about structure is very simple : is the molecule linear or bent? Instead, in the case of polyatomic molecules the number of possible geometric configurations increases and with it the number of questions that one should answer. Unfortunately, at the same time the experimental knowledge of the equilibrium structures becomes less accurate and the statistics less ample. It is nevertheless important to test the transferability of the quantum structural parameters appropriate for crystals to complex molecules, within present knowledge, and thus hopefully stimulate further experimental work.

In this chapter we present structural classifications for $s-p$ bonded tetra-atomic compounds in both solid and molecular phases[14]. In full analogy with our investigation of AB_2 compounds, we have constructed structural maps whose Cartesian coordinates are linear combinations of either pseudopotential or nodal valence electron orbital radii (VEOR). Our

results for AB_3 and A_2B_2 molecules are reported in section 4.1 and 4.2, while those for AB_3 crystals structures are discussed in section 4.3.

4.1 AB_3 molecules

We recall that the most symmetrical structure for an AB_3 moecule is planar and corresponds to an equilateral triangle formed by the B atoms, with the A atom placed at the center (D_{3h} symmetry). As we have discussed in chapter 1 (section 1.2), the long standing Walsh arguments[28] concern the transition from this planar symmetric shape to the pyramidal one (C_{3v} symmetry or NH_3-type) and consider the number of valence electrons of the compound, N, as the only structural parameter. The planar shape is predicted as long as $N < 24$ and for $N = 28$, while the pyramidal modification is predicted for $N = 25$ and 26. More sophisticated pictures[5] of the molecular bonding agree in identifying a critical number $N = 24$ for the valence electrons, beyond which distortion from D_{3h} symmetry should occur, either planar or three-dimensional. For a few selected species, and in particular for $N > 24$, several proposals exist in the literature to figure out which are the electronic properties responsible for these distortions. Burdett[5], for example, has adopted an Angular Overlap Model (AOM, see chapter 1) to investigate the single particle energy level changes on distortion of the high symmetrical D_{3h} geometry to a planar conformation with C_{2v} symmetry(T, Y or arrow shaped). He has then applied this scheme to 28

electron molecules ($ClBr_3$ and ClF_3), to account for their slightly different C_{2v} planar geometries and to predict the values of their bond angles.

According to present experimental knowledge of molecular shapes, most of the compounds with $N > 24$ are pyramidal, with the exception of $ClBr_3$ and ClF_3, and all the known species with $N = 24$ have a D_{3h} geometry in their ground state[66]. Compounds with $N < 24$, instead, are not planar and symmetrical, with the only exception of NO_3 (as indicated by recent infrared laser spectroscopy in the gas phase[67]), but display a rather large variety of possible equilibrium structures[68,69].

Our investigation of AB_3 molecules concentrates on the class of species with $N < 24$, the only for whch statistically meaningful structural maps can be constructed. We stress that this is indeed the class of tetra-atomic compounds whose geometric conformations have never been successfully classified within a comprehensive scheme. The structural plots we report in the following for these compounds (fig. 4.1 and 4.2) use as coordinates either Zunger-Cohen (ZC) elemental coordinates or Compound Coordinates derived from nodal radii, which are defined in chapter 2 (section 2.1).

The actual geometries of $N < 24$ AB_3 molecules are shown in figures 4.1 and 4.2. These collect the 37 $s-p$ bonded species for which equilibrium shapes have been given in the literature, as deduced from either experiment[68] (mostly infrared and Raman spectra in rare gas matrices) or calculations of the electronic structure[69]. The equilibrium geometries found within this family are pyramidal configurations for the compounds of group V elements,

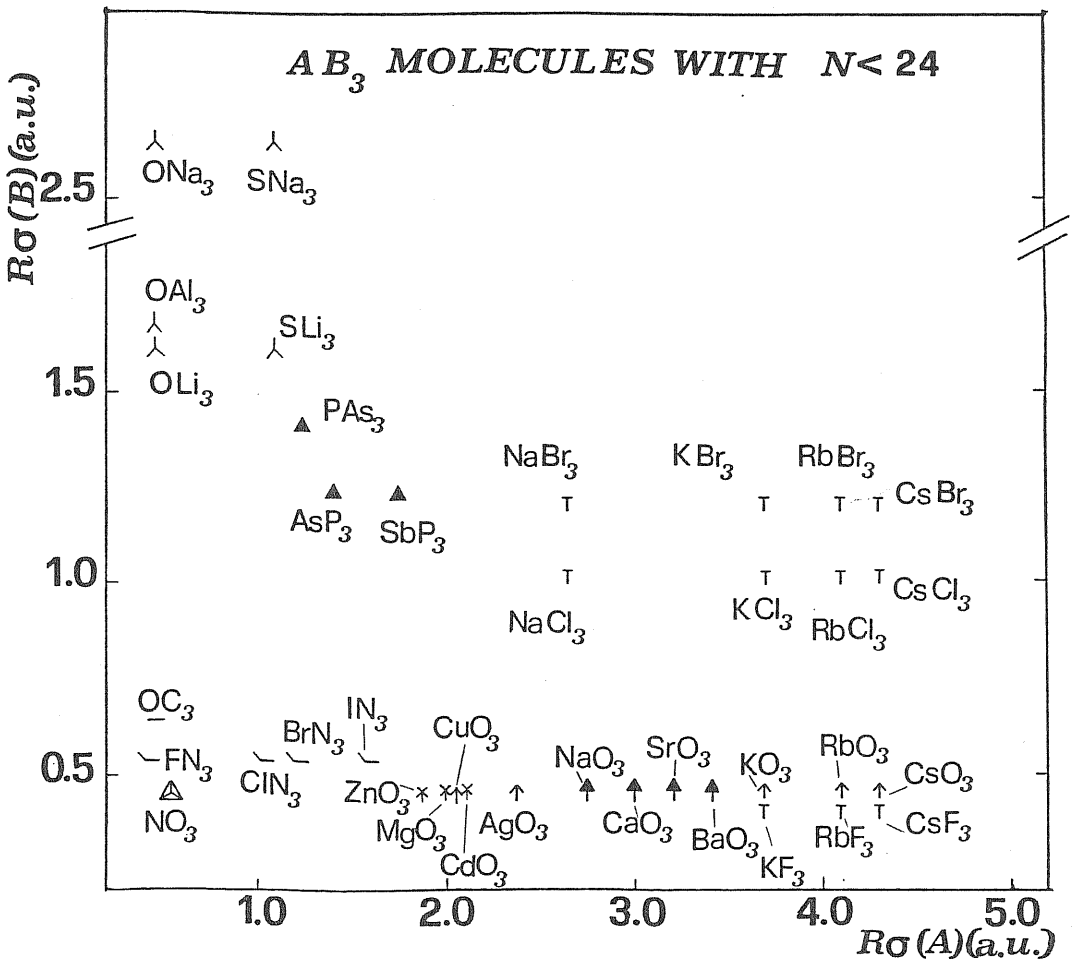

Fig. 4.1 Elemental coordinates plot for AB_3 molecules with $N < 24$. The structural information used for these compounds is from references 67-69.

HN_3-type conformations for the halogen-azides, T shapes for the alkali trihalides (symmetrical only in the case of trifluorides), Y and arrow shapes for both oxides and sulfides. The latter can be distinguished by the different identity of the central atom, which is B for the trioxides and A for both the mono-oxides and sulfides. All these structural differences are brought out

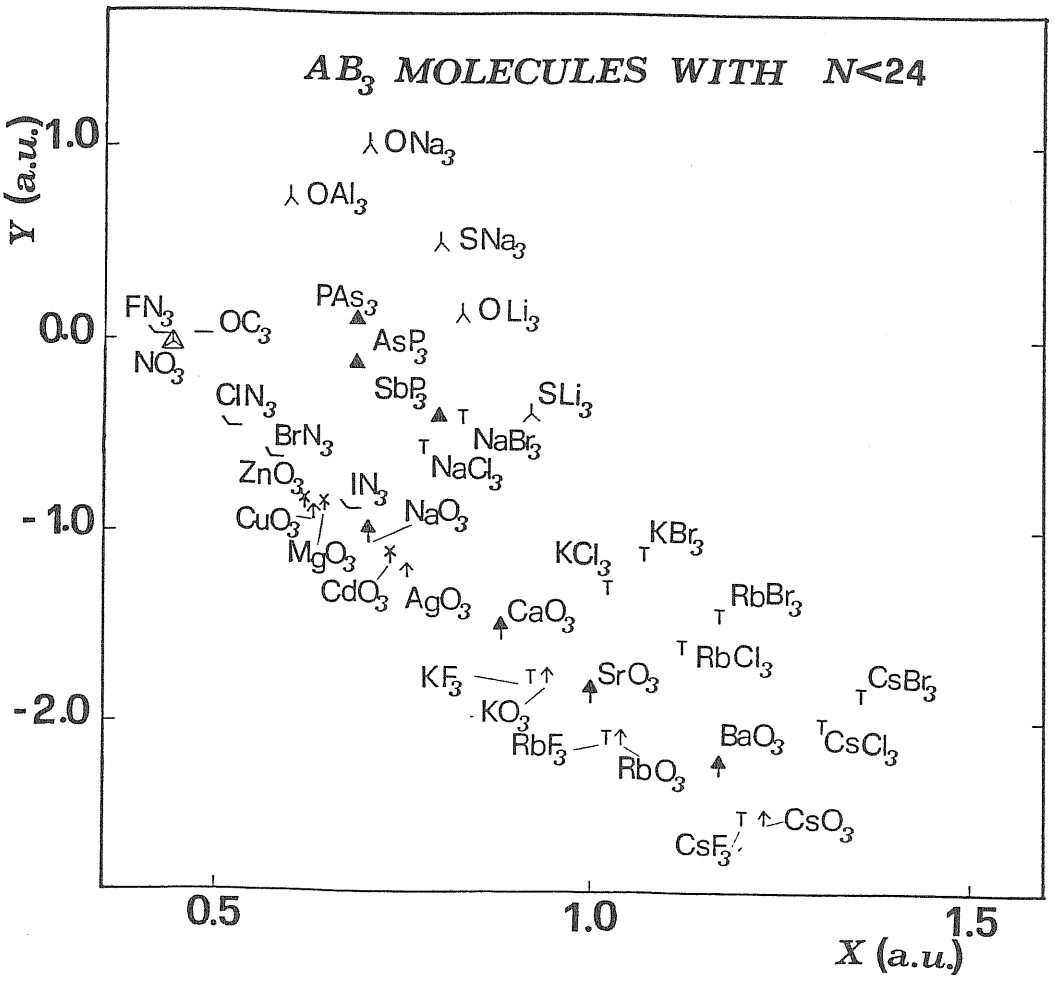

Fig. 4.2 Compound coordinates plot for AB_3 molecules with $N < 24$. The structural information used for these compounds is from references 67-69.

clearly in the two plots of figures 4.1 and 4.2. Moreover, the comparison between the vibrational frequencies, extrapolated from infrared and Raman spectra, for the trioxides of sodium and of the alkaline-earth elements with those for the trioxides of Li, K, Rb and Cs, has suggested that compounds belonging to the former group are not planar. (See, e.g., L. Andrews (1981)

in ref. 70). In the case of NaO_3, this suggestion is strongly supported by the results of an electron spin resonance experiment[71]. The distinction between two- and three-dimensional trioxides is the only feature not well resolved in a plot with elemental coordinates derived from nodal radii. We have also found, in analogy with AB_2 species, that ZC compound coordinates are not as successful as the elemental ones of fig. 4.2. We notice that the species expected to be the most ionic ones are found at large negative values of Y and/or large values of X in fig. 4.2, as was the case for AB_2 molecules. Those that can reasonably be supposed to show relevant covalent character in their bond, such as the mono-oxides and sulfides , have instead small values of the Y and/or X coordinates. Again in analogy with triatomic compounds, N turns out to be a relevant structural parameter, in the sense that neither species with $N = 24$ nor those with $N > 24$ can be placed on the same plots that are appropriate to classify molecules with $N < 24$.

In searching for schemes that can account for both molecular shapes and crystal structures, we have examined the transferability to molecules of the coordinates recently proposed by Villars[10] and Pettifor[26] to classify AB_3 solids. We recall that the former uses three coordinates, of which N is one, while the latter uses two entirely phenomenological elemental parameters (see chapter 1, section 1.1). None of the above schemes seems to be useful for AB_3 molecules. In fact, Villars' scheme needs a very large statistics in order to have a sufficient number of compounds at each value of N. On the other hand, a classification of AB_3 molecules in a (χ_A, χ_B) map , χ being

Pettifor's empirical chemical scale, does not give as accurate an account of their structures as figures 4.1 and 4.2 do.

4.2 A_2B_2 molecules

In the case of A_2B_2 molecules, structural information is available for about 40 species[72,73]. It is derived from infrared absorption and Raman spectra in matrices and electron diffraction experiments, and based upon suggestions from thermochemical data and Hartree-Fock calculations. The known species include alkali dihalides, dioxides of mono- , di- and tri-valent ions and a few dichalcogenides. They seem to be all planar and to form rings (mostly having rhombohedral shape), apart from C_2N_2 and probably B_2O_2 which are linear and N_2O_2 which is bent at both nitrogen atoms[72]. It is thus not worthwhile showing quantum diagrams for A_2B_2 compounds, but it is easy to see that VEOR-structural parameters, within either the compound or the elemental scheme, separate well these three special cases and confine them near the origin of the plots. Schnuelle and Parr[74] indicated a critical number of valence electrons $N = 22$ as marking the border between linear symmetric and other shapes. In fact, in their picture of the electron distribution, $N = 22$ corresponds to completed octets at the terminal atoms (say B) plus a triple bond between the two central atoms (say A). This type of bonding is realistic only for covalent species such as C_2N_2 but is unstable against increase of ionicity or delocalization of the charge density.

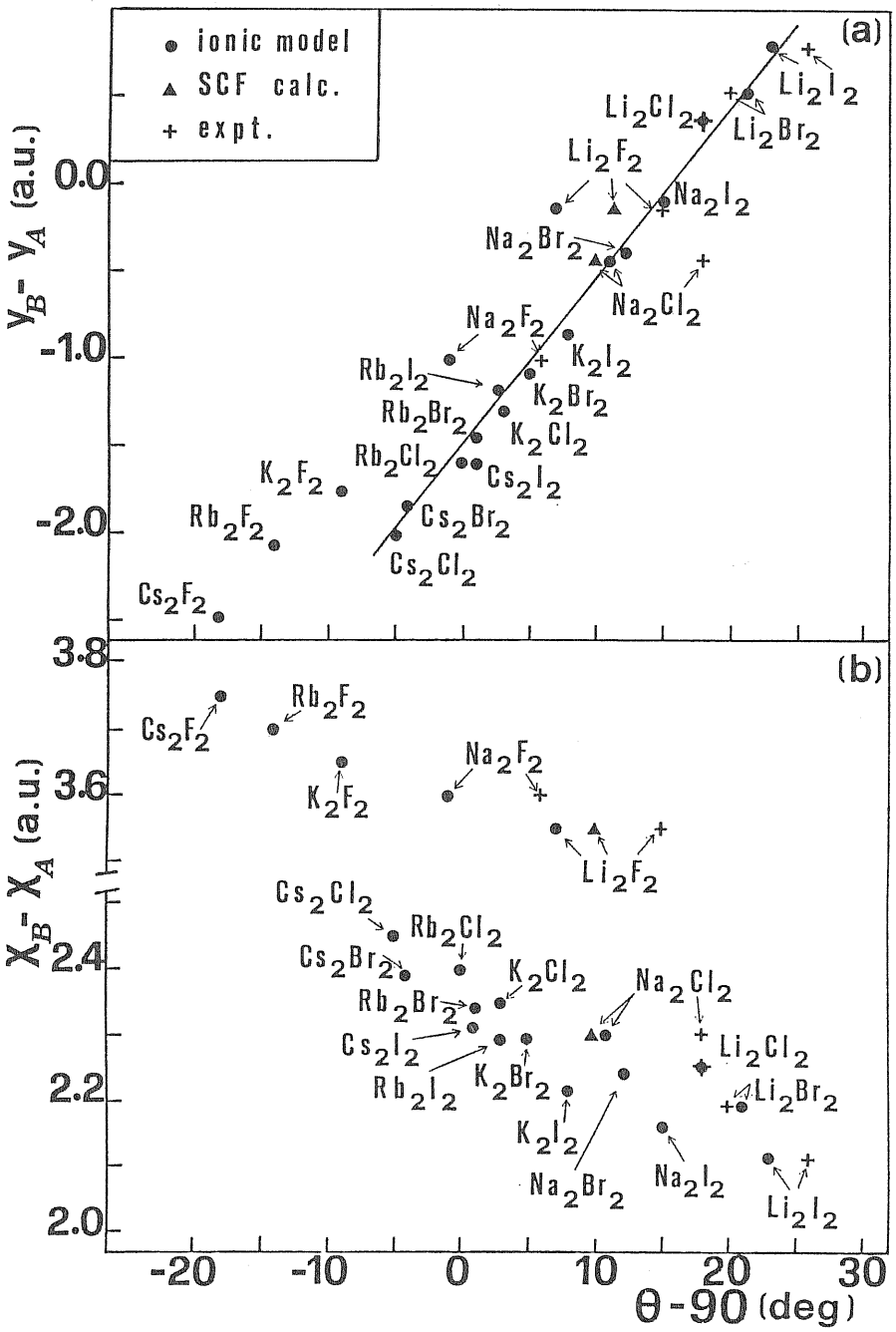

Fig. 4.3 Correlation between the bond angle $\theta = BAB$ and respectively, the $Y = y_B - y_A$ coordinate (a) and the $\chi_{AB} = \chi_B - \chi_A$ coordinate costructed from Petifor's chemical scale (b) for alkali dihalides molecules A_2B_2 molecules. The result of ionic model calculations are from ref. 75. Those of Hartree-Fock-Self- Consistent-Field calculations are from ref. 18 and 73 for Na_2Cl_2 and Li_2F_2 respectively.

As in the case of AB_2 compounds, we have looked at trends in the values of the bond angles. The statistics is rather poor for A_2B_2 molecules, and only in the case of alkali dihalides a trend can be identified, since experimental information[73] can be implemented with the results of ionic models[75]. For double octet AB_2 molecules, Y was found to be related to the tendency to bend. In the case of tetramers, it is natural to look at the deviation of the bond angle θ from 90 degrees, i.e., at the distortion from the ideal square shape. Fig. 4.3(a) indicates that a linear relationship exists between θ and the parameter Y ; since the latter measures the mismatch of the average core radii of the two atomic species, it can again be related to the ionicity of the compound. A similar correlation is found with the ZC coordinate Y_{ZC} and also with both the differences of the Pauling Radii[38] of the two ions and , as shown in ref. 75, of the Tosi-Fumi[76] radii. This simple correspondence seems to be lost when we use Pettifor's chemical scale to construct our structural coordinate in Fig. 4.3(b).

4.3 AB_3 solids

We turn now to apply to crystal structures the same classification schemes that we have adopted for AB_3 molecular shapes. Once more we divide compounds with $N = 24$ from those with $N < 24$.

Amongst the former, only 19 compounds of non transition elements are structurally determined[44,55]. These are the trihalides of elements belonging

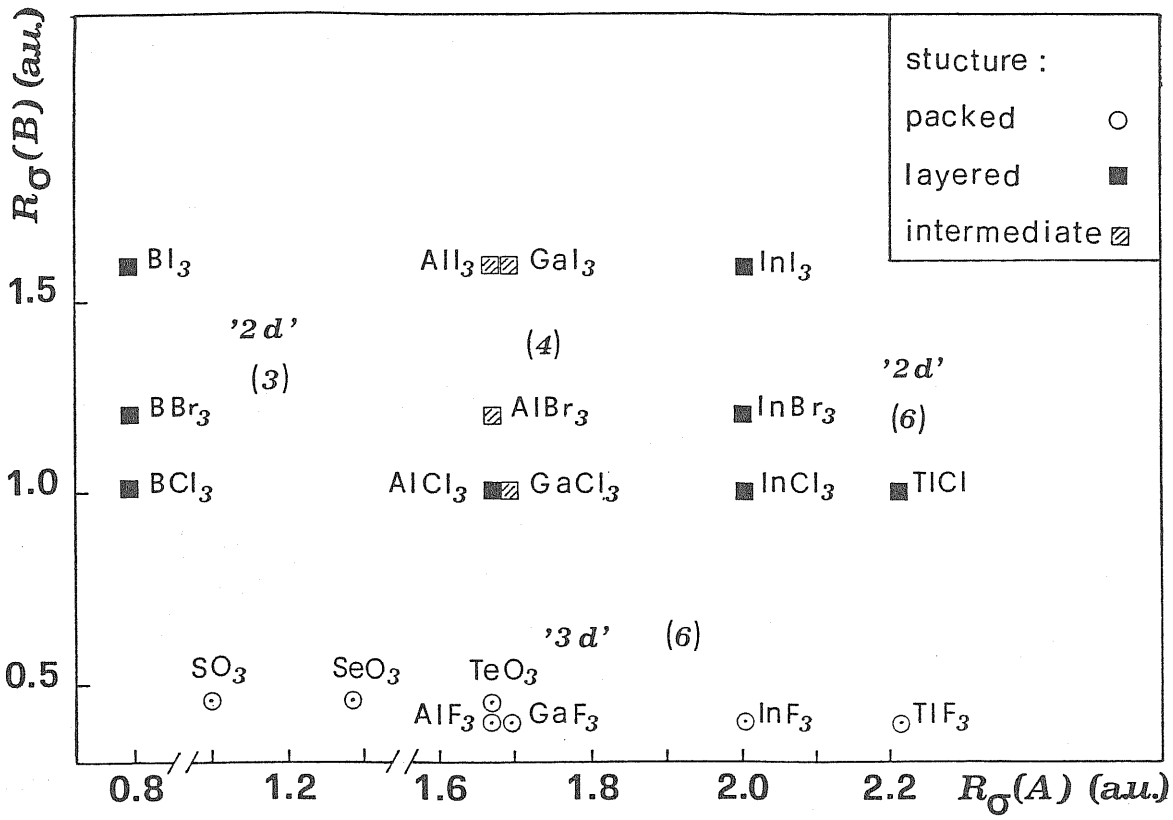

Fig. 4.4 Elemental coordinates plot, based on pseudopotential radii, for AB_3 solids with $N = 24$.

to group III and the trioxides of S, Se and Te. As indicated in fig. 4.4 and 4.5, they appear in different domains of the plots , depending on whether the atomic configuration is layered or not (full/empty symbols) and on the A atom coordination number (CN). Shaded symbols label crystals with a kind of "intermediate" structure[55]. All of them are polycompounds of the type A_2B_6; they have a monoclinic structure, exception made for $GaCl_3$ which is triclinic with CN= 4. In relation to fig. 4.4, Y is again seen to correlate with

the coordination number: in the upper part of the plane we find the trihalides of boron, which are hexagonal layers with CN= 3; at more negative values of Y are placed the intermediate structures with CN= 4. Finally, crystals with CN= 6 are found to have large negative values of Y, and are correctly separated into three and two dimensional (3D and 2D) compounds. It is interesting that InI_3 which is found in both the layered (red modification) and in the intermediate (yellow modification In_2I_6) configurations is indeed found at the border between the 2D and the intermediate structure domains in both figures 4.4 and 4.5. With reference to the 3D compounds, we remark that Villars[44] classifies SO_3 and SeO_3 as tetragonal SeO_3 structures, while TeO_3 as a $CuNi_3$ structure. Amongst the three-fluorides, they are classified as VF_3 structures, with the exception of TlF_3 (YF_3 structure), by Hulliger[55]. Although we have not marked explicitly these different crystal structures, it is easy to see that they are correctly separated in our plots. The only structure which is not accounted for in both structural maps of figures 4.4 and 4.5 appears to be $AlCl_3$, which is a layered structure, incorrectly placed in the intermediate domain.

The structural problem for the class of AB_3 compounds with $N < 24$ is definitely more complicated than that for $N = 24$ crystals. This family displays indeed a large variety of crystal structures[43,44,55], several of them having a small number of representatives, and contains also compounds with non-stoichiometric composition and polycompounds. VEOR-based structural parameters can successfully separate crystals with different

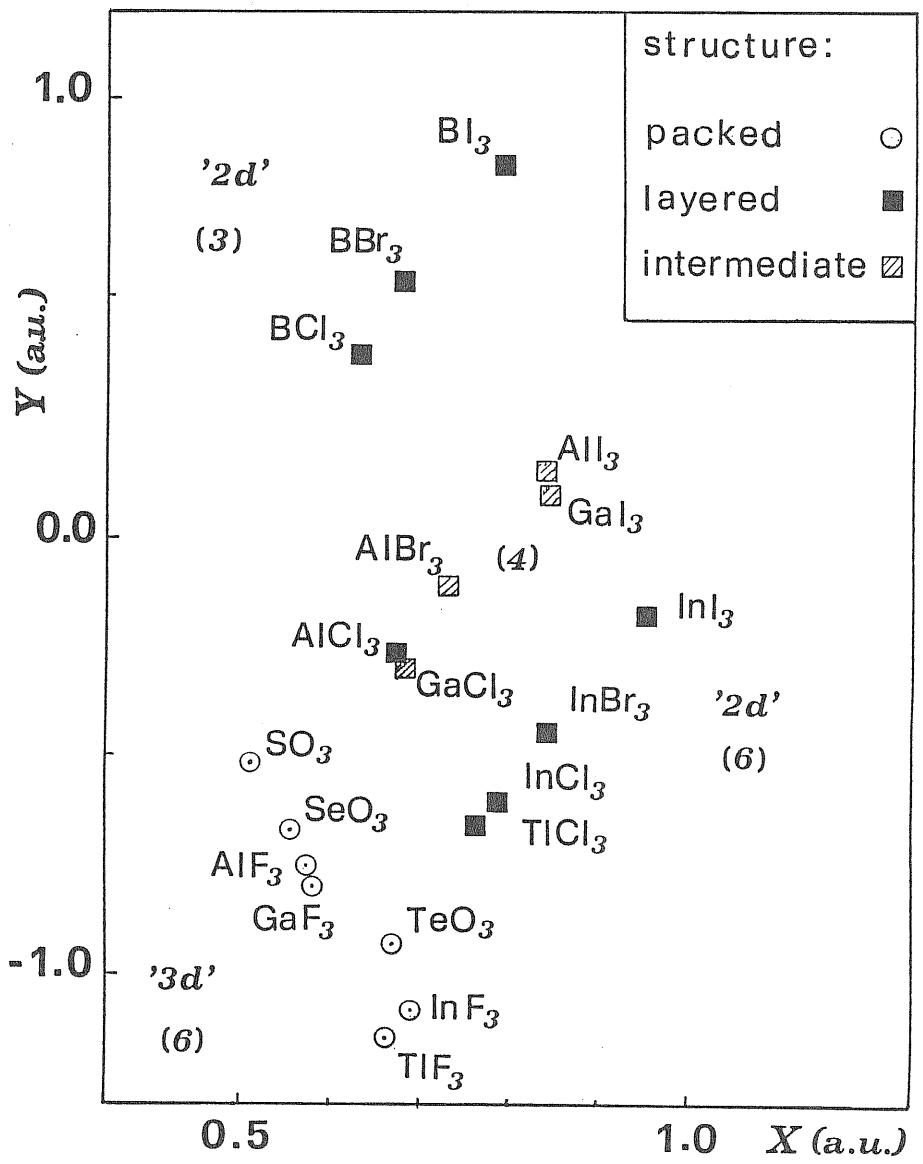

Fig. 4.5 Compound coordinates plot, based on nodal radii, for AB_3 solids with $N = 24$.

coordination numbers and distinguish 3D from 2D atomic arrangements. Intermetallic phases with CN= 14, 12, 11 are clearly distinguished from each other and separated from solids having coordination number from 6 to 8.

Amongst these the layered compounds, which have CN= 6, appear in a separate domain. Several different crystal structures are also resolved in VEOR-based plots. However, not all of the different ordered and disordered arrangements displayed by intermetallic compounds find a clear distinction in our structural maps. Another difficulty which we have encountered concerns compounds containing first row elements, namely lithium and beryllium. They are misplaced in both the pseudopotential and nodal radii plots. The reasons of these difficulties, not at all surprising due to the complexity of the problem, need further investigation in order to be completely understood.

Chapter 5

STABILITY AND IONIZTION INDUCED STRUCTURAL TRANSITIONS IN SODIUM CHLORIDE MICROCLUSTERS: $Na_2Cl_2^{(+)}$ AND $Na_2Cl^{(+)}$

We now turn to introduce and then discuss the results of our ab initio investigation of the sodium chloride microclusters $Na_2Cl_2^{(+)}$ and $Na_2Cl^{(+)}$, as well as those of our test calculations for the neutral and ionized monomer $NaCl^{(+)}$.

Characterization through mass spectra or time-of-flight measurements hinges on ionization via electron impact or photons. Thus direct information on cluster stability refers to ionized species. Fig. 5.1 shows a mass spectrum of clusters formed by quenching NaCl vapours in He gas and ionizing them with a low energy electron source. Two kinds of aggregates can be seen,i.e. $(Na_nCl_n)^+$ and the more intense series $(Na_nCl_{n-1})^+$. The intensity of a given line in a mass spectrum is influenced by many factors : the stability of the neutral clusters entering the ionization chamber, the cross section for ionization, the probability of fragmentation and finally the stability of the ionized products. However, the observation of a large abundance of halogen deficient aggregates relative to the stochiometric ones

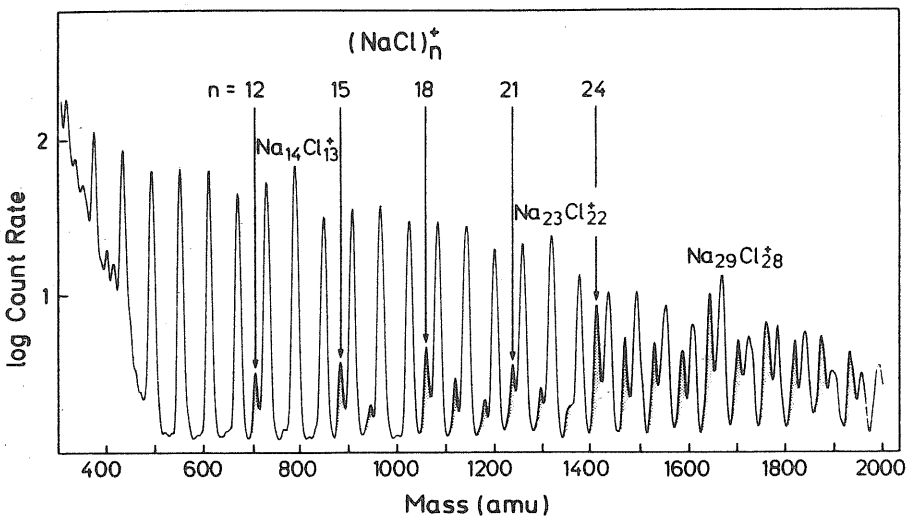

Fig. 5.1 Mass spectrum of sodium chloride clusters formed by quenching NaCl vapor. (From ref. 17)

can be readily understood in an ionic model, where one assumes that the electron is removed upon ionization from a specific chlorine ion and that the resulting chlorine atom is only weakly bound to the $(Na_nCl_{n-1})^+$ cluster. Indeed, cluster ions of composition $(Na_nCl_n)^+$ are observed only if the temperature of the condensed vapours is low enough[78], so that the vibrations of the neutralized halogen do not lead to dissociation when the Coulomb attraction is changed into the weaker induced dipole interaction. Alkali halides clusters have also been produced by low-flux rare gas sputtering of the corresponding crystals and then detected by the method of secondary ion mass spectroscopy (SIMS)[79]. In agreement with the results discussed above, the SIMS positive spectra show two series of aggregates, the most prominent of which corresponds again to the non-stoichiometric clusters $(M_nX_{n-1})^+$.

Alkali halide clusters M_nX_m of a broad size range have been obtained from vapour condensation by either adiabatic expansion[77] or cooling through an inert gas[17,78]. Experimental characterization of the ionization process of (M_nX_{n-1}) neutral systems has been recently achieved for the dialkali monohalide molecules [77]. These have been generated in supersonic nozzle beams, which result from an adiabatic expansion of high temperature vapours containing alkali metal and alkali halides. Vertical ionization potentials of several $MM'X$ species have then been determined by photoionization threshold measurements.

In spite of the growing wealth of experimental data, ab initio theoretical investigations on ionic aggregates are still few and often limited to small neutral aggregates. Most of them have been carried out in the Hartree-Fock approximation. Amongst the alkali halide dimers, only lithium fluoride has been studied by ab initio methods (see C. P. Baskin *et. al.* in ref.73), with the major aim of assessing its ground state equilibrium geometry. As far as triatomic aggregates are concerned, only the alkali bihalide molecules MX_2 (M = Li, Na; X = F, Cl) have been investigated[80], in order to examine their stability against dissociation into $MX + M$. Very recently Dunlapp[82] has reportd the results of ionic model and ab initio (both Hartree-Fock and Local density) calculations for nine atom cluster ions of LiF, LiI, NaI, KI, RbI, CsI and sodium halides, which show that the most stable structure for these systems is invariably a slightly puckered plane.

Ionic model calculations on neutral and ionized aggregates (M_nX_n)

and $(M_nX_{n-1})^+$ of several sizes and composition have been reported by Martin[17,81]. Many features in cluster mass spectra can be qualitatively explained by these model calculations. They also allow a partial understanding of the ionization processes, under the assumption that the electron removed upon ionization is taken out from a specific ion. The equilibrium structures for many of the neutral and charged aggregates examined by Martin turn out to be significantly dependent on the details of the model[81]. In particular, if the Born-Mayer model is refined by the inclusion of polarization forces, crucial changes in the symmetry of the ground state equilibrium geometry of several clusters are found. Progress in this approach would seem to depend on the development of interatomic potentials derived from ab initio calculations[83].

We have studied the equilibrium properties of $(NaCl)_2$ and Na_2Cl in both neutral and ionized states within the Hartree-Fock (HF) approximation[18]. Our calculations are focused on the ionization processes and demonstrate that they involve symmetry breaking in both $(NaCl)_2$ and Na_2Cl. Specifically, a linear Na_2Cl^+ species is the final product of both the ionization of Na_2Cl and the ionization plus dissociation of Na_2Cl_2, the dissociation process of $(Na_2Cl_2)^+$ into $(Na_2Cl)^+$ and a chlorine atom requiring, in fact, very little energy. An ionic model is quite consistent with the molecular orbital picture of the bond that we obtain for the dimer. This is no longer the case for the neutral dialkali chloride species and thus an ionic model cannot properly account for its ionization process.

Our calculations use a single-configuration Hartree-Fock (SCHF) method to evaluate the electronic ground state of Na_2Cl_2, $Na_2Cl_2^+$, Na_2Cl and Na_2Cl^+ in a number of different structures. Sufficient information is available from experiment for the very small NaCl aggregates to establish to which extent the description we use for the bond is reliable. In particular, experimental data are available on dissociation energies relative to various reaction paths [77,84], on ionization potentials [17] and also on structural parameters in the case of the sodium chloride dimer [85].

In addition, the validity of the SCHF approach for the description of the equilibrium properties has been tested in the case of NaCl and $NaCl^+$, against the results of generalized-valence-bond configuration-interaction (GVB-CI) calculations[19]. A brief description of the GVB and CI approximations is reported in Appendix I. Some details of the computational method which we have used are described in section 5.1 of this chapter. The results of our GVB-CI calculations for the monomers are presented in section 5.2, while those for $Na_2Cl_2^{(+)}$ and $Na_2Cl^{(+)}$ are reported in section 5.3 and 5.4 respectively. Further discussion of these results in section 5.5 concludes the chapter.

5.1 Method

All our calculations have been carried out in a pseudopotential scheme. More specifically, the Coulomb,exchange and core orthogonality effects of the assumed chemically inert core electrons of both sodium and chlorine

have been replaced by the ab initio effective core potentials (ECP) reported by Wadt and Hay[86]. These pseudopotentials have been derived for most elements of the periodic table from all-electron numerical HF atomic wavefunctions and fitted to analytical representations for use in molecular calculations. The procedure for generating an ECP from ab initio numerical wavefunctions is similar to that reported in chapter 2, section 2.1, for generating the ZC pseudopotentials[9]. The essential difference between the two approaches lies in the approximation chosen to solve the AE atomic Schroedinger equation: HF in the case of ECPs and LDA for deriving ZC pseudopotentials. We notice that in the ECP scheme the Na and Cl valence electrons are defined to belong to the outermost s and p orbitals.

Wadt and Hay[86] have presented a number of tests on the accuracy of their ECP. In particular, they compare the results of calculations for the energy curve of the NaCl molecule, at the GVB(1) level (see Appendix I), as carried out in an all-electron scheme and in the pseudopotential scheme. The agreement between the two calculations is excellent, the relative errors being 0.5% in the equilibrium distance R_e and 1% in the binding energy D_e. Further tests have been made on the Na and Cl atoms. In our calculation of the total energy of sodium, which in an ECP approach coincides with its first ionization potential (IP), we find for the latter the value of 4.91 eV, in satisfactory agreement with the measured value of 5.12 eV. With regard to Cl, Wadt and Hay report a comparison between all-electron and ECP calculations of its electron affinity. Though the experimental value, 3.6 eV,

is understimated by 16-17% in both calculations, owing to the small number of configurations employed, the agreement between the two results is at the level of 1%. The choice of the basis set used in our calculations has been based again on the work of Wadt and Hay and is consistent with the choice of the pseudopotentials.

It consists of energy optimized s and p primitive gaussians for both sodium and chlorine, constructed for use with ECP's, to which a further p function to describe the negative ion as well as d polarization gaussians on Cl are added. The $(s+p)$ gaussian sets reported in ref. 86 for Na and Cl are built up in the following way . Initial guesses for the exponents of each primitive function are determined by a least squares fit to the atomic pseudo-orbitals. Then the exponents to be used in molecular calculations are obtained by energy optimization of the atomic ground state. The valence p basis for sodium is derived by energy optimization of the $s^1p^1(^3P)$ excited state. The complete basis set which we have used is Na$(3s,3p)$, Cl$(3s,4p,1d$), where the figures indicate the number of gaussians used to represent each wavefunction of given z-component of the angular momentum. There are therefore 12 gaussians for the Na atom (three s and nine p) and 21 gaussians for the Cl atom (three s, twelve p and six d).

5.2. Results for NaCl and $NaCl^+$

The alkali halides molecules in the neutral state have been the subject of numerous experimental and theoretical investigations[83,87,88]. Much of the theoretical interest in these systems derives from the behaviour of their two lowest adiabatic potential curves as functions of the internuclear distance : they display an avoided crossing with an interchange of ionic and covalent character and, hence, show a nonadiabatic behaviour. The ionic dissociation limit, $M^+(^1S) + X^-(^1S)$ is usually the first excited dissociation limit above the ground state atoms, $M^+(^2S) + X^-(^2P)$. The energy difference ΔE between these two limits is determined by

$$\Delta E = (ionization\ potential)_M - (electron\ affinity)_X.$$

At large internuclear distances, the potential curve arising from the interaction of the ions to give a $^1\Sigma^+$ state behaves as $\Delta E - \frac{e^2}{R}$ (relative to the energies of the separated atoms), while the covalent potential curve, again of $^1\Sigma^+$ symmetry, arising from the ground state atoms varies very slowly at large R. Consequently, if the interaction between the ionic and covalent curves is ignored, they are expected to intersect at $R = R_x = \frac{e^2}{\Delta E}$. On the other hand, if the electronic structures are allowed to relax by optimal mixing of ionic and covalent configurations, no intersection between these two $^1\Sigma^+$ potential curves is expected, leading to a sharp bending away

(avoided crossing) in the potentials curves. A concomitant sharp change in the electronic configurations takes place at about R_x. This, in turn, induces large variations in terms neglected in the adiabatic approximation, namely the operators:

$$< 1^1\Sigma^+|\frac{\partial}{\partial R}|2^1\Sigma^+ > \frac{\partial}{\partial R}$$

and

$$< 1^1\Sigma^+|\frac{\partial^2}{\partial R^2}|2^1\Sigma^+ > \frac{\partial}{\partial R}$$

Thus in alkali halides molecules a nonadiabatic behaviour is expected at internuclear distances of about R_x.

To our knowledge, two thorough studies of the ground and excited states of alkali halides molecules have been reported in the literature. Both of them have been carried out by ab initio configuration interaction methods. Kahn *et. al.*[88] have calculated adiabatic potential curves for the four lowest $^1\Sigma^+$ states of the LiF molecule, from which a set of diabatic curves are generated, by a procedure based on the Rittner model[89] of the ionic state. Very accurate calculations for the ground and first excited states of the NaCl monomer have recently been reported by Clementi and coworkers[83]. They involve systematic distance by distance basis set optimizations and a very large number of configurations.

We have carried out CI calculations of the total energy of the NaCl

Table 5.1 Master reference configurations set for NaCl. Each of the n configurations listed ,except the first, is specified as single excitation relative to the ground state electronic configuration $A(1\sigma^2 2\sigma^2 1\pi^4)$.

n	Configuration
1	$A(1\sigma^2 2\sigma^2 1\pi^4)$
2	$2\sigma \rightarrow 3\sigma$
3	$2\sigma \rightarrow 4\sigma$
4	$2\sigma \rightarrow 5\sigma$
5	$2\sigma \rightarrow 6\sigma$
6	$1\pi_x \rightarrow 2\pi_x$
7	$1\pi_x \rightarrow 3\pi_x$
8	$1\pi_y \rightarrow 2\pi_y$
9	$1\pi_y \rightarrow 3\pi_x$

Table 5.2 Master reference configurations set for $NaCl^+$. Each of the n configurations listed ,except the first, is specified as single excitation relative to the ground state electronic configuration $A(1\sigma^2 2\sigma^2 1\pi^3)$.

n	Configuration
1	$A(1\sigma^2 2\sigma^2 1\pi^4)$
2	$2\sigma \rightarrow 3\sigma$
3	$2\sigma \rightarrow 4\sigma$
4	$2\sigma \rightarrow 5\sigma$
5	$2\sigma \rightarrow 6\sigma$
6	$1\pi_x \rightarrow 2\pi_x$
7	$1\pi_x \rightarrow 3\pi_x$

molecule in both the neutral and ionized state[19]. Our calculations are limited to the ground state potential curves, since we are mainly concerned with the equilibrium properties of the two systems, to be compared with the corresponding quantities computed by the SCHF method. These calculations have been performed with CI wavefunctions including all single and double excitations (1+2) from self consistent generalized valence bond orbitals (see Appendix I). Table 5.1 lists the set of correlated pairs which we have included at the GVB level, usually referred to as the master reference set. All but the 3s valence electrons of chlorine, which give rise to the 1σ orbital, are explicitly correlated. Excitations from the 2σ orbital describe bond electron correlations, while those from the π_x and π_y orbitals account for correlations involving electrons out of the bond. A CI wavefunction has then been constructed from all (1+2) excitations relative to the reference set of table 5.1. The master reference set used for the $^2\Pi$ ground state of the ionized monomer is given in table 5.2. Only correlations involving doubly occupied orbitals are explicitly considered.

At the equilibrium internuclear distance, which is calculated to be $2.41\mathring{A}$ against the measured value $R_e = 2.36\mathring{A}$, the ground state of NaCl is characterized, as expected, by a highly ionic bond. A shift of the electronic charge of 0.85e from the metal to the halogen is estimated from GVB results on Mulliken populations, the charge density being polarized in the direction opposite to the charge shift. Table 5.3 reports our calculated equilibrium properties for the neutral molecule with both SCHF and CI

Table 5.3 Hartree-Fock (HF) nd Configuration-Interaction (CI) results for some equilibrium properties (bond distance R_{eq}, dissociation energy with respect to the free atoms E_0 and dipole moment μ) of the neutral NaCl molecule, compared with the corresponding experimental values.

Equilibrium Properties	HF	CI	Expt.†
R_{eq} (Å)	2.40	2.41	2.361
E_0 (eV)	3.22	3.78	4.23
μ (Debye)	10.0	10.0*	9.002

† from ref.98
* GVB result

wavefunctions. The equilibrium distance is essentially insensitive to the inclusion of electronic correlations. On the other hand, if we estimate the correlation energy of the molecule E_{corr} from the relation :

$$E_{corr} = |E_{HF} - E_{CI}|$$

where E_{HF} and E_{CI} are the total energies of the monomer computed respectively within the SCHF and CI approximations, it turns out to be almost constant for values of R near R_{eq}. While SCHF wavefunctions yield quite accurately the equilibrium distance, the inclusion of correlation is crucial in determining the binding energy of the molecule. Our CI value, though a significant inprovement on the HF one, is still an understimate of the experimental value. This is a consequence of our understimation of the chlorine atom electron affinity. A much larger number of configurations than

we have used should be included in constructing the total wavefunction, in order to eliminate the discrepacy with experiment, as shown by Clementi *et. al.*[83]

With regard to the calculated dipole moment $\mu(R)$ of the molecule as a function of R, we may attempt a contact with phenomenological models such as the well known Rittner model[89], by subtracting from it the value eR associated with the full transfer of one electron from the metal to the halogen atom. The residue can be interpreted as an electron dipole moment associated with the deformation of the closed shells of a supposed Cl^- component of the molecule.An effective polarizability $\alpha_-(R)$ of such a Cl^- ion can hence be estimated after multiplication by R^2. It is pleasing to find that α_- around $R = 3\mathring{A}$ has a value of the order of $3\mathring{A}^3$, which is similar to that determined from refractive index data for the polarizability of Cl^- in alkali halide crystals[63], and that $\alpha_-(R)$ decreases rapidly with decreasing R, undoubtely because of quenching of ionic deformability from overlap effects. However, at a more quantitative level (GVB), the dipole moment at $R = R_{eq}$ is an overstimate of the experimental value (10.0 vs. 9.0 Debye). This means that our GVB approximation for the wavewfunction as well as the HF one, sligthly overstimate the ionicity of the molecular bond. Very preliminary calculations, again performed in a pseudopotential framework, seem to indicate that the opposite is true in the LD approximation of the Density Functional Theory. In the latter case the dipole moment is found to be 8.2 Debye against the measured value of 9.0 Debye.

The $^2\Pi$ ground state of the molecular ion $NaCl^+$, obtained by removing an electron from the highest π orbital of the NaCl molecule, is found to be rather weakly bound. The minimum at the equilibrium bond length, calculated as $R_{eq} = 2.95\mathring{A}$, is very shallow, in accord with the observation of broad bands in photoelectron spectra[90]. In a vertical ionization process the electron which is being removed is highly localized on the chlorine site, as can, e.g., be deduced from a Mulliken Population analysis. When the molecule relaxes towards equilibrium after ionization, a very tiny shift of electronic charge from the chlorine atom to the sodium ion is seen to take place : however, the hole left by the ionization process is essentially localized on chlorine and the molecular bonding arises primarily from the polarization of the chlorine atom in the field of the sodium ion. The Mulliken population on the Chlorine site varies from 6.96e at $R = R_e(NaCl)$ to 6.94 at $R = R_e(NaCl^+)$, to increase then rapidly toward its dissociation limit value of 7.0e at larger internuclear distances.

As in the case of the neutral molecule, the equilibrium geometry is found to be insensitive to the inclusion of electronic correlation. The calculated R_{eq} is the same with either CI or SCHF wavefunctions. On the other hand, correlation effects are crucial in the calculation of ionization potentials.The HF approximation understimates both the vertical (VIP) and the adiabatic (AIP) ionization potentials by more than 1 eV. Indeed the SCHF calculated values are 8.18 eV and 7.92 eV for the VIP and AIP respectively, against the measured values (see, e.g.,K. D. Jordan in ref. 87) of 9.34 eV and 8.93

eV. In our CI calculation we obtain instead 8.78 eV and 8.52 eV. Though the latter values constitute an improvement on the HF ones, they are still understimates of the experimental data, again because of our understimate of the chlorine electron affinity.

5.3 Results for Na_2Cl_2 and $Na_2Cl_2^+$

A. Na_2Cl_2

We have calculated the total energy of Na_2Cl_2 in both planar and linear geometries, finding the rhombic structure shown in Figure 5.2 to be the most stable. The Na-Cl bond length d in the dimer slightly increases (by about 7%) with respect to the isolated monomer (see Table 5.4 ; our value for NaCl is $R_e = 2.40$ Å against $R_e^{expt.} = 2.36$ Å).

This is accompanied by a slight decrease of the charge transfer to the halogen, the Mulliken population (MP) on Cl being 7.84 in the dimer against 7.86 in the monomer at equilibrium (cf. MP=7.84_5 in the monomer a R=d). The experimental value for d is obtained from electron diffraction measurements on vapours[85], which however are believed to contain both monomers and dimers in unknown percentage (see J. Berkowitz inref. 87).

Figure 5.3(a) shows the electron density $\rho(\underline{r})$ of Na_2Cl_2 at equilibrium ($D_{2h}, {}^1A_{1g}$ state) in the plane of the bond, referred to that of the free ions. Comparison with a similar charge-difference map for the monomer (Figure 5.3(b)) shows that the bonding of the dimer arises from an accumulation of

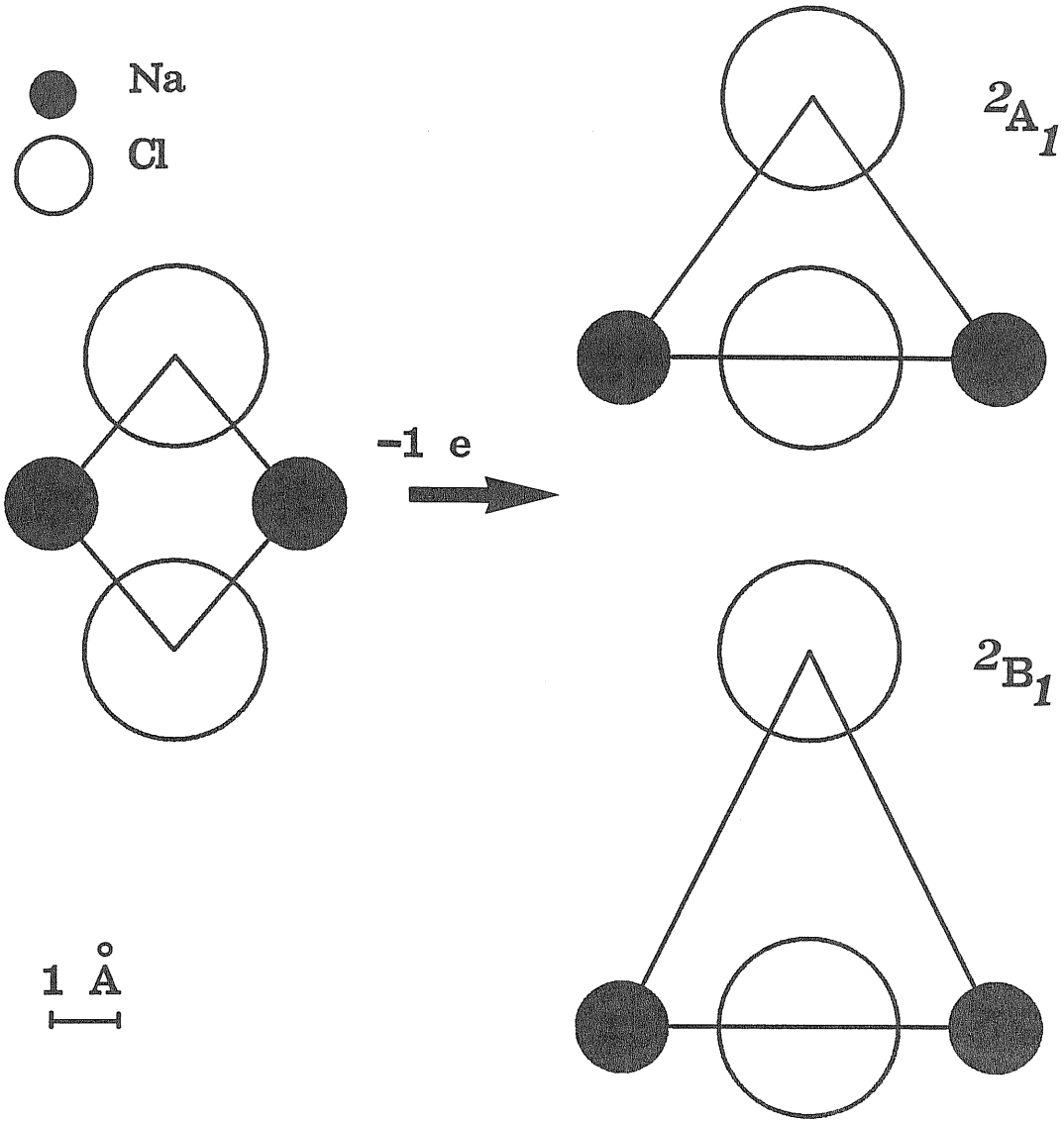

Fig. 5.2 Calculated equilibrium structures of the Na_2Cl_2 molecule (left) and of the $Na_2Cl_2^+$ molecular ion (right). Interatomic distances are on the indicated scale.

electronic charge along the Cl-Cl bond at the expense of polarization charge along the Na-Cl bond in the monomer.

Our calculations yield dissociation energies for Na_2Cl_2 into both free ions and free molecular monomers within about 5% of the measured values[84,91] (see Table 5.4). We also find a metastable state for Na_2Cl_2 in an asymmetric linear configuration (Na-Cl-Na-Cl), at about 0.3 eV above the equilibrium

Table 5.4 Results for Na_2Cl_2 and $Na_2Cl_2^+$

Compound	$d_{(NaCl)}$(Å)		Θ_{NaClNa}(deg)		D_e^i(eV)[a]		D_e(eV)[b]		IP(eV)	
	calc.	*expt.*	*calc.*	*expt.*	*calc.*	*expt.*	*calc.*	*expt.*	*calc.*	*expt.*
									vertical	
Na_2Cl_2 (D_{2h},$^1A_{1g}$)	2.566	2.50[c]	80	72[c]	13.05	13.6±9 [d]	2.14	2.04[e] 2.24[f]	9.89	10.3[g]
									adiabatic	
									8.10	/
$Na_2Cl_2^+$ (C_{2v},$^2A_1$)	(2.50,4.26)	/	(180,72)	/	7.63	/	0.04	0.07[d]		
$Na_2Cl_2^+$ (C_{2v},$^2B_1$)	(2.50,5.59)	/	(180,53)	/	7.60	/	0.01	0.07[d]		

[a] $D_e^i(Na_2Cl_2)=|E(Na_2Cl_2)-2\times E(Na^+)-2\times E(Cl^-)|$

$D_e^i(Na_2Cl_2^+)=|E(Na_2Cl_2^+)-2\times E(Na^+)-E(Cl^-)-E(Cl)|$

[b] D_e=dissociation energy with respect to the most stable products:

$D_e(Na_2Cl_2)=|E(Na_2Cl_2)-2\times E(NaCl)|$

$D_e(Na_2Cl_2^+)=|E(Na_2Cl_2^+)-E(Na_2Cl^+)-E(Cl)|$

[c]ref.85; [d]ref.91; [e]ref.84; [f]ref.84; [g]ref.17.

configuration. Figure 5.4 shows the minimum energy path in the (d, θ) coordinates around equilibrium. Evidently, along this path the energy varies strongly with the bond angle, which, however, correlates only weakly with the Na-Cl bond length.

B. Vertical ionization

The level diagram of the sodium chloride dimer is shown in Figure 5.5

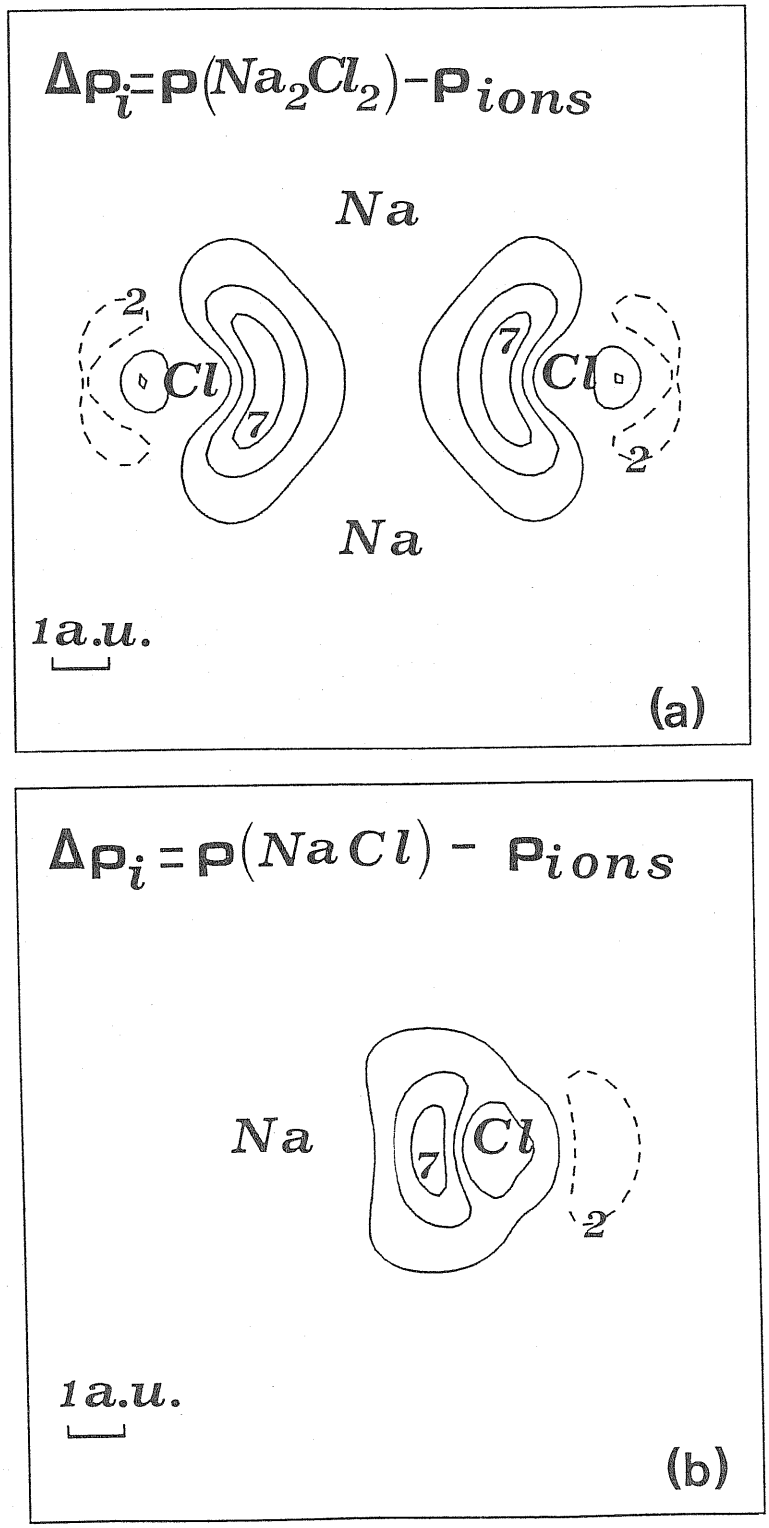

Fig. 5.3 Charge density $\Delta\rho_i$ of the neutral species referred to that of the free ions, $\rho_{ions} = \Sigma_k(\rho(\mathrm{Cl}_k^-) + \rho(\mathrm{Na}_k^+))$, for the dimer (a)) and the monomer (b)). Contour values are in units of $0.001e/(a.u.)^3$, with spacing of $0.003e/(a.u.)^3$. Here and in the following figures of density maps, dashed lines refer to negative values, while solid lines refer to positive values of the electron density; symbols indicate the positions of the nuclei.

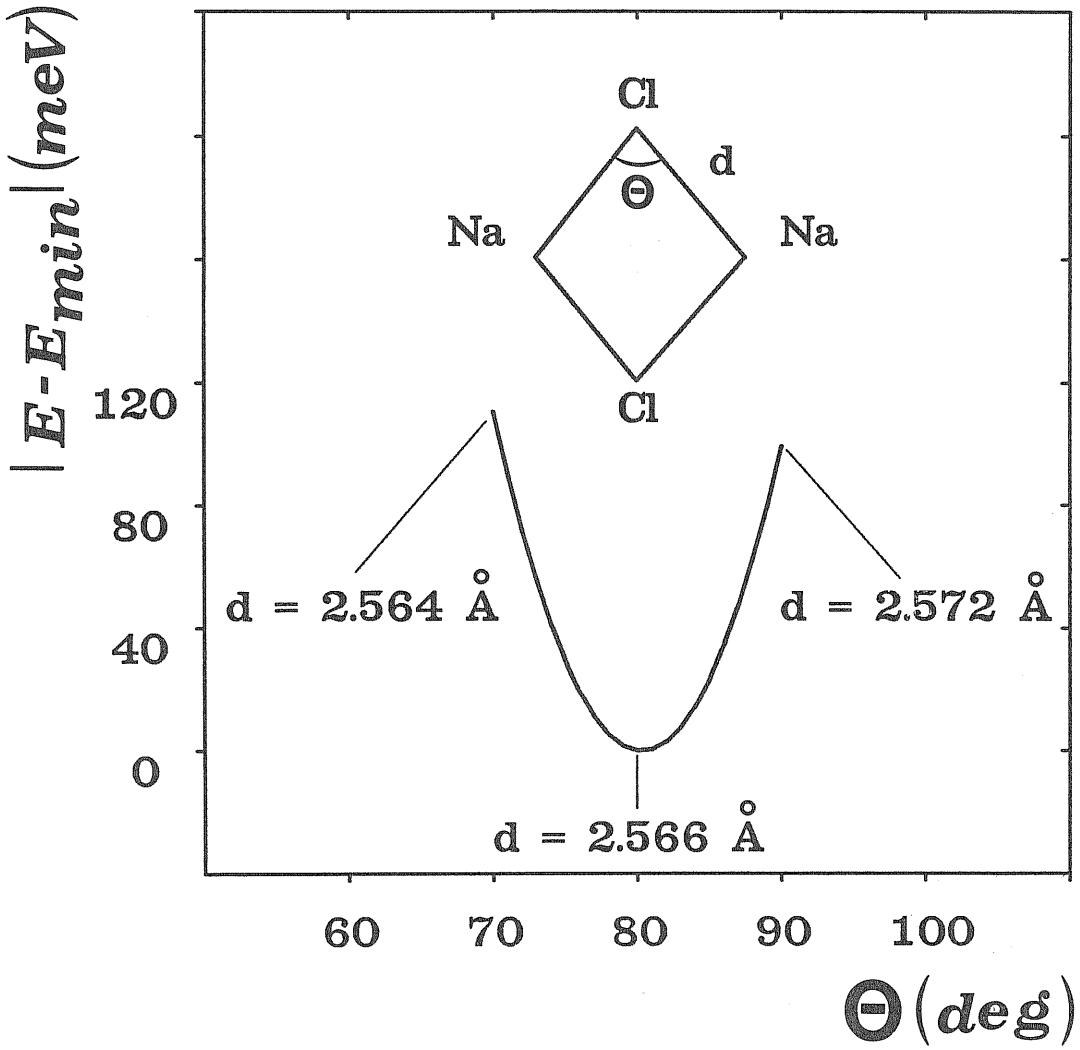

Fig. 5.4 Minimum energy path for the Na_2Cl_2 dimer.

and compared with those of the ionized species with a hole in two different antibonding orbitals, i.e. along the Cl-Cl axis (B_{1u}) and out of the bond plane (B_{2g}). The one-electron energy levels deriving from the p states of chlorine cover a range of about 0.9 eV. Within the "Koopman approximation", the two lowest ionization potentials (IP's) correspond to removal of the electron from the B_{2g} and B_{1u} states (10.56 eV and 10.63 eV, respectively) (see Figure 5.5). Electronic relaxation lowers both IP's by about 0.7 eV and appears to

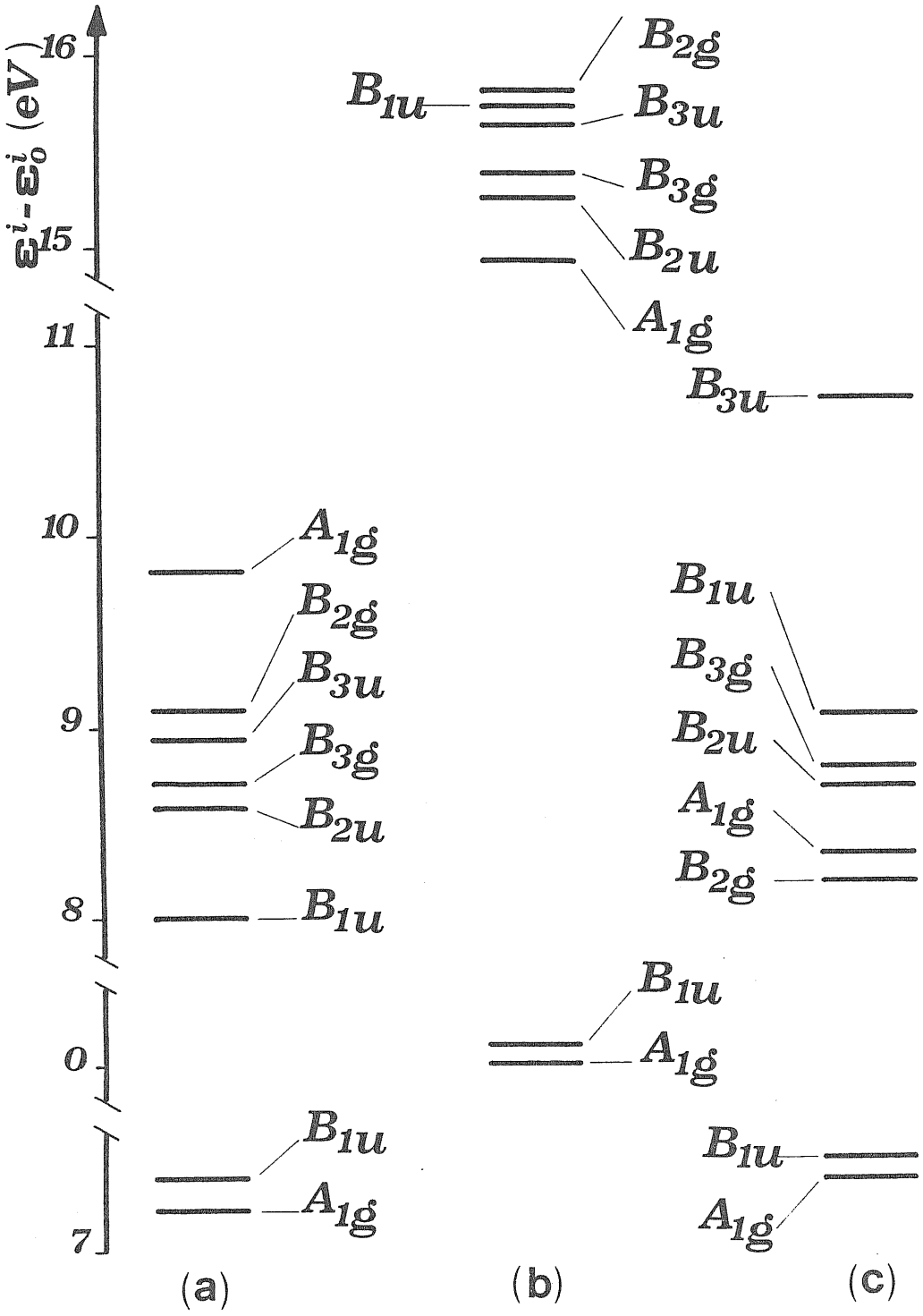

Fig. 5.5 Level diagrams of Na_2Cl_2 (D_{2h},$^1A_{1g}$ state ,b)) and of $Na_2Cl_2^+$ in the same geometrical configuration , in the D_{2h}, $^2B_{1u}$ state (a)) and in the D_{2h}, $^2B_{2g}$ state (c)). Single particle eigenvalues ϵ^i are classified according to the D_{2h} point group and referred to the lowest level, ϵ^i_o, of the neutral dimer.

be stronger for the B_{1u} state.

The distribution of the hole density is shown in Figure 5.6 for both symmetries after electronic relaxation. It is clear that in both cases the hole is localized on the halogens. In order with the HF approximation, the value that we obtain for the vertical IP is lower than the experimental value[17] by about 0.4 eV. This is also a consequence of our understimate of the electron affinity of the halogen.

C. $Na_2Cl_2^+$

If we keep the ionized dimer in the D_{2h} symmetry, its structure relaxes towards a rhombus with a Na-Cl bond length d=2.71 Å and a bond angle of about 120°, the hole being in the B_{1u} orbital. This is a metastable state consisting in essence of a Cl_2^- molecule, with d_{Cl-Cl}=2.65 Å as in the free Cl_2^- ion, but strongly stabilized by the field of the two alkali ions, with a stabilization energy of 7eV. The energy gain relative to the free Cl_2 molecule is as high as 1.64 eV.

On the other hand, an infinitesimal distorsion of the rhombus relative to the Na-Na axis in either the B_{2g} or the B_{1u} state suffices to induce neutralization of one of the chlorines. This drives a symmetry breaking $D_{2h} \rightarrow C_{2v}$, i.e. a structural transition to a triangular shape in both cases (see Figure 5.2). The energy difference between the resulting triangular configurations turns out to be negligible (0.03 eV). As expected, the Cl-Cl distance is much shorter in the $^2A_1$ state (deriving from $^2B_{1u}$(D_{2h})) than

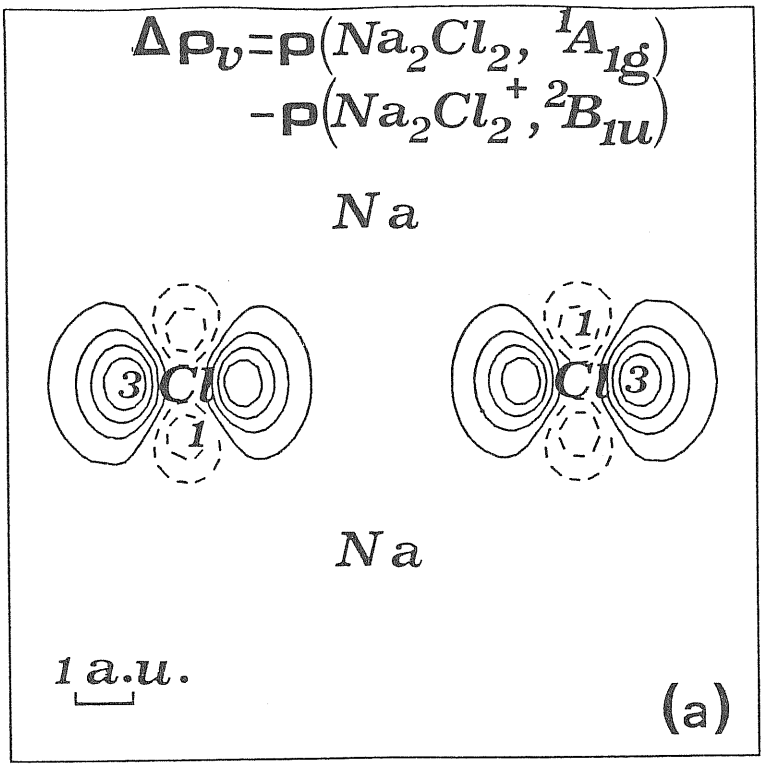

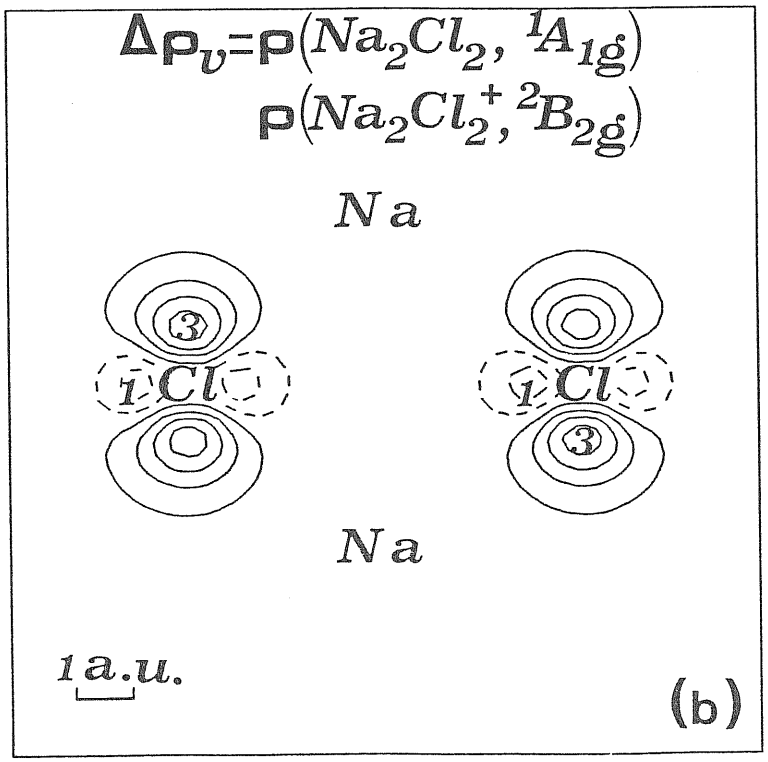

Fig. 5.6 Charge density $\Delta\rho_v$ of the Na_2Cl_2 molecule relative to the $Na_2Cl_2^+$ molecular ion in two states: D_{2h}, $^2B_{1u}$(a), in the bond plane YZ), and D_{2h}, $^2B_{2g}$ (b), in the XZ plane) (see text). Contour values are in units of $0.01e/(a.u.)^3$, with spacing of $0.008e/(a.u.)^3$.

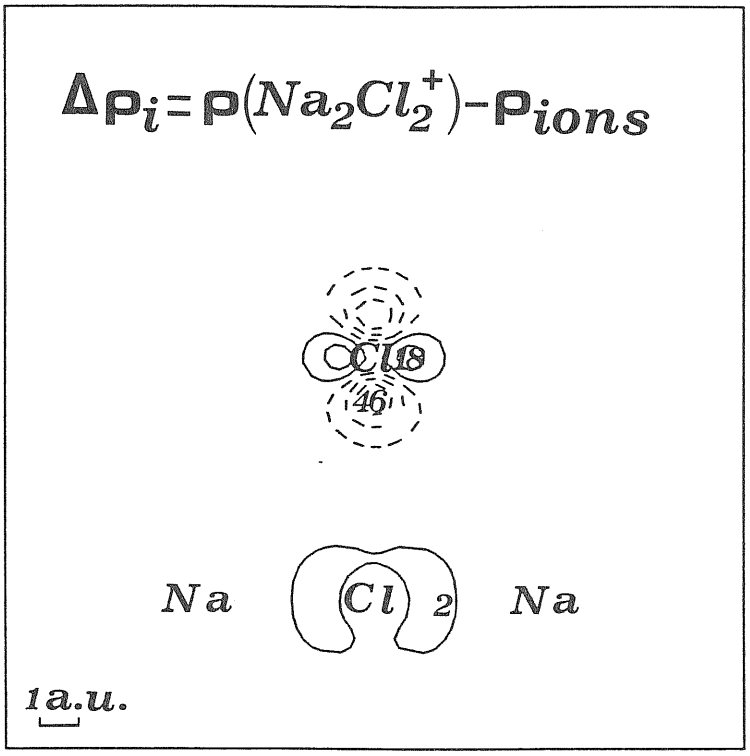

Fig. 5.7 Charge density $\Delta\rho_i$ of the $Na_2Cl_2^+$ molecular ion in the C_{2v}, $^2A_1$ state referred to that of the free ions, $\rho_{ions} = \Sigma_k(\rho(Cl_k^-) + \rho(Na_k^+))$. Contour values are in units of $0.01e/(a.u.)^3$, with spacing of $0.016e/(a.u.)^3$.

in the $^2B_1$ state (deriving from $^2B_{2g}(D_{2h})$). The closest Na-Cl distance shrinks upon ionization and does not depend on the specific state (see Table 5.4). The result of relaxation can be viewed as a linear Na_2Cl^+ cluster with a chlorine atom weakly bound to it, the energy being lower by about 1.8 eV than in the " vertically ionized " species. The MP's on the halogens are 7.00 and 7.79 against 7.84 in the neutral dimer. The localization of the hole is shown in Figure 5.7, which illustrates the charge density of $Na_2Cl_2^+$ in the $^2A_1$ state relative to the free ions.

5.4 Results for Na_2Cl and Na_2Cl^+

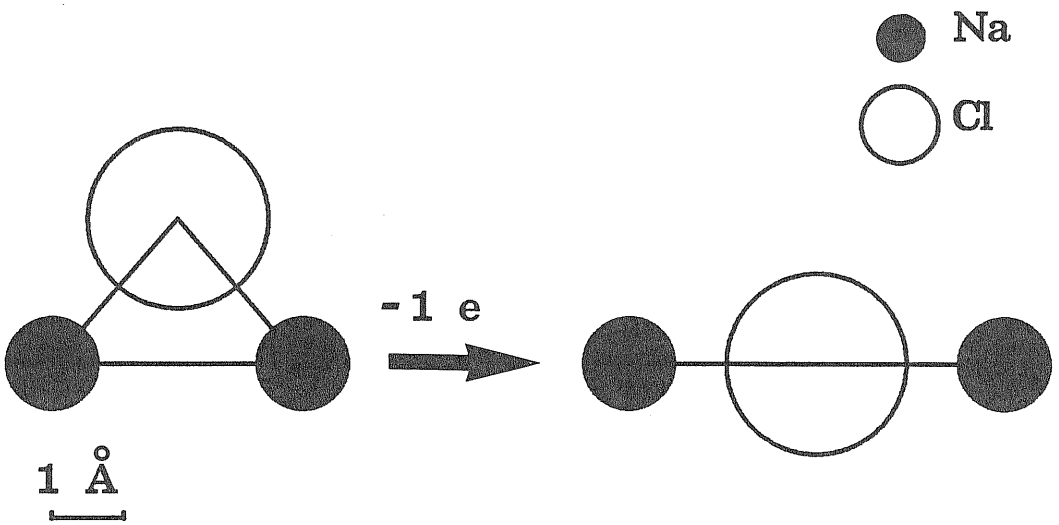

Fig. 5.8 Calculated equilibrium structures of the Na_2Cl molecule (left) and of the Na_2Cl^+ molecular ion (right). Interatomic distances are on the indicated scale.

Figure 5.8 shows the equilibrium structures that we calculate for Na_2Cl and Na_2Cl^+. The numerical results are summarized in Table 5.5. In the following we discuss the different bonding properties that correspond to different geometries and how they are affected by ionization.

A. Na_2Cl

Figure 5.9 reports the electron density of Na_2Cl in three different structures and also the variation of the corresponding total energy with one of the structural parameters. The triangular arrangement in Figure 5.8 is the most stable and, as expected, has slightly less ionic bond character than the others (MP(Cl)=7.81). The highest-lying singly occupied molecular orbital is delocalized and has a strong contribution from *s* orbitals on the two sodium atoms (see Figure 5.9(d)). The binding with respect to NaCl + Na is relatively weak (see Table 5.5).

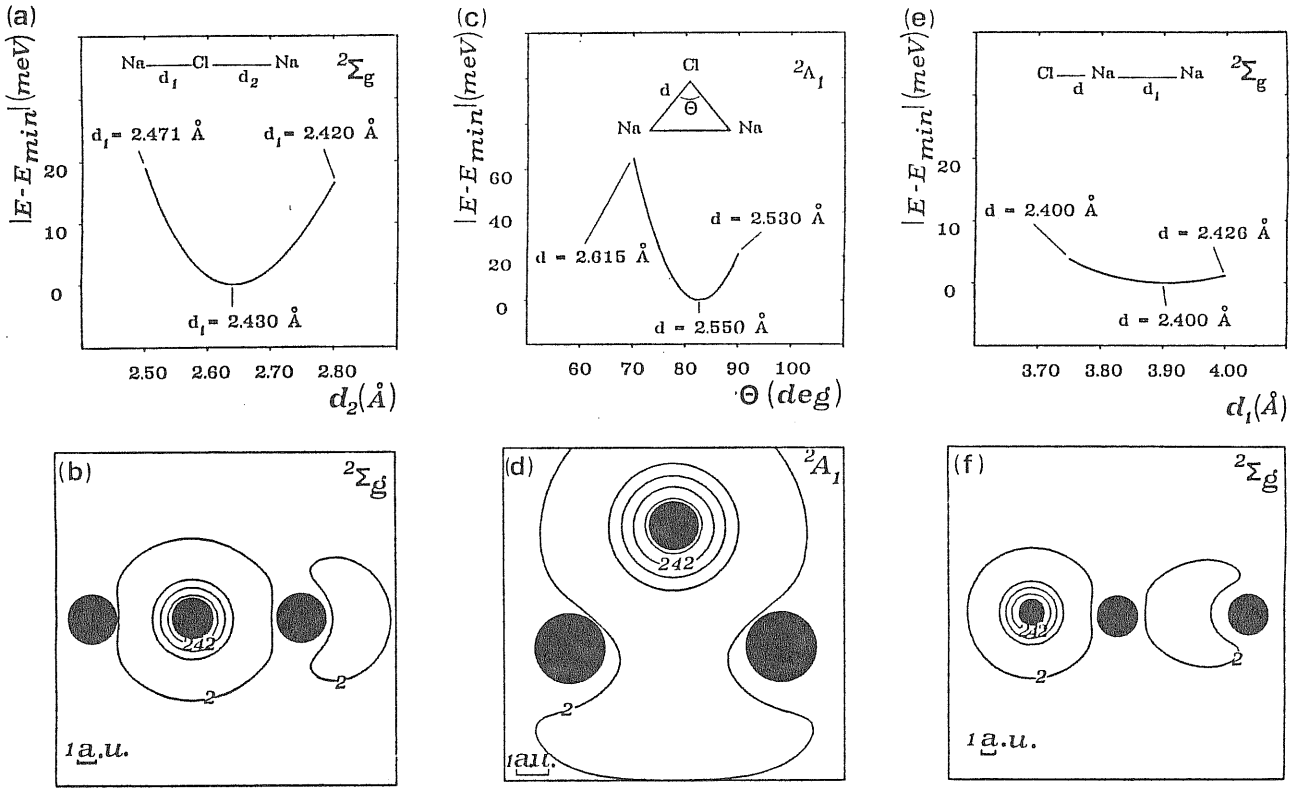

Fig. 5.9 Minimum energy paths for Na_2Cl in the triangular ground state (c)) and in two metastable linear configurations (a) and e)), and corresponding charge density plots (d), b) and f)). Contour values are in units of $0.001e/(a.u.)^3$, with spacing of $0.08e/(a.u.)^3$. Full circles indicate the core sizes of the two atoms (◯ Na, ○ Cl).

Polarization effects are responsible for a weak binding of the NaCl molecule with an essentially "atomic" sodium in the two linear structures shown in Figures 5.9(b) (asymmetric Na-Cl-Na configuration) and 5.9(f) (Cl-Na-Na configuration). In the latter the binding is almost negligible and

Table 5.5 Results for Na_2Cl and Na_2Cl^+

Compound	$d_{(NaCl)}$(Å)	Θ_{NaClNa}(deg)	D_e^i(eV)[a]		D_e(eV)[b]		IP(eV)	
			calc.	*expt.*[c]	*calc.*	*expt.*[c]	*calc.*	*expt.*[c]
							vertical	
Na_2Cl (C_{2v},$^2A_1$)	2.550	82	5.26	5.51±.03	0.74	0.78±.03	4.54	4.1±.1
							adiabatic	
							3.51	/
Na_2Cl^+ ($D_{\infty h}$,$^1\Sigma_g$)	2.50	180	4.43	5.00±.03	2.13	1.80± .20		

[a] $D_e^i(Na_2Cl)=|E(Na_2Cl)-E(Na_2^+)-E(Cl^-)|$

$D_e^i(Na_2Cl^+)=|E(Na_2Cl^+)-E(Na_2^+)-E(Cl)|$

[b] $D_e(Na_2Cl)=|E(Na_2Cl)-E(NaCl)-E(Na)|$

$D_e(Na_2Cl^+)=|E(Na_2Cl^+)-E(NaCl)-E(Na^+)|$

[c] ref.77.

insensitive to the location of the extended Na orbital (Figure 5.9(e)).

B. Vertical ionization

The vertical ionization threshold of Na_2Cl corresponds to the removal of the unpaired electron from the highest occupied molecular orbital, which, as noted above, is mostly concentrated between the two sodium atoms. This is clearly seen in the differential charge density map in Figure 5.10, showing the electron density of the neutral molecule relative to the ionized molecule in the triangular structure after electronic relaxation. We find that the relaxation

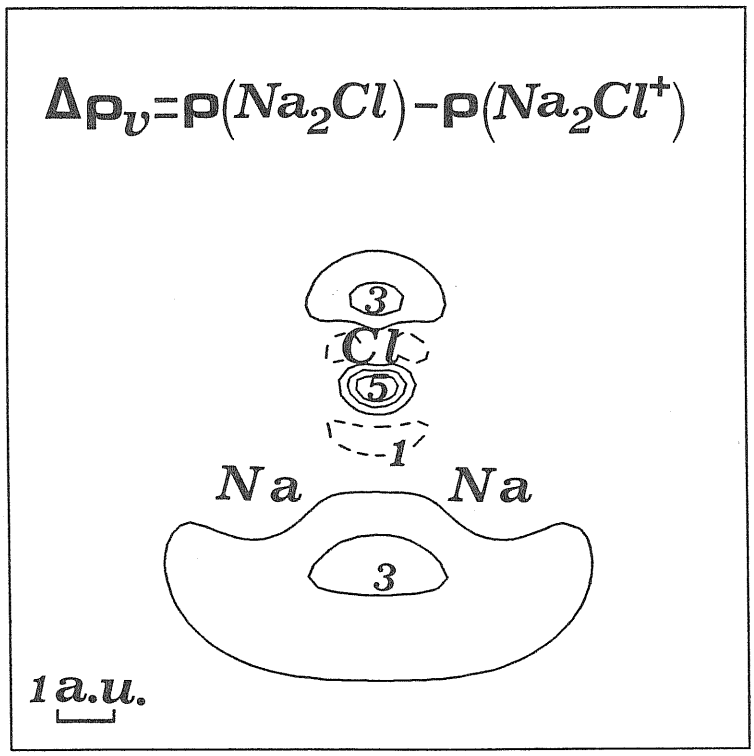

Fig. 5.10 Charge density $\Delta\rho_v$ of the Na_2Cl molecule relative to the Na_2Cl^+ molecular ion in the same configuration. Contour values are in units of $0.001e/(a.u.)^3$, with spacing of $0.002e/(a.u.)^3$.

tends to further delocalize the hole and shifts the IP by only 0.03 eV. Our calculated value for the vertical IP is surprisingly somewhat higher than the experimental datum [77], by about 0.4 eV. This could be due to an inaccuracy in the pseudopotential description of sodium, which, at variance from the case of Na_2Cl_2, is directly involved in the ionization process of Na_2Cl. We also note that the vertical IP of the Na-Cl-Na linear species is about 3.5 eV.

C. Na_2Cl^+

In the case of Na_2Cl as well we find that ionization is accompanied by a

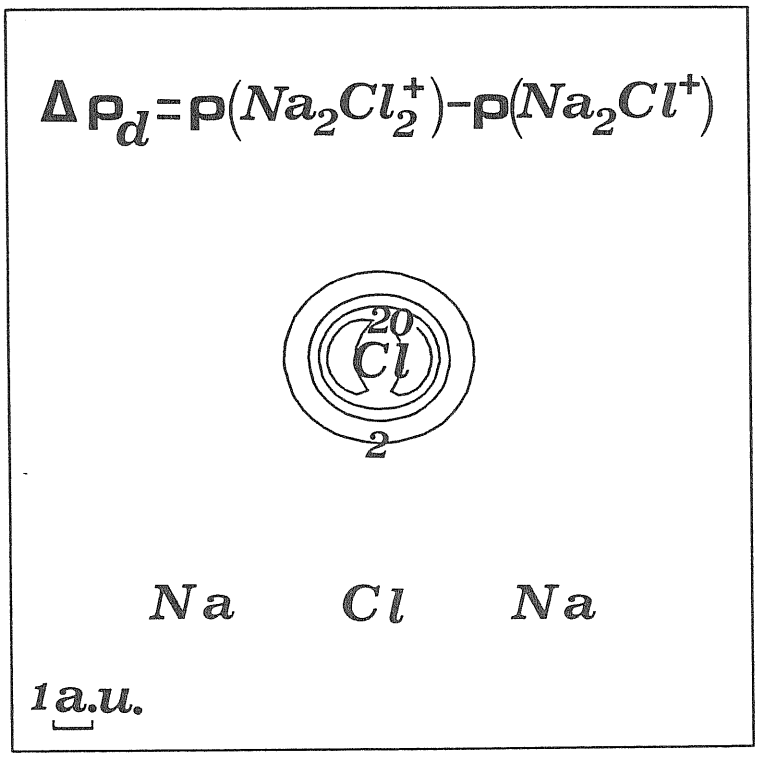

Fig. 5.11 Charge density $\Delta\rho_d$ of $Na_2Cl_2^+$ relative to Na_2Cl^+.Contour values are in units of $0.01e/(a.u.)^3$, with spacing of $0.06e/(a.u.)^3$.

structural change. A transition to the linear symmetric shape shown on the right hand side of Figure 5.8 is found to further stabilize the singly ionized triatomic molecule and to lower the IP by about 1 eV (see Table 5.5). The electron density piles back around the halogen (MP(Cl)=7.79) and the binding energy turns out to be very close to that of the neutral dimer (see Tables I and II). The same structure is the final ionization product of the metastable state of Na_2Cl in the linear asymmetric Na-Cl-Na arrangement , whereas the Cl-Na-Na arrangement is unstable against ionization.

As can be seen from the values of $d_{(NaCl)}$ in Table 5.4 and Table 5.5, the

stable structure of the Na_2Cl^+ cluster is identical to that of this aggregate in the presence of an extra chlorine atom ($Na_2Cl_2^+$). Figure 5.11 shows the difference between the electron densities of the two compounds and reveals once more the neutralization of the additional weakly bound atomic halogen in $Na_2Cl_2^+$. In agreement with evidence from mass spectra[79], the chlorine-deficient ionized aggregate is more stable than the stoichiometric cluster and, as expected, is its most probable dissociation product.

5.5 Discussion

The calculations presented above allow us to understand how the bonding and the structural properties of the neutral sodium chloride dimer evolve after ionization and why eventually mass spectroscopy can reveal the chlorine-deficient ionized aggregate in much stronger abundance than the stoichiometric one. The SCHF-pseudopotential method seems a useful approach to the study of the equilibrium properties of these aggregates. Dissociation energies for several paths are found in reasonable agreement with experiment. Chemi-ionization reactions of alkali dimers with homonuclear halogen molecules have been produced and the energetically allowed paths for these reactions carefully analyzed[92]. In agreement with these chemi-ionization experiments, we find that the formation reaction $Na_2+Cl_2 \rightarrow Na_2Cl^+ + Cl^-$ is highly probable, while the reaction $Na_2+Cl_2 \rightarrow Na^+ + NaCl + Cl^-$ is highly improbable since the energy of the products is significantly higher than that of the reactants. For a complete study of dissociation

processes one should of course transcend the HF approximation.[83]

A number of more or less refined ionic models have been put forward for both Na_2Cl_2[75,93] and Na_2Cl^+[91,92,94], which use in general interionic potentials fitted to the properties of NaCl. For Na_2Cl_2 we notice that a shell model [75], adjusted to both the monomer and the crystal, gives results in close agreement with our own. In the case of Na_2Cl^+, Lin *et al.* [94] have shown that the polarizability of the anion in an ionic model is a crucial parameter and that a value significantly smaller (by a factor 2/3) than the polarizability of the free anion is necessary to obtain a linear structure at equilibrium and a dissociation energy in rough agreement with experiment.

We believe that, as the size of the aggregate increases, the same mechanism found here for the smallest cluster is still involved in determining the features of the observed mass spectra. Ionization should remain a drastic process and involve important structural changes. Therefore, at variance from aggregates of rare-gas atoms and simple metals[95], magic numbers in the mass spectra of ionic systems do not reflect the relative stability of the neutral parent clusters of the same composition.

Chapter 6

SUMMARY AND CONCLUSIONS

As we have discussed in Chapter 1 of this thesis, semiempirical approaches to molecular shapes and crystal structures have so far been developed on different footings. In the case of solids, great success has been achieved recently in the classification of a large class of compounds by means of simple structural parameters defined for the atomic constituents.[7–12] In the case of molecules[5], several phenomenological criteria to account for the shapes of the main group species have been proposed in the literature. Though useful, to a large extent, in rationalizing the geometries of restricted classes of molecules, none of them seems to provide a successful scheme to account for structural trends in wide families of compounds, such as all the AB_2 or AB_3 species.

We have shown, in chapters 2 and 4, that a unified classification scheme for structural properties of $s-p$ bonded tri- and tetra-atomic aggregates, in both the molecular and the solid phase, can be constructed through the use of Quantum Structural Diagrams (QSDs). These diagrams are defined by two Cartesian coordinates expressed as linear combinations of Valence Electron Orbital Radii (VEOR), the latter being derived from ab initio calculations on

the free atoms. We have examined the tranferability from solids to molecules of coordinates based on radii from either pseudopotential (Zunger-Cohen radii[9]) or all electron (nodal radii[24]) calculations. Our results indicate a substantial equivalence of the two schemes.

We notice that transition metal compounds have been explicitly excluded from our plots based on s and p VEOR, since we believe that d orbital contributions are needed for a complete account of their structural properties.

The first result of our QSDs is that the number N of total valence electrons in the compound is a relevant parameter in structural classification, in agreement with Walsh criterion[28] for molecular shapes and with Villars' classification scheme for solids[10]. While crystal structures are known for many solids, the available experimental information for the molecular phase is not sufficient to construct statistically meaningful plots for the various values of N. However, at least in the case of molecules, it is not necessary to define a fine scale on the N axis, such as that used by Villars in classifying crystals. A distinction between double-octet (DO) and sub-DO compounds for AB_2 species, and between compounds with $N = 24$ and with $N < 24$ for AB_3 species is sufficient to yield successful structural separations. It is not clear, however, how to extend our approach to molecular ions. This would be interesting especially with the aim of predicting structural transitions upon ionization or electron capture.

The VEOR based structural maps for solids reported in the literature

(Andreoni[11] and Burdett *et.al.*[12]) for DO AB_2 compounds, and those which we have constructed[13,14] for sub-DO AB_2 and for AB_3 crystals with $N < 24$ provide the following remarkable results:

(i) they allow a satisfactory separation between different crystal structures; (ii) they account for trends in the coordination number; (iii) they distinguish between packed and layered compounds, always appearing in two distinct domains of the plane.

Some species are however found to be misplaced in the plots used to investigate crystals. A careful analysis of the structure and bonding of the specific misplaced compound has often indicated the reasons why the maps constructed cannot account for its conformation. (In the case of mercury dihalides, for example, both the frozen core approximation and the disregard of *d* orbital contributions may be responsible for the difficulties encountered in their classification). The corresponding QSDs for molecules do not reveal the same problems met with solids, due to the simpler structural question to be solved in the former case.

In the case of AB_2 molecules, the maps which we have constructed[13] perfectly discriminate between linear and bent species and account for the trend in the apex angle of bent compounds. The structural plots for AB_3 molecules[14] successfully distinguish planar from threedimensional geometries and also several different distortions of ideal symmetric shapes. Finally, the different planar structures displayed by molecules belonging to the A_2B_2 family are clearly separated by VEOR-based structural parameters.

The results of our plots for AB_2 and A_2B_2 molecules have allowed us to establish a correlation between the apex angles of these compounds and one of the structural parameters used, i.e., our Y coordinate defined as the difference of the averages core sizes of the atomic constituents. More precisely, Y has been found to be related to the tendency of AB_2 molecules to bend and to the angular deviation from the ideal square shape for rhombohedral A_2B_2 species.

The existence of these correlations has in turn suggested a direction where a physical interpretation of the coordinates used may be sought. Insight into the physical meaning of our structural parameters has been gained by a first principle investigation of the linear-to-bent structural transition in the family of DO AB_2 molecules[15]. We have performed all-Eeectron (AE), Hartree-Fock frozen core calculations on DO AB_2 molecules with different core sizes. B has been taken as a model fluorine atom with a fixed core size, while A has been taken to model a group-II atom with twelve electrons and its atomic dimensions have been varied to define different Y coordinates for the AB_2 species. We have first established the role of the central atom single particle orbitals in determining the molecular geometry. It turns out that, provided that the atomic constituent A gives rise together with B to an ionic compound AB_2, i.e., provided that $3s$ valence level of A is high enough in energy to permit a charge transfer A$\rightarrow$B, it is the position of the A $2p$ core level which determines the molecular equilibrium structure as linear or bent. Hence, the elemental y coordinate associated with the central

atom, which by definition weights more the p radii than the s one, is expected to suitably condense the orbital properties which are necessary and sufficient to describe a linear-to-bent transition in the class of the species examined. The above findings are also consistent with our results for conformation and binding of alkaline-earth dihalide molecules in an ionic model[56].

Our calculations have allowed us to establish a first principle relationship between the bond angle θ of DO AB_2 molecules and the structural coordinates Y and furthermore to find an analytic representation of the binding energy of these compounds, as function of θ and Y. In agreement with the results of our QSD for triatomic molecules with $N = 16$, we have again found a critical value Y_c of the Y coordinate associated with the compound, such that species with $|Y| < |Y_c|$ have a linear shape, while those with $|Y| > |Y_c|$ have a bent geometry in their ground state. The squared angular deviation from planarity of bent molecules, $\Delta\theta^2$, has been established to vary linearly with Y, except in the immediate neighborhood of Y_c. In the transition region near Y_c, the functional dependence of $\Delta\theta$ from the so called bond ionicity Y is more complicated. The behaviour $\Delta\theta(Y)$ has suggested a simple form for the binding energy $E(\theta, Y)$ of DO AB_2 molecules. The difference between E in the bent and in the linear structures has been expressed as a linear combination of a quadratic and a quartic term in $\Delta\theta$, with coefficients depending on Y. Such an expression has turned out to reproduce very accurately the energy of an AB_2 with a fixed core size, as θ varies, and to provide a general representation for the energy of DO AB_2

species when both Y and θ vary.

Our ab initio study of the linear-to-bent transition has therefore established significant connections between the Y structural coordinate and both the physical factors underlying the structural transition and some properties of the AB_2 family compounds. This clearly constitutes only a first step towards a complete understanding of the physical meaning of the VEOR-based coordinates. Further investigations are certainly needed. In the case of molecules, a study of the square-to-rhombohedral distortion in the class of A_2B_2 compounds and an analysis of how Y is related to the properties of AB_3 species could provide further insight into the interpretation of the structural parameters. In the case of solids, the interpretations of the (Y, X) coordinates reported so far in the literature has always been formulated on phenomenological grounds[41]. Due to the greater complexity of the structural problem in the solid than in the molecular phase, an investigation for crystals corresponding to that we have provided for molecules should first be adressed to AB compounds. A relevant contribution in this direction could come from an ab initio study of the correlations between the (Y, X) coordinates and the physical properties determining, e.g., the transition from the NaCl to CsCl structure. Such an investigation could be accomplished by AE frozen core calculations on a model AB ionic solid with the NaCl structure, whose core size of the cation is suitably enlarged to reproduce a transition to the CsCl structure.

In this connection, we mention that ab initio all-electron calculations

of the electronic properties of crystalline silver halides , by means of the Linearized-Augmented-Plane-Wave (LAPW) method[96], are part of our work in progress. In order to test our computer code[97] for simple ionic solids, as well as to test the validity of the frozen core approximation for these systems, we are carrying out AE calculations for the NaCl solid.These calculations could provide an appropriate starting point for the investigation mentioned just above, about the correlation between the sodium-chloride-to-cesium-chloride structural transition and the coordinates (Y, X).

While the first part of this thesis has been devoted to the problem of equilibrium structure for tri- and tetra-atomic compounds, the second part has been concerned with ionization induced structural transitions in specific systems, namely sodium chloride microclusters. The ab initio calculations which we have presented have allowed us to understand how bonding and structure of the neutral sodium chloride tri- and tetra-atomic compounds evolve after ionization, and why eventually mass spectroscopy can reveal chlorine-deficient ionized aggregates in much stronger abundance than stoichiometric ones. We have indeed shown that ionization is a drastic process involving symmetry braking for both Na_2Cl_2 and Na_2Cl. The neutral bent Na_2Cl evolves towards a linear structure after ionization, while the rhombohedral dimer adopts a triangular conformation upon removal of one electron. The latter is found to be very weakly bound against dissociation into a non stoichiometric ionized aggregate and a chlorine atom. We believe that, as the size of the aggregate increases, the same mechanism found

here for the smallest cluster is still involved in determining the features of the observed mass spectra. Ionization should remain a drastic process and involve important structural changes.

The Single-Configuration-Hartree-Fock method which we have used, turns out to be a useful approach to the study of the equilibrium properties of sodium chloride aggregates. Dissociation energies for several paths are found in reasonable agreement with experiment. In particular, we have found complete agreement with chemi-ionization experiments on compounds formation.

Our calculations have also allowed us to make contact with the ionic models proposed in the literature for sodium chloride compounds and to discuss to what extent the picture they provide for the bonding in these materials is reliable. In particular, an ionic model is found to be quite consistent with the molecular orbital picture of the bond that we obtain for the dimer. This is no longer the case for the neutral dialkali chloride species and thus an ionic model cannot properly account for its ionization process.

Appendix

GENERALIZED VALENCE BOND AND CONFIGURATION INTERACTION METHODS

The Hartree-Fock (HF), Generalized Valence Bond (GVB) and Configuration Interaction (CI) methods [3]are, in their essence, different approximations to the total wavefunction of N interacting electrons in the field of given fixed nuclei. If a N electron system is characterized by the hamiltonian :

$$H = \sum_{p=1}^{N} h(p) + \sum_{p>q=1}^{N} \frac{1}{r_{pq}}, \qquad (A.1)$$

where $h(p)$ contains all one-electron terms involving electron p, the total energy of any electronic wavefunction can be written as :

$$E = \sum_{i,j}^{n} D_j^i h_{ij} + \sum_{i,j} {}_{k,l} D_{kl}^{ij} (ik|jl) \qquad (A.2)$$

where

$$h_{ij} = < \phi_i | h | \phi_j > \qquad (A.3)$$

$$(ik|jl) = < \phi_i(1)\phi_j(2) | \frac{1}{r_{12}} | \phi_k(1)\phi_l(2) >,$$

and $\{\phi_j\}_{j=1}^n$ is a set of n single particle functions, in term of which the total wavefunction is described. D_j^i and D_{kl}^{ij} are appropriate density matrix elements. If the total wavefunction is expressed through orthonormal orbitals

$$< \phi_i | \phi_j >= \delta_{ij}, \tag{A.4}$$

the one and two electron density matrices in (A.2) can be brought into diagonal form and the total energy written in the following simplified way

$$E = 2\sum_{i=1}^{n} f_i h_{ii} + \sum_{i,j=1}^{n} (a_{ij} J_{ij} + b_{ij} K_{ij}), \tag{A.5}$$

where $J_{ij} =< \phi_i | \mathbf{J_j} | \phi_i >$ and $K_{ij} =< \phi_i | \mathbf{K_j} | \phi_i >$ indicate the usual Coulomb and exchange energies, respectively and J_j and K_j the corresponding operators. The energy coefficients $\{2f_i = D_i^i; a_{ij} = a_{ji} = D_{ij}^{ij}; b_{ij} = b_{ji} = D_{ji}^{ij}\}$ are independent from the orbital set $\{\phi_j\}_j$.

In the HF scheme, the total wavefunction Ψ of N electrons is approximated by the antisymmetrized product of n single particle orbitals ϕ_j, chosen to be orthonormal to each other

$$\Psi = \mathbf{A} | (\phi_1 \alpha)(\phi_1 \beta)...(\phi_n \alpha)(\phi_n \alpha) > . \tag{A.6}$$

A is the antysimmetrizer or determinant operator and α and β are the Pauli spin functions. If the total electronic wave function of a molecule is written in the HF approximation, it generally doesn't lead to an adequate description of bond dissociation. Let's consider, as an example, the simple case of the

hydrogen molecule H_2. Near the equilibrium internuclear distance R_{eq}, the ground state of H_2 is properly described by the closed-shell HF wavefunction

$$\mathrm{A}|\phi\phi\alpha\beta> . \qquad (A.7)$$

In the dissociative limit, the system consists of two isolated hydrogen atoms and is therefore described by the open-shell singlet wavefunction

$$\mathrm{A}|\phi_1\phi_2(\alpha\beta-\beta\alpha)> . \qquad (A.8)$$

Since eq. (A.7) consists of a single, doubly occupied molecular orbital, it cannot describe the separated atom limit. Conversely, the required orthogonality between ϕ_1 and ϕ_2 prevents eq. (A.8) from describing the molecular bond. A wavefunction with the proper behavior at all internuclear separations can be constructed by relaxing the orthogonality restriction between single particle orbitals

$$\mathrm{A}|\phi_1\prime\phi_2\prime(\alpha\beta-\beta\alpha)>=\mathrm{A}|(\phi_1\prime\phi_2\prime+\phi_2\prime\phi_1\prime)\alpha\beta>, \qquad (A.9)$$

where $<\phi_1\prime|\phi_2\prime>=S_{12}=0$. The wavefunction expressed by eq. (A.9) is the simplest example of generalized valence bond function. For any molecular system, eq. (A.6) can be generalized to allow selected electron pairs to be described in term of singly occupied overlapping orbitals (as in the simple valence bond method). If the various orbitals are then solved for selfconsistency, the resulting wavefunction is referred to as a generalized bond

wavefunction. More specifically, the GVB method replaces the conventional HF-closed-shell orbital description of a singlet pair by a so called GVB pair, consisting of two non orthogonal orbitals coupled into a singlet

$$\phi_a\phi_a\alpha\beta \rightarrow \phi_{1a}\phi_{2a}(\alpha\beta - \beta\alpha), \qquad (A.10a)$$

or equivalently

$$\phi_a\phi_a\alpha\beta \rightarrow (\phi_{1a}\phi_{2a} + \phi - 2a\phi_{1a})\alpha\beta. \qquad (A.10b)$$

Using this prescription, the HF wavefunction

$$\mathbf{A}|\phi_1\phi_1\alpha\beta...\phi_m\phi_m\alpha\beta\phi_{m+1}\alpha...\phi_n\alpha > \qquad (A.11)$$

is extended to the GVB form

$$\mathbf{A}|\phi_{11'}\phi_{21'}(\alpha\beta - \beta\alpha)...\phi_{1m'}\phi_{2m'}(\alpha\beta - \beta\alpha)\phi_{m+1}\alpha...\phi_n\alpha >, \qquad (A.12)$$

where $< \phi_{1i'}|\phi_{2i'} >= S_i$. In eq. (A.12) each singlet electron pair is allowed to correlate. However, for most chemical problems many such correlations can be ignored and only selected electron pairs (generally those describing chemical bonds) need be represented by GVB pairs. The wavefunction (A.12) singlet couples as many orbital pairs as is possible for a given eigenstate of spin. This "perfect pairing" assumption in the construction of the coupling scheme can be relaxed by allowing full functional freedom for spin eigenstates.

In this way other linearly independent ways of coupling orbitals than that used in eq. (A.12) are taken into account in the construction of the total wavefunction. The energy of the GVB eigenfunction so far developed cannot be expressed in the relatively simple form of eq. (A.5), since the density matrices entering eq. (A.2) can't be put in a diagonal form. In order to obtain E in the desired form of eq. (A.5), suitable single particle orbitals orthogonal to each other are constructed from the original GVB orbitals. Different techiques can be adopted to build up the new set of orbitals, depending on which kind of pairing is considered Perfect pairing or separeted pairing of spin eigenfunctions.

Once the total wavefunction has been expressed in the form of eq.(A.5), it is solved for selfconsistency. This means that one seeks those orbitals $\{\phi_j\}_j$ for which E is stationary (at a minimum) with respect to any arbitrary varation in any of the orbitals. Two necessary and sufficient variational conditions are derived for the minimization of E

$$< \delta\phi_\nu | \mathbf{F}_\nu | \phi_\nu >= 0 \qquad (A.13a)$$

$$< \delta\phi_\nu | \mathbf{F}_\nu - \mathbf{F}_\mu | \phi_\mu >= 0 \qquad (A.13b)$$

$\mathbf{F_i}$ is the generalized Foch operator

$$\mathbf{F_i} = f_i \mathbf{h} + \sum_j (a_{ij}\mathbf{J_j} + b_{ij}\mathbf{K_j}) \qquad (A.14)$$

Condition (A.13a) ensures $\delta E = 0$ for each variation $\delta\phi_\nu$ in orbital ϕ_ν that is

orthogonal to all occupied orbitals. Condition (A.13b) ensures instead that $deltaE = 0$ for each $\delta\phi_\nu$ overlapping any occupied orbital.

The configuration interaction method is a straightforward application of the Ritz method of linear variations to the calculation of electronic wavefunction. This method employs a linear expansion *ansatz* for the trial wavefunction Ψ of a N electron system

$$\Psi = \sum_{s=1}^{n} C_s \Phi_s. \qquad (A.15)$$

Here the Φ_s are predetermined expansion functions and the linear coefficients C_s are the parameters which are varied to make the total energy $E[\Psi]$,functional of Ψ, stationary. The expansion functions Φ_s are often referred to as "configurations". They are constructed as linear combinations of products of one elctron functions (spin-orbitals), those being chosen so that Φ_s satisfies all of the symmetry conditions which Ψ is required to satisfy. A linear combination of Slater determinants is required, generally, in order to satisfy spin and space symmetry conditions. The choice of the spin orbital set $\{\phi_j\}_j$ used to construct the configuration Φ_s is of paramount importance in determining the ultimate success of a CI calculation. First, the one- electron function space spanned by the orbital set determines the best result that can be obtained when all possible CFs which can be constructed from the given set are included in the CI expansion, and no further approximations are made. This so called "full CI" result is invariant with respect to any

unitary transformation of the orbital set. Second, the particular choice of the individual orbitals within a given space, is of crucial importance in determining the convergence rate of the CI expansion. The term " convergence" refers to the number of CFs needed to achieve results of a particular quality within a given orbital set.

REFERENCES

[1] M. L. Cohen and S. Louie, Ann. Rev. Phys. Chem. **17**, 537 (1984).

[2] P. C. Hohemberg and W. Kohn, Phys. Rev. **136**, B864 (1964); W. Kohn and L. J. Sham, *ibid.* **140**, A1133 (1965).

[3] For Hartree-Fock and Generalized Valence Bond methods see, e.g., F. W. Bobrowicz and W. A. Goddard in:*The Electronic Structure of Atoms and Molecules*, H. F. Schäfer ed. (Addison-Wesley, Reading, Massachusetts, 1972), Ch.4; for Configuration Interaction method, see I. Shavitt *ibid.*, Ch.6.

[4] For a review see, e.g., E. Mooser, Nuovo Cimento **2D**, 1613 (1983); A. N. Bloch and G. C. Schatteman in: *Structure and Bonding in crystals* (Academic, New York, 1981), Ch.4 and A. Zunger, *ibid.*, Ch. 5.

[5] J. K. Burdett, *Molecular Shapes* (J. Wiley, New York, 1980).

[6] Surf. Sci. **156** and **157** (1985).

[7] J. St. John and A. N. Bloch, Phys. Rev. Lett. **33**, 1095 (1974); J. R. Chelikowsky and J. C. Phillips, Phys. Rev. B **17**, 2453 (1978).

[8] W. Andreoni, A. Baldereschi, E. Biemont and J. C. Phillips, Phys. Rev. B **20**, 4814 (1979).

[9] A. Zunger and M. L. Cohen, Phys. Rev. B **20**, 4082 (1979); A. Zunger, Phys. Rev. B **22**, 5839 (1980).

[10] P. Villars, J. Less-Common Met. **92**, 215 (1983); *ibid.* **99**, 33 and 102,

199 (1984); *ibid.* **109**, 93 (1985).

[11] W. Andreoni, Helv. Phys. Acta **58**, 226 (1985).

[12] J. K. Burdett, G. D. Price and S. L. Price, Phys. Rev. B **24**, 2903 (1981).

[13] W. Andreoni, G. Galli and M. P. Tosi, Phys. Rev. Lett. **55**, 1734 (1985); W. Andreoni and G. Galli, J. Phys. Chem. of Minerals (in press).

[14] G. Galli and W. Andreoni (to be published).

[15] G. Galli and W. Andreoni (to be published).

[16] M. P. Tosi, Sol. St. Phys. **16**,1 (1964), F. Seitz and D. Turnbull eds. (Academic Press, New York)

[17] See, e.g., T. P. Martin, Physica **127** B, 214 (1984) and references therein.

[18] G. Galli, W. Andreoni and M. P. Tosi, Phys. Rev. A (in press).

[19] G. Galli, W. Andreoni and M. P. Tosi (unpublished).

[20] E. Mooser and W. B. Pearson, Acta Crystallogr. **12**, 1015 (1959).

[21] J. C. Phillips, Rev. Mod. Phys. **42**, 317 (1970); J. A. Van Vechten, Phys. Rev. **182**, 891 (1969); *ibid.* **187**, 1007 (1969).

[22] E. S. Machlin and B. Loh, Phys. Rev. Lett. **45**, 1642 (1980).

[23] J. R. Chelikowsky, Phys. Rev. A **26**, 3433 (1982).

[24] W. Andreoni, A. Baldereschi and G. Guizzetti (unpublished).

[25] L. Pauling, J. Am. Chem. Soc. **147**, 542 (1947).

[26] D. G. Pettifor, Solid State Commun. **51**, 31 (1984); D. G. Pettifor and R. Podloucky, Phys. Rev. Lett. **53**, 1080 (1985); D. G. Pettifor, J. Phys. C **19**, 285 (1986).

[27] J. C. Phillips, A. Zunger, A. N. Bloch and J. R. Chelikowsky, Phys. Rev. Lett. **55**, 260 (1985); D. G. Pettifor and R. Poudloucky, Phys. Rev. Lett. **55**, 261 (1985).

[28] A. D. Walsh, J. Chem. Soc. 2266 (1953).

[29] R. S. Mulliken, Rev. Mod. Phys. **14**, 204 (1942).

[30] P. K. Mehrotra and R. Hoffmann, Theor. Chim. Acta **48**, 301 (1978).

[31] K. Ruedeberg, J. Chem. Phys. **66**, 375 (1977).

[32] N. H. March, J. Chem. Phys. **74**, 2973 (1981).

[33] L. S. Bartell, J. Chem. Educ. **45**, 754 (1968).

[34] R. G. Pearson, J. Am. Chem. Soc. **91**, 1252 and 4947 (1969); R. G. Pearson, Proc. Natl. Acad. Sci. USA **72**, 2104 (1975).

[35] R. E. Rundle, J. Am. Chem. Soc. **85**, 112 (1963).

[36] See, e.g.,E. Heilbronner and H. Bloch, *The HMO Method and Its Application*, (J. Wiley, New York, 1976).

[37] R. J. Gillespie, *Molecular Geometry* (Van Nostrand-Reinhold, London, 1972).

[38] L. Pauling, *The Nature of the Chemical Bond* (Cornell. Univ. Press, Ithaca, New York, 1960); see also R. Mc. Weeny, *Coulson's Valence* (Oxford University Press, 1979).

[39] J. K. Burdett, Acc.Chem. Res. **15**, 34 (1982).

[40] M. Natapoff, J. Phys. Chem. Solids **36**, 57 (1975); *ibid.* **37**, 59 (1976); Chem. Phys. Lett. **78**, 375 (1981).

[41] J. C. Phillips, Solid State Commun. **22**, 549 (1977); E. S. Machlin,

T. P. Chow and J. C. Phillips, Phys. Rev. Lett.**38**, 1292 (1977).

[42] M. L. Cohen, Science **179**, 1189 (1973).

[43] Landoldt-Börnstein, *Crystal Structure Data of Inorganic Compounds* VII (Springer, Berlin Heidelberg, 1973).

[44] P. Villars and L. D. Calvert, *Pearson's Handbook of Crystallographic Data for Intermetallic Phases* (American Society for Metals, Metals Park 1985).

[45] L. Wharton, R. A. Berg and W. Klemperer, J. Chem. Phys. **39**, 2023 (1963); A. Büchler, J. L. Stauffer and W. Klemperer, J. Am. Chem. Soc. **86**, 4544 (1964).

[46] See, e.g., *Infrared and Raman Spectroscopy*, E. G. Brame Jr. and J. Grassel (Marcell Dekker Inc., New York and Basel, 1976)

[47] See, e.g., *Electron Spin Resonance* N. M. Atheron (J. Wiley, New York, 1973).

[48] A. F. Wells, *Structural Inorganic Chemistry* (Claredon, Oxford, 1975).

[49] R. W. G. Wyckoff, *Crystal Structures*, vol.1 (Interscience, New York 1964)

[50] J. C. Phillips , J. Non-Cryst. Solids **43**, 37 (1981).

[51] R. D. Shannon, Acta Cryst. **A32**, 751 (1976).

[52] D. E. Mann, G. V. Calder, K. S. Seshadri, D. White and M. J. Linevsky, J. Chem. Phys. **46**, 1138 (1967); G. V. Calder, D. E. Mann, K. S. Seshadri, M. Allavena and D. White, J. Chem. Phys. **51**, 2093 (1969) ; V. P. Spiridonov, A. G. Gershikov, A. B. Altman,

G. V. Romanov and A. A. Ivanov, Chem. Phys. Lett. **77**, 41 (1981).

[53] L. Andrews in: "*Vibrational Spectra and Structure*", vol.IV, p. 9 (Elsevier,1975): alkali-dioxides; L. Andrews, J. Am. Chem. Soc. **98**, 2147 and 2152 (1976): alkali-dihalides; L. Andrews and B. S. Ault, J. Mol. Specrt. **68**, 114 (1977): Ca_2O; L. Andrews, E. S. Prochaska and B. S. Ault, J. Chem. Phys. **69**, 556 (1978): MgO_2; B. S. Ault and L. Andrews, J. Chem. Phys. **62**, 2312 (1975): CaO_2, SrO_2, BaO_2; A. Buchler, J. L. Stauffer and W. Klemperer, J. Chem. Phys. **40**, 3471 (1964): Cu-dihalides; R. L. Dekock and M. R. Barbachyn, J. Inorg. Nucl. Chem. **43**, 2645 (1981): B_2O; A. V. Demidov, A. G. Gershikov, E. Z. Zasorin, V. V. Spiridonov and A. A. Ivanov, Zhurn. Strukt. Khim. **24**, 9 (1983): Ga_2O, In_2O, Tl_2O; M. A. Douglas, R. H. Hauge and J. L. Margrave, High. Temp. Sci. **16**, 35 (1983): Al_2O; W. C. Easley and W. Weltner, J. Chem. Phys. **52**, 1489 (1970): BC_2; G. Galli, W. Andreoni and M. P. Tosi, Phys. Rev. A (1986), in press: Na_2Cl; W. R. M. Graham, K. I. Dismuke and W. Weltner, J. Chem. Phys. **61**, 4793 (1971): LiC_2, NaC_2, KC_2, CsC_2; R. S. Grev and H. S. Schaefer III, J. Chem. Phys. **80**, 3552 (1984) and reference therein: SiC_2; G. Herzberg, *Molecular Spectra and Molecular Structure III*(Van Nostrand Reinhold, New York, 1966): CN_2, C_2N, BO_2, C_3, N_3 ; D. L. Hildebrand and E. Murad, J. Chem. Phys. **53**, 3403 (1970): Na_2O; A. Hinchcliffe and J. C. Dobson, Mol. Phys. **28**, 543 (1974): Li_2S; A. Hinchcliffe and J. C. Dobson, Chem. Phys. **8**, 158 (1975): Na_2S;

Z. H. Kafafi, R. H. Hauge, L. Fredin and J. L. Margrave, J. Phys. Chem. **87**, 797 (1983) and R. S. Grev and H. S. Schaefer III, J. Chem. Phys. **82**, 4126 (1985): Si_2C; K. J. Kelsall and K. D. Carlson, J. Phys. Chem. **84**, 951 (1980): GaO_2, InO_2, TlO_2; R. R. Lembke, R. F. Ferrante and W. Weltner, J. Am. Chem. Soc. **99**, 416 (1977): SiN_2; T. P. Martin and H. Schaber, Spectrochim. Acta **38A**, 655 (1982): Mg_2S, Ca_2S, Sr_2S, Zn_2S, Cd_2S, MgS_2, CaS_2, SrS_2, ZnS_2, CdS_2; A. Mavridis and J. F. Harrison, J. Am. Chem. Soc. **104**, 3827 (1982): Li_2C; D. Milligan and M. J. Jacox, J. Chem. Phys. **43**, 3734 (1965): C_2O; A. Neubert, K. F. Zmbov, K. A. Gingerich and H. R. Ihle, J. Chem. Phys. **77**, 5218 (1982): Li_2Sb, $LiSb_2$; E. S. Prochaska and L. Andrews, J. Chem. Phys. **72**, 6782 (1980): Zn_2O, ZNO_2, CdO_2; R. C. Spiker, L. Andrews and C. Trindle, J. Am. Chem. Soc. **94**, 2401 (1972): LiN_2; R. C. Spiker and L. Andrews, J. Chem. Phys. **58**, 702 and 713 (1973): Li_2O, K_2O, RB_2O, Cs_2O; D. E. Tevault, J. Chem. Phys. **76**, 2859 (1982): Cu_2O, CuO_2; D. E. Tevault, J. Chem. Phys. **77**, 577 (1982): AgO_2; C. Thomson, J. Chem. Phys. **58**, 216 (1973): B_2C; G. Verhaegen, F. E. Stafford and J. Dowart, J. Chem. Phys. **40**, 1622 (1964): BSi_2.

[54] D. A. Garland and D. M. Lindsay, J. Chem. Phys. **78**, 2813 (1983) and J. A. Horward, R. Sutcliffe and B. Mile, Chem. Phys. Lett. **112**, 84 (1984): Li_3; D. M. Lindsay, D. R. Herschbach and A. L. Kwiram, Mol. Phys. **32**, 1199 (1976): Na_3; G. A. Thompson and D. M. Lindsay, J.Chem. Phys. **74**, 959 (1981): K_3; M. D. Morse, J. B. Hopkins,

P. R. R. Langridge-Smith and R. E. Smalley, J. Che. Phys. **79**, 5316 (1983): Cu_3; J. A. Howard, K. F. Preston and B. Mile, J. Am. Chem. Soc. **103**, 6626 (1981) and K. Kernisant, G. A. Thompson and D. M. Lindsay, J. Chem. Phys. **82**, 4739 (1985): Ag_3; G. Pacchioni and J. Koutecky, Chem. Phys. **71**,181 (1982) and Ber. Bunsenges. Phys. Chem. **88**, 242 (1984): Ge_3, Be_3, Mg_3, Ca_3; R. S. Grev and H. S. Schaefer III, Chem. Phys. Lett. **119**, 111 (1985) , K. Ragavachari, J. Chem. Phys. **84**, 5672 (1986) and D. Tomanek and M. A. Schlüter Phys. Rev. Lett. **56**, 1055 (1986): Si_3; T. H. Upton, Phys. Rev. Lett. **56**, 2168 (1986): Al_3.

[55] F. Hulliger, *Structural Chemistry of Layer-Type Phases* (Reidel, Dordrecht 1976).

[56] G. Galli, M. P. Tosi, Nuovo Cimento D **4**, 431 (1984).

[57] C. Salez and A. Veillard, Theor. Chim. Acta, **11**, 441 (1968)

[58] A. D. McLean and G. S. Chandler, J. Chem. Phys. **72**, 5639 (1980).

[59] M. Weinert, R. E. Watson and J. Davenport, Phys. Rev. B **72**, 2115 (1985).

[60] D. Cubicciotti, J. Phys. Chem. **65**, 1058 (1961); T. E. Brackett and E. B. Brackett, J. Phys. Chem. **66**, 1542 (1962).

[61] P. Brumer and M. Karplus, J. Chem. Phys. **58**, 3903 (1973).

[62] See e.g. R. A. Cochran, Crit. Rev. Solid State Sci. **2**,1 (1971).

[63] J. R. Tessman, A. H. Kahn and W. Shockley, Phys. Rev. **92**, 890 (1953).

[64] P. S. Yuen, R. M. Murfitt and R. L. Collin, J. Chem. Phys. **61**, 2382 (1974).

[65] P. A. Akishin and V. P. Spiridonov, Kristallografiya **2**, 475 (1957).

[66] Landoldt-Börnstein, *Structure Data for Free Polyatomic Molecules* II/7 (Springer, Berlin Heidelberg, 1976).

[67] T. Ishiwata, I. Tanaka, K. Kawaguchi and E. Hirota, J. Chem. Phys. **82**, 2196 (1985).

[68] K .S. Krasnov, N. V. Philippenko, V. A. Bobkova, N. L. Lebedeva, E. B. Morozov, T. I. Ustinova and G. A. Romanova, *Molecular Constants of Inorganic Compounds* (Khimia, Leningrad 1979), cited by G. L. Gutsev and A. I. Boldyrev, Chem. Phys. Lett. **92**, 262 (1982): Li_3O, Na_3O, Li_3S, Na_3S; R. D. Brown, J. Am. Chem. Soc. **105**, 6496 (1984): C_3O; D. E. Tevault, R. A. DeMarco, and R. R. Smardzewski J. Chem. Phys. **75**, 4168 (1981): AgO_3 ; D. E. Tevault, R. L. Mowery, R. A. DeMarco, and R. R. Smardzewski, J. Chem. Phys., **74**, 4342 (1981): CuO_3 ; L. Andrews and R. C. Spiker Jr., J. Chem. Phys. **59**, 1851 and 1863 (1973): alkali dioxides; E. S. Prochaska and L. Andrews, J. Chem. Phys. **72**, 6782 (1980): ZnO_3, CdO_3; L. Andrews, E. S. Prochaska and B. S. Ault, J. Chem. Phys. **69**, 556 (1978): MgO_3; D. M. Thomas and L. Andrews, J. Mol. Spectrosc. **50**, 220 (1974): CaO_3, SrO_3, BaO_3; B. S. Ault and L. Andrews, J. Chem. Phys. **64**, 4853 (1976): alkali trichlorides and tribromides; B. S. Ault and L. Andrews, Inorg. Chem. **16**, 2024 (1977): alkali trifluorides;

G. A. Ozin, J. Chem. Soc. A (GB) 2307 (1970): AsP_3, SbP_3, PAs_3 ; R. L. Cook and M. C. L. Gerry, J. Chem. Phys. **53**, 2525 (1970): ClN_3 ; D. C. Frost, C. B. MacDonald, C. A. McDowell and N. P. C. Westwood, Chem. Phys. **47**, 111 (1980): ClN_3, BrN_3; E. Gipstein and J. F. Haller, Appl. Spectrosc. **20**, 417 (1966): FN_3; Von U. Engehardt, M. Feuerhahn and R. Minkwitz, Z. Anorg. Allg. Chem. **440**, 210 (1978): IN_3.

[69] P. von Rayne' Schleyer, E. U. Wuerthwein and J. A. Pople, J. Am. Chem. Soc. **104**, 5839 (1982): Li_3O and Na_3O; M. E. Schwartz and C. M. Quinn, Surf. Sci. **106**, 259 (1981): Al_3O; E. D. Brown and E. H. N. Rice, J. Am. Chem. Soc. **106**, 6475 (1984): C_3O.

[70] L. Andrews, B. S. Ault, J. M. Grzybowski and R. O. Allen, J. Chem. Phys. **62**, 2461 (1975).

[71] F. J. Adrian, V. A. Bowers, E. L. Cochran, J. Chem. Phys. **61**, 5463 (1974).

[72] J. Berkowitz in *Alkali Halide Vapors: Structure, Spectra and Reaction Dynamics*, Ch.5, P. Davidovits and D.L. McFadden (Academic, New York 1979); L. Andrews, J. Chem. Phys. **50**, 4288 (1969); *ibid* **54**, 4935 (1975),: Li_2O_2; *ibid* **57**, 1327 (1972) L. Andrews, T. Huang, C. Trindle, J. Chem. Phys. **77**, 1065 (1973): K_2O_2, Rb_2O_2, Cs_2O_2; B. S. Ault and L. Andrews, J. Chem. Phys. **62**, 2312 (1975): Ca_2O_2, Sr_2O_2, Ba_2O_2; J. S. Anderson and J. S. Ogden, J. Chem. Phys. **51**, 4189 (1969): Si_2O_2; J. S. Ogden and M. J. Ricks, J. Chem. Phys. **52**, 352 (1972): Ge_2O_2; *ibid* **53**, 896 (1970): Sn_2O_2; C. M. Western, P. R. R. Langridge-Smith

and B. J. Howard, Mol. Phys. **44**, 145 (1981) and P. Brechignac, S. De Benedictis, N. Halberstadt, B. J. Whitaker and S. Avrillier, J. Chem. Phys. **83**, 2064 (1985): N_2O_2; G. Herzberg, *Molecular Spectra and Molecular Structure III* (Von Nostrand-Reinhold, New York, 1966): C_2N_2, C_2O_2; K. M. Maloney, S. K. Gupta and D. A. Lynch Jr., J. Inorg. Nucl. Chem. **38**, 49 (1976): M_2X_2 with M=Al,In,Tl and X=O,S,Se,Te; A. N. Syverud, J. Inorg. Nucl. Chem. **38**, 2163 (1976): B_2O_2, Al_2O_2, B_2S_2, Al_2S_2, Al_2Se_2, Al_2Te_2, Ga_2Te_2, In_2S_2, In_2Se_2, In_2Te_2; B. J. Kelsall and K. Douglas Carlson, J. Phys. Chem. **84**, 951 (1980): Tl_2O_2; P. Klaeboe, E. Rytter, C. E. Sjorgen and T. Tomita, Proc. SPIE Int. Soc. Opt. Eng. **289**, p.283 (Int. Conf. on Fourier Transform Infrared Spectroscopy, Columbia SC, USA, 1981): Al_2Cl_2, Ga_2Cl_2, Al_2I_2.

[73] D. White, K. S. Seshadri, D. F. Dever, D. E.!Mann and M. J. Linevsky, J. Chem. Phys. **39**, 2463 (1963), C. P. Baskin, C. F. Bender and P. A. Kollman, J. Amer. Chem. Soc. **95**, 5868 (1973) Li_2F_2; K. S. Krasnov, V. S. Timoshinin, T. G. Danilova and S. V. Khandozhko, *Molekulyarnye Postoyannye neorganicheskikh soedineii (Molecular Constant of Inorganic Compounds)* (Izd. Khimiya, Leningrad, 1968) cited by S. J. Cyvin in *Molecular Structure and Vibrations* p. 49, (Elsevier ,1972): Na_2F_2; S. H. Bauer, T. Ino and R. F. Porter, J. Chem. Phys. **33**, 685 (1960): Li_2X_2 with X=Cl,Br,I; P. A. Akisin and N. G. Rambidi, Z. Phys. Chem. (Leipzig) **213**, 111 (1960): Li_2F_2, Na_2Cl_2.

[74] G. W. Schnuelle and R. G. Parr, J. Amer. Chem. Soc. **94**, 8974 (1972).

[75] D. O. Welch, O. W. Lazareth, G. J. Dienes and R. D. Hatcher, J. Chem. Phys. **64**, 835 (1976).

[76] M. P. Tosi and F. G. Fumi, J. Phys. Chem. Solids **25**, 45 (1964).

[77] M. M. Kappes, P. Radi, M. Schär and E. Schumacher, Chem. Phys. Lett. **113**, 243 (1985).

[78] R. Pflaum, P. Pfau, K. Sattler and E. Recknagel, Surf. Sci. **156**, 165 (1985).

[79] F. Honda, G. M. Lancaster, Y. Fukuda and J. W. Rabalais, J. Chem. Phys. **69**, 4931 (1978).

[80] B. Maessen and P. Cade, J. Chem. Phys. **80**, 2618 (1984).

[81] J. Diefenbach and T. P. Martin, J. Chem. Phys. **83**, 4585 (1985) and references therein.

[82] B. I. Dunlap, J. Chem. Phys. **84**, 5611 (1986).

[83] P. K. Swaminathan, A. L. Laaksonen, G. Corongiu and E. Clementi, J. Chem. Phys. **84**, 867 (1986).

[84] R. C. Miller and P. Kusch, J. Chem. Phys. **25**, 860 (1956); G. M. .Rothberg, J. Chem. Phys. **34**, 2069 (1961).

[85] P. A. Akisin and N. G. Rambidi, Z. Phys. Chem. (Leipzig), **213**, 111 (1960).

[86] W. R. Wadt and P. J. Hay, J. Chem. Phys. **82**, 284 (1985).

[87] See, e.g., K. D. Jordan in: *Alkali Halide Vapors: Structure, Spectra and Reaction Dynamics*, Ch. 15 (Academic Press, New York, 1979, Eds.

P. Davidovits and D. L. Mc Fadden);J. Berkowitz *ibid.* Ch. 5; S. Berry *ibid.* Ch3.

[88] L. R. Kahn, P. J. Hay and I. Shavitt, J. Chem. Phys. **61**, 3530 (1974).

[89] E. S. Rittner, J. Chem. Phys. **19**, 1030 (1959).

[90] A. W. Potts, T. A. Williams and W. C. Price, Proc. Roy. Soc. A **341**, 147 (1974).

[91] J. Berkowitz, C. H. Batson and G. L. Goodman, J. de Chemie Physique, **77**, 631 (1980).

[92] G. P. Reck, B. P. Mathur and E. W. Rothe, J. Chem. Phys. **66**, 3847 (1977).

[93] P. Brumer and M. Karplus, J. Chem. Phys. **64**, 5165 (1976).

[94] S. M. Lin, J. G. Wharton nd R. Grice, Mol. Phys. **26**, 317 (1973) .

[95] K. Sattler in: "*Festkorperprobleme, Advances in Solid State Physics*", vol. XXIII (Vierweg, Braunschweig, 1983, Eds. P. Grosse).

[96] H. J. F. Jansen and A. J. Freeman, Phys. Rev. B **30**, 561 (1984).

[97] The computer code for all-electron LAPW calculations of the electronic structure of crystals has been kindly provided to me by Dr. S. Massidda, who has also taught to me the basic features of the LAPW method.

[98] K. P. Huber and G. Herzberg, *Molecular spectra and Molecular Structure IV. Constants of Diatomic Molecules* (Van Nostrand-Reinhold, New York 1979).